AMERICAN UNIVERSITY OF BEIRUT

TUNING THE PHOTOPHYSICAL PROPERTIES OF CONJUGATED POLYELECTROLYTES USING SILVER NANOPARTICLES AND AMPHIPHILIC MACROMOLECULES

by
GHINWA HASSAN DARWISH

A thesis
submitted in partial fulfillment of the requirements
for the degree of Master of Science
to the Department of Chemistry
of the Faculty of Arts and Sciences
at the American University of Beirut

Beirut, Lebanon
April 2015

AMERICAN UNIVERSITY OF BEIRUT

TUNING THE PHOTOPHYSICAL PROPERTIES OF CONJUGATED POLYELECTROLYTES USING SILVER NANOPARTICLES AND AMPHIPHILIC MACROMOLECULES

by
GHINWA HASSAN DARWISH

Approved by:

Dr. Pierre Karam, Assistant Professor — Advisor
Chemistry

Dr. Tarek Ghaddar, Associate Professor — Member of Committee
Chemistry

Digambara Patra
Dr. Digambara Patra, Associate Professor — Member of Committee

Date of thesis defense: April 23, 2015

AMERICAN UNIVERSITY OF BEIRUT

THESIS, DISSERTATION, PROJECT RELEASE FORM

Student Name: ____
Last First Middle

○ Master's Thesis ○ Master's Project ○ Doctoral Dissertation

☐ I authorize the American University of Beirut to: (a) reproduce hard or electronic copies of my thesis, dissertation, or project; (b) include such copies in the archives and digital repositories of the University; and (c) make freely available such copies to third parties for research or educational purposes.

☐ I authorize the American University of Beirut, **three years after the date of submitting my thesis, dissertation, or project,** to: (a) reproduce hard or electronic copies of it; (b) include such copies in the archives and digital repositories of the University; and (c) make freely available such copies to third parties for research or educational purposes.

____

Signature Date

ACKNOWLEDGMENTS

I would like to express my deepest gratitude and appreciation to my advisor Dr. Pierre Karam for his encouragements, patience, support, guidance, and for providing me the opportunity to work in his lab and to benefit from his experience. Words are not enough to thank him for his continues support, for encouraging me to think creatively and pursue research projects in different directions. Without his guidance and persistent help this thesis would not have been possible.

I would like to express my sincere thanks to my committee members, Dr. Tarek Ghaddar and Dr. Digambara Patra for their help, advice, guidance, and for offering me valuable comments toward improving my work.

I thank my labmates in Dr. Karam's research group for their support and help: thank you Jihane Abou Zeid, Aya Sakaya, Hassan Fakeeh, and Samir Abo Shahin.

My sincere thanks also go to my friends and colleagues at the chemistry department especially Malik Jaafar , Remi Fayad, Rasha Al Moussawi, and Dani Saliba.

I also thank the chemistry department staff at AUB and the CRSL staff for their continuous support and help.

Last but not least, I deeply thank with love my family especially my mother Lina Tohmi and my sister Layal Darwish for their unconditional trust, love, and encouragement. I cannot forget friends who went through hard times together, cheered me up, and celebrated each accomplishment: Zouheir El Halabi, Reham abou Amer , Hala Najem, Elham El khatib, Zainab El Khatib, and Rana Salami.

AN ABSTRACT OF THE THESIS OF

Ghinwa Hassan Darwish for Master of Science
Major: Chemistry

Title: Tuning the Photophysical Properties of Conjugated Polyelectrolytes Using Silver Nanoparticles and Amphiphilic Macromolecules

The optoelectronic, semiconducting, and light amplifying properties of conjugated polyelectrolyte (CPEs) make them promising class of materials for applications in light emitting diodes, solar cells, biosensing and bioimaging. A major drawback, however, is their large extent of reversible and irreversible photobleaching leading to their short survival time and low quantum yield. The photophysical properties of CPEs are highly dependent on their microenvironment and backbone conformation. When extended, the polymer quantum yield increases substantially and its photostability improves. In this thesis work, we report on the enhancement of the photophysical properties of an anionic conjugated polyelectrolyte poly[5-methoxy-2-(3-sulfopropoxy)-1,4phenylenevinylene] (MPS-PPV) when positioned at precise distance from the core of metallic nanoparticles and upon its complexation with an amphiphilic polymer.

Using silver nanoparticles coated with a nano-layer of silica modified with 3-(Aminopropyl)trimethoxysilane, we were able to achieve 3.5 folds fluorescence enhancement on the emission intensity of MPS-PPV. Parameters such as silica shell thickness, particle concentration and surface charge are discussed in details on how to get the highest fluorescence enhancement.

Upon complexation with an amphiphilic polymer (polyvinylpyrrolidone), the anionic conjugated polyelectrolyte MPS-PPV was prepared as small nanoparticles with exceptional photostability and brightness. The polymer fluorescence was enhanced by 23 folds. Single molecule experiments revealed a complete suppression of blinking. In addition, a remarkable amount of photons were emitted per nanohybrid particle ($\sim 10^9$, on average) after only losing 18% of the original intensity. This number is many folds greater than most of the popular organic fluorescent dyes. We believe that an intimate contact between the two polymers is shielding the conjugated polymer from the destructive photo-oxidation effects.

In the last section, we discuss the use of antioxidants to improve on the photostability of MPS-PPV. CPEs backbone is exceptionally vulnerable to singlet oxygen. By exploiting the scavenging properties of hydrophobic and hydrophilic antioxidants, we were able to further improve the photophysical properties of pristine MPS-PPV and the nanohybrid particles reported earlier.

TABLE OF CONTENT

LIST OF ILLUSTRATIONS

FIGURES PAGES

LIST OF TABLES

TABLES PAGES

CHAPTER 1

INTRODUCTION

1.1 Overview on the advances of fluorescence spectroscopy:

Advances in fluorescence spectroscopy over the past decades have led to seminal work in fundamental and applied sciences. For instance, it provided unique opportunities for real-time tracking of molecules, which led to an exquisite level of understanding of many important biological phenomena and catalytic processes at the single molecule level.[1] It also allowed accurate measurements of association and dissociation of proteins and unraveled the interplay of interaction with other oligonucleotides and specific receptors.[1-2] This wealth of information allowed subsequently the advancement of the field of basic medicine through the development of targeted potent drugs and manufacturing of advanced materials and optoelectronic devices.[3-] In this chapter, we will cover the basic fundamentals in fluorescence spectroscopy and the recent advancements in this field. We will then present and highlight the unique photophysical properties of conjugated polymers, their wide range of applications in the field of material science and medicine, and the efforts undertaken to improve their photostability and quantum yield.

1.2 Jablonski Energy Diagram

Fluorescence spectroscopy provides an easy tool to detect molecules with high sensitivity and low detection limit (down to a single molecule). When a molecule is excited, the relaxation pathway greatly depends on its environment. The different energy levels involved in the absorption and emission of a photon by a fluorophore are schematically illustrated with the classical Jablonski energy diagram proposed in 1935 by Professor Alexander Jablonski (1898-1980).[4]

Figure 1.1 represents a typical Jablonski diagram where S_0 is the singlet electronic ground state and S_1 and S_2 are, respectively, the first and second singlet excited states represented as a stack of horizontal lines (vibrational levels). S_0 and S_1 are separated by the absorbance energy gap. The bold-black lines represent electronic energy levels. At each of these electronic energy levels, the fluorophore can assume a number of vibrational energy levels, represented as thinner-grey lines and depicted as 0, 1, 2, etc. For simplicity, rotational energy states are ignored in this representation.

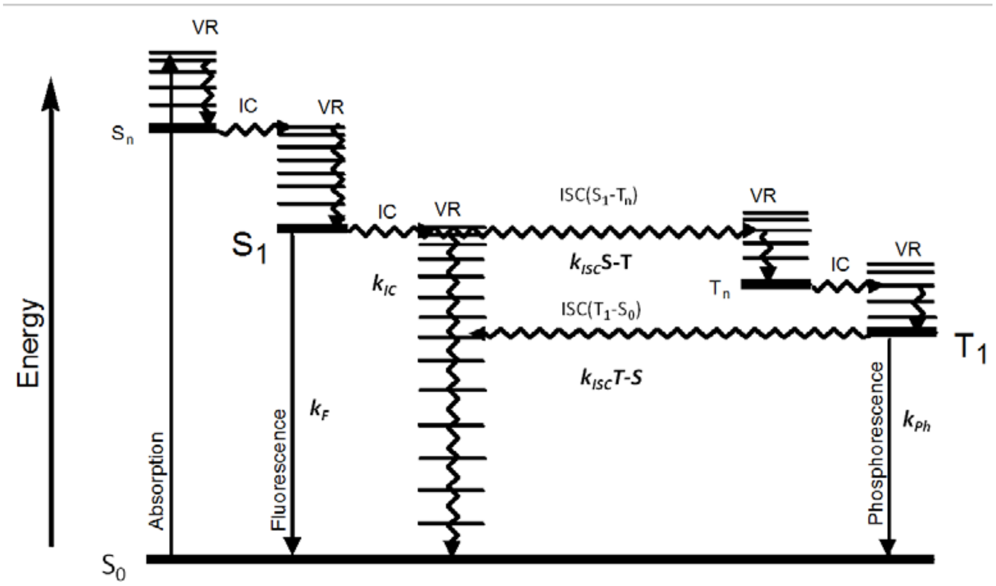

Figure 1.1: Jablonski diagram. S_n represents the electronic states. VR stands for the vibrational relaxation. IC stands for internal conversion. ISC stands for intersystem crossing.

Transitions associated with absorption or emission of a photon are represented as straight arrows, while those corresponding to internal conversion or non-radiative relaxation processes (Figure 1.1) are depicted as wavy arrows.

1.2.1 Absorption

A fluorophore absorbs a photon as a result of the interaction of the electric field vector of light with electrons in the ground state of a molecule, which occurs on the sub-femtosecond time-scale ($<10^{-15}$ seconds). The molecule is usually excited to a higher vibrational energy level in the first electronic excited state S_1.

1.2.2 Excited State Relaxation

Immediately after its excitation, the molecule relaxes to the lowest vibrational energy level of the first singlet excited state. This relaxation process is much slower than the absorption, and it typically lasts a few picoseconds. It involves both internal vibrational relaxations, also termed internal conversion (IC), and solvent reorganization around the photoexcited molecule. Any excess vibrational energy is converted into heat.

1.2.3 Emission

The fluorophore may relax to the ground electronic state via emission of a photon. This process may occasionally take hundreds of nanoseconds, although typically emission occurs in less than 10 ns. Since the energy associated with the photon emitted is less than that of the absorbed photons, emission is shifted to longer wavelengths from absorption. This phenomenon is known as Stokes shift.

The emission spectrum of a fluorophore is usually a mirror image of the absorption spectrum. Figure 1.2 presents an absorption and emission spectrum of the cyanine dye Cy3, which results from several favored electronic transitions from the ground state to the excited energy states. The shoulder at 518 nm corresponds to the transition from the lowest vibrational level in the ground state to the second vibrational level in the excited state. The absorption maximum at 550 nm corresponds to the electronic transition from the ground state to the first vibronic energy level in the excited state. On the emission side of the spectrum, the maximum emission peak at 566 nm and the shoulder peak at 606 nm correspond to the relaxation to different vibronic energy levels of the ground state.

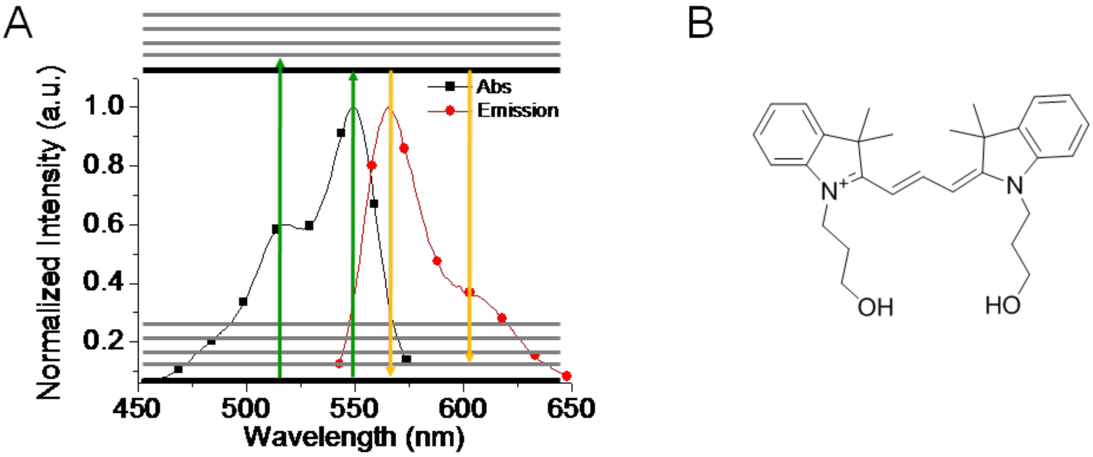

Figure 1.2: (A) Absorption (■) and emission (●) spectra of Cy3, and (B) its chemical structure.

As such, fluorescence spectroscopy has emerged as a sensitive and reliable technique to measure analytes in low range concentrations and down to the single molecule level.

This method enabled unraveling the dynamics of interaction of multiple proteins and protein/oligonucleotides in a spatial scale smaller than the optical diffraction limit.[1] Until recent years, the movement of Kinesin along microtubule filaments remained elusive until the use of fluorescence microscopy in 2004.[5] Kinesin is a homodimer motor protein powered by adenosine triphosphate (ATP) hydrolysis. The active movement of Kinesin supports several cellular functions such as meioses, mitoses and signaling molecules.[5] Yildiz *et al*. used single molecule fluorescence microscopy to track the movement of a single labeled Kinesin head. They showed for the first time strong evidence in support of the hand-over-hand walking model for Kinesin mobility (Figure 1.3).[5]

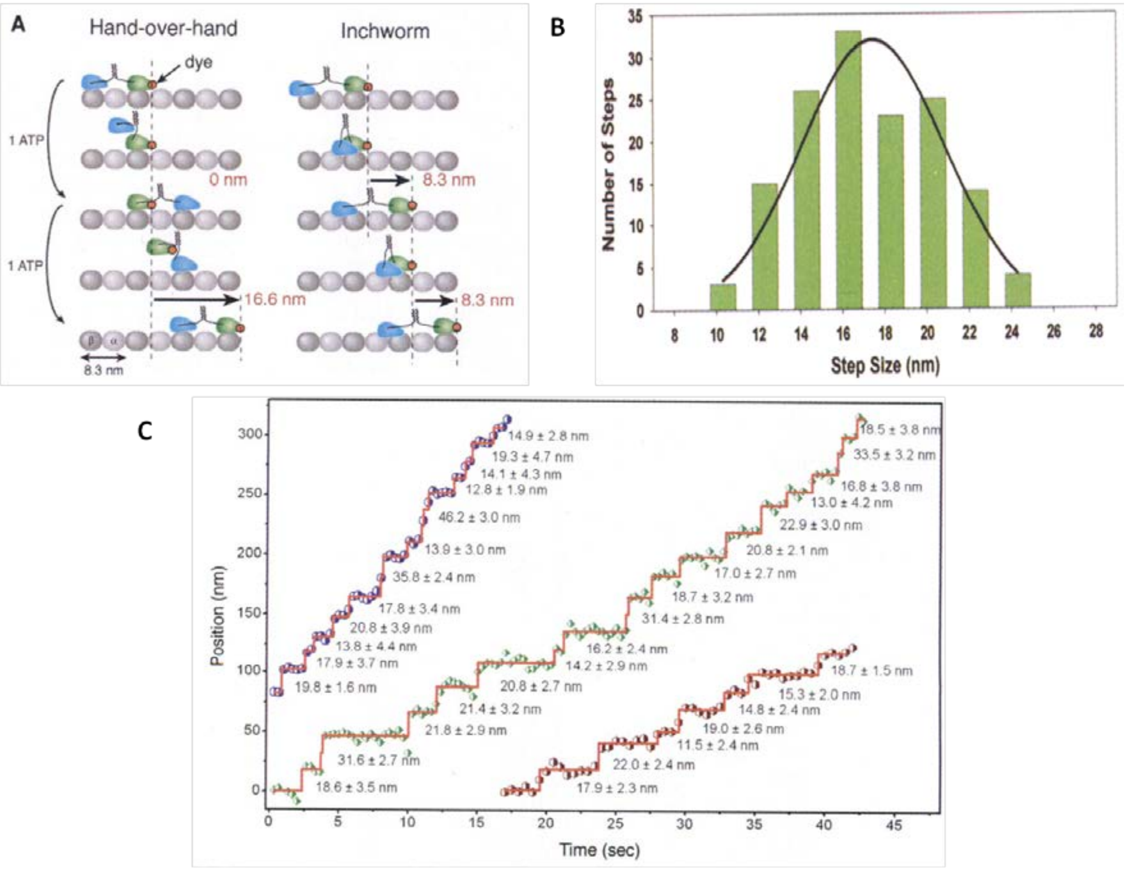

Figure 1.3: (A) Examples of two alternative classes of mechanisms for processive movement by kinesin. The hand-over-hand model (left) predicts that a dye on the head of kinesin will move alternately 16.6nm, 0nm, 16.6nm, whereas the inchworm mechanism (right) predicts uniform 8.3nm steps. (B) The kinesin step size histogram, the average step size is 17.3 ± 3.3 nm. The black solid line is a Gaussian fit. (C) Position versus time for Kinesin motility. The numbers correspond to the step size ± standard error of the mean. (Reprinted with permission from Yildiz *et al.*).[5]

Another example that strongly illustrates the impact of fluorescence techniques on biochemical applications is the use of specific indicators to detect the physiological role of cytoplasmic Ca^{2+} and to quantify its concentration. Ca^{2+} ions are important intercellular messengers for controlling numerous biological processes. With the development of Ca^{2+} specific probe, Grynkiewicz *et al.* have made it possible to study the role of Ca^{2+} as an intercellular messenger in a single cell, adherent cells layers or bulk tissues.[6]

1.2.4 Non-Radiative Decay

The process described earlier concerns only with the radiative decay. However, some molecules may decay via non-radiative pathways, which may involve unimolecular processes such as internal conversion (IC) to the ground state (**section 1.2.2**), intersystem crossing (ISC) to the triplet manifold, unimolecular chemical reactions, as well as bimolecular processes such as energy transfer and chemical reactions.

1.2.4.1 Internal Conversion

As previously discussed in **section 1.2.2**, the energy of the electronically excited state is given off to vibrational modes of the molecule. The excitation energy is, therefore, transformed into heat in competition with emission and other processes.

1.2.4.2 Intersystem crossing

The molecule may relax to a lower excited triplet state in a phenomenon known as intersystem crossing. Once in the triplet manifold, three photophysical processes (in addition to chemical reactions) may in turn take place; emission of a photon through phosphorescence, a back transition to the excited singlet state, or internal conversion to the singlet ground state. Molecules in the triplet excited state decay slowly, which often results in an increased probability of a reaction. Of particular importance is the sensitization of singlet oxygen which may in turn react with the molecule leading to its accelerated photobleaching.[7,8] Conjugated polyelectrolytes are especially prone to this phenomena. We will discuss later this destructive effect in details and our efforts to shield this class of macromolecules.

1.2.5 Quantum yield and lifetime

Fluorophores in the absence of any quenching interactions are characterized by their quantum yield and lifetime. Quantum yield is defined as the number of emitted photons out of the number of absorbed photons, or as the competition between the radiative decay rate and other decay rates (Equation 1.1). The lifetime is defined as the average time a molecule spends in the excited state before it relaxes to the ground state, or as the inverse of all possible decay rates (Equation 1.2).[9,10]

The quantum yield is given by:

$$\phi_0 = \frac{\Gamma}{\Gamma + k_{nr}} \qquad \textbf{Equation 1.1}$$

The lifetime is given by:

$$\tau_0 = \frac{1}{\Gamma + k_{nr}} \qquad \textbf{Equation 1.2}$$

Where ϕ_0 is the fluorescence quantum yield, Γ is the emissive rate of the fluorophore, k_{nr} is the nonradiative decay rate to S_0, and τ_0 is the life time of the excited state.

1.3 Förster Resonance Energy Transfer

Förster resonance energy transfer (FRET) was first formally proposed in the 1940s by Theodor Förster (1910-1974), who showed that electronic excitation energy can be transferred from a donor fluorophore to an acceptor chromophore in close proximity through non-radiative dipole–dipole coupling, with an efficiency dependent on the inverse of the sixth power of the distance separating the two (Equation 1.3).

$$E_{FRET} = \frac{1}{1+\left(\frac{R}{R_0}\right)^6} \qquad \textbf{Equation 1.3}$$

Where R is the distance between donor and acceptor and R_0 is the characteristic distance at which 50% energy is transferred.

R_0 is calculated by the following equation:

$$R_0^6 = \frac{9000(\ln 10)\phi_D \kappa^2 J(v)}{128\pi^5 N_A n^4} \qquad \textbf{Equation 1.4}$$

Where ϕ_D is the quantum yield of the donor molecule, N_A is Avogadro’s number, n is the index of refraction of the medium, κ^2 is an orientation factor and $J(v)$ is the normalized spectral overlap of the donor emission and the acceptor absorption, as shown below:

$$J(v) = \frac{\int \varepsilon_A(\lambda) f_D(\lambda) \lambda^4 d\lambda}{\int f_D(\lambda) d\lambda}$$ **Equation 1.5**

Where $\varepsilon_A(\lambda)$ (the molar absorptivity) is in units of $M^{-1}.cm^{-1}$ and f_D is the corrected fluorophore intensity of the donor. For instance, R_0 for Cy3 and Cy5, a classical single molecule FRET pair, is equal to 55 Å.

Resonance energy transferred between two fluorescent molecules is incredibly sensitive to distance and is thus instrumental in measuring small distance variations ranging from a few up to 100 angstroms. FRET has opened the door to a new and powerful field in biophysics enabling dynamic studies in a number of biological processes.[11]

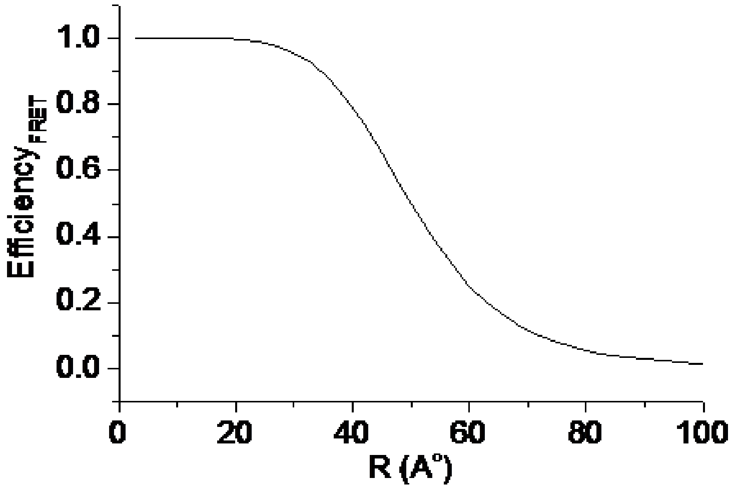

Figure 1.4: Simulated FRET efficiency distance-dependence between cyanine dyes Cy3 and Cy5.

Liu *et al.* have applied single-molecule FRET to decipher the initial stage of reverse transcription (RT) of the human immunodeficiency virus (HIV) genome.[12] They showed that the RT of the HIV genome is initiated from the tRNA–vRNA complex (Figure 1.5). This complex has a structural and a dynamic property at the initial stage that differs from the later stage of RT. This information is critical for designing anti-HIV drugs.[12]

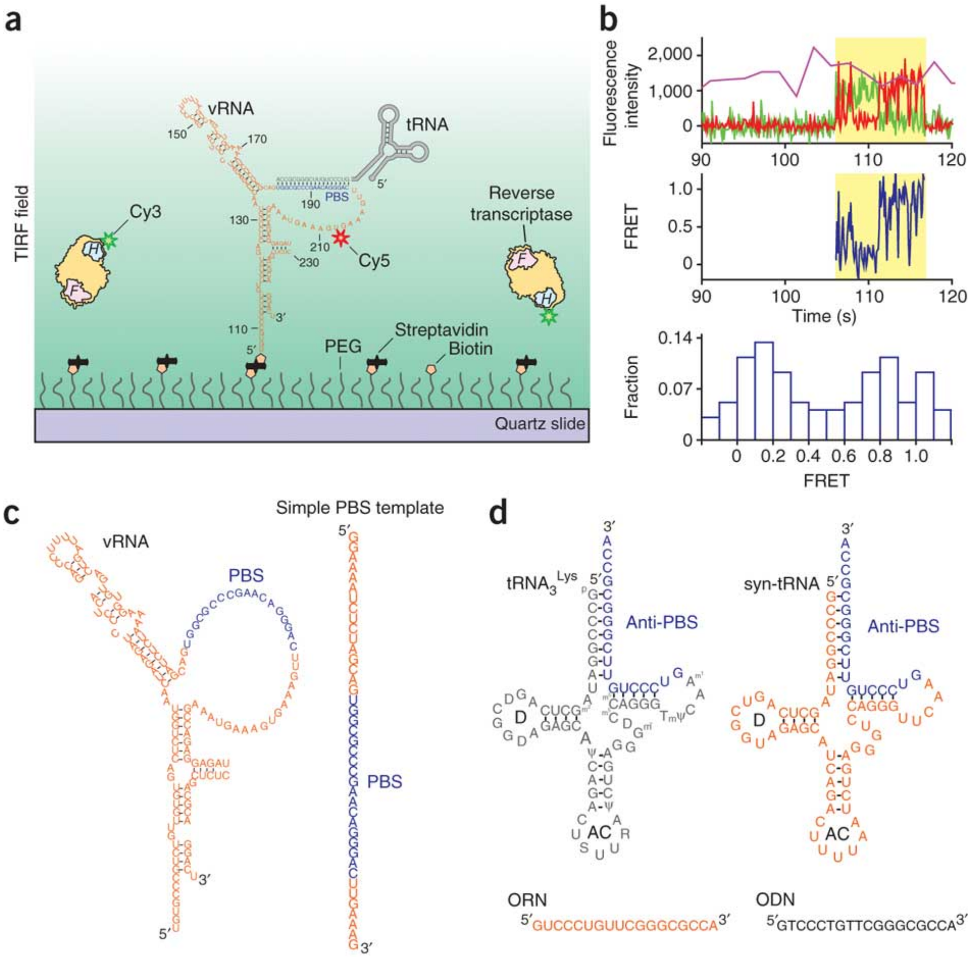

Figure 1.5: Single-molecule FRET assay for probing the structural dynamics of the initiation complex. (Reprinted with permission from Liu *et al.*).[12]

Single molecule fluorescence spectroscopy also allowed the determination of the free energy surface of folding for small cold-shock proteins, which cannot be obtained from ensemble experiments. The cold-shock protein termini were modified with a green fluorescent donor dye and a red fluorescent acceptor dye. The single-molecule Förster resonance energy transfer (FRET) measurement probed the distance changes as the protein folded over time. Studying the folding process at the single-molecule level can help in describing the distribution of pathways of this heterogeneous process.[13]

However, the need for photostable and bright fluorescent materials for long exposure SMS imaging is one of the most pressing factors limiting live cell imaging development. Quantum dots (QDs) partially fulfilled this need.

QDs have exceptional photophysical properties including: high quantum yield, high photostability, narrow emission bandwidth, size-tunable band gap, and solution processability, which make them excellent materials for long exposure and low laser power imaging applications.[14] These properties are strongly dependent on the structural contrast of the QDs.[14-15] Wu *et al.* compared the photostability of streptavidin conjugated to a QD (CdSe/ZnS) to that of one of the most stable organic dyes (Alexa 488) in the presence and absence of an antifading medium.[15] QDs showed great stability against photobleaching (Figure 1.6 **(A)** Red); the signals of QD 630 showed no obvious change for the entire 3 minutes illumination period. Whereas the labeling signals of Alexa 488 demonstrated quick photobleaching; the intensity started to disappear after 10s (Figure 1.6 **(A)** Green). In the presence of an antifade medium, the organic dye photostability was improved but not to be compared to quantum dots.[15]

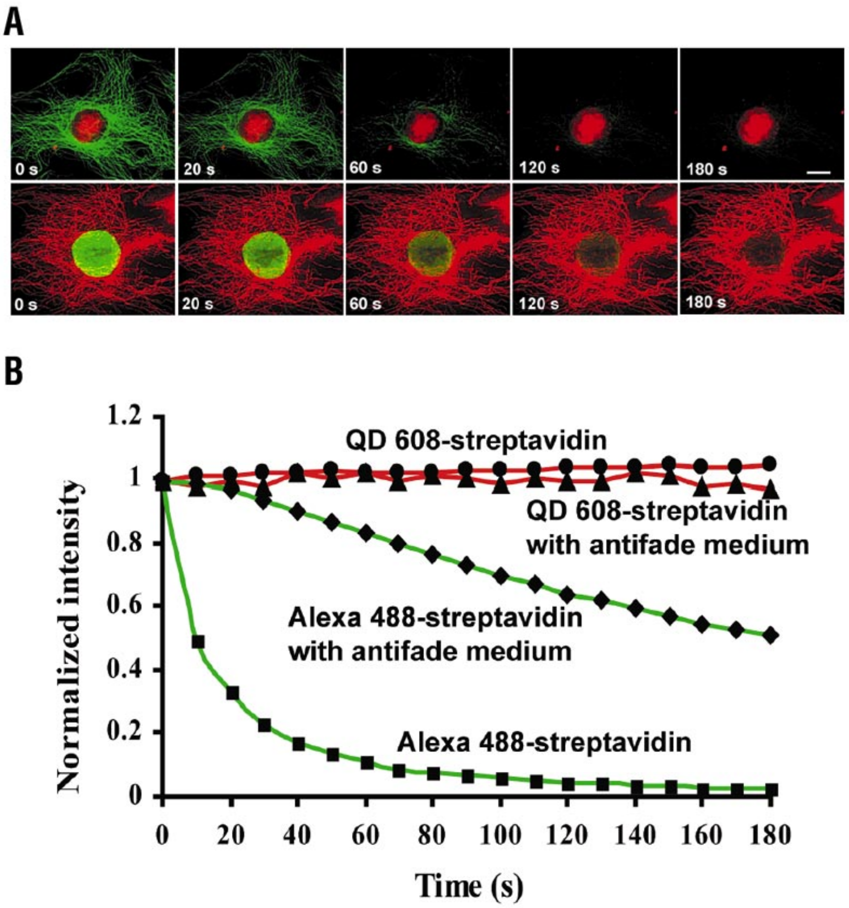

Figure 1.6: Photostability comparison between QDs and Alexa 488. (A) Top row: Nuclear antigens were labeled with streptavidin conjugated to QDs (CdSe/ZnS) (red) and microtubules were labeled with Alexa 488 (green). Bottom row: Microtubules were labeled with streptavidin conjugated to QDs (red), and nuclear antigens were labeled with Alexa 488. (B) Quantitative analysis of changes in intensities of streptavidin conjugated to QDs (CdSe/ZnS) (stained microtubules) and Alexa 488–streptavidin (stained nuclear antigens) in the presence and absence of antifade mounting medium Vectashield. (Reprinted with permission from Wu *et al.*).[16]

As such, quantum dots provided an excellent tool for long exposure imaging experiments.[14] Images could be acquired for several minutes and biological processes could be probed and studied for longer times than what organic and protein based fluorescent dye provided.

Despite the great advantage brought by the emergence of QDs as bright fluorescent probes, they are considered non-biocompatible material with adverse toxic effects on living cells. As such, they were limited to studies which involve fixed cells. In addition, a single QD particle emission suffers from photoblinking limiting their application in single particle tracking applications.[16]

Thus, the need for fluorescent materials with exceptional photostability, brightness, non-photoblinking, and most importantly, biocompatibility, attracted a lot of research interest to meet these requirements.

Conjugated polymers seemed like great candidates to fulfill all the aforementioned requirements. They are a class of organic compounds with alternating single and double bonds within their backbone, which allows them to have unique optoelectronic properties.[17, 18] In what follows, we will start with a brief history of conjugated polymers followed by addressing their biocompatibility and then discuss their photophysical properties, and some of their applications.

1.4 Brief history of conjugated polyelectrolytes

Polyacetylene, also known as Cuprene (Figure 1.7), was the first synthesized conjugated polymer, a highly cross-linked, irregular molecule resulting from acetylene polymerization in the presence of a copper-containing catalyst.[19] In 1958, Natta *et al.* polymerized acetylene in hexane using a mixed catalyst of alkyl aluminum and titanium tetraalkoxide, which yielded a linear non-conductive polyacetylene.[20] In 1974, Shirakawa and his co-workers succeeded in synthesizing a non-conductive silvery thin polymer film by using the Ziegler-Natta catalyst.[19] In 1977, Shirakawa, MacDiarmid and Heeger oxidized polyacetylene with oxidizing agents such as halogen vapor or AsF_5, which resulted in 10^9 more conductive polymers than the silvery film; yet, it was still insoluble.[21] In 1987, Wudle, Heeger, and their co-workers prepared the first water-soluble conducting polymers, which were 3-(2-sulfonatoethyl) substituted and 3-(4-sulfonatobutyl)-substituted polythiophenes (Figure 1.8). [22]

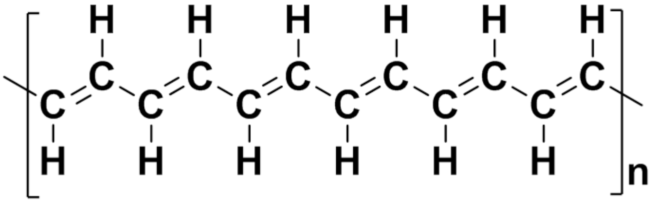

Figure 1.7: Chemical structure of Polyacetylene (Cuprene).

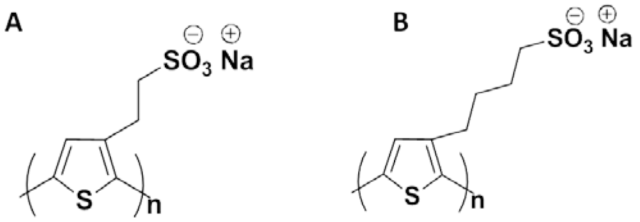

Figure 1.8: Chemical structures of 3-(2-sulfonatoethyl) substituted (A) and 3-(4-sulfonatobutyl)-substituted (B) polythiophenes.

1.5 Photophysical properties of conjugated polyelectrolytes:

Conjugated polyelectrolytes provide a unique set of photophysical properties including high conductivity, π-electron polarization, exciton and charge transport, variable band gap for light absorption and emission, and chemical sensitivity.[22] These properties are controlled by the structural conformation of the conjugated polyelectrolyte and their surrounding environment (nature of the solvent, its polarity and the power of solvation).

The delocalization of π-electrons along the polymer's conjugated backbone is highly affected by the degree of aggregation of the chromophore segments, which in turn affects their photo-physical properties. Understanding the energy transfer mechanism is crucial for the application of conjugated polymer in bioimaging and sensing devices.[23,24]

The delocalization of electrons along the backbone of conjugated polymers offers attractive optical and electronic properties. Their large extinction coefficient, their highly emissive properties, their ability to translate a binding (or unbinding) event into an easily measurable optical or electrochemical response, and their highly efficient intra- and interchain energy transfer makes them an excellent choice for chemical sensing.[25]

The energy migration in conjugated polymer can occur through both the intramolecular and intermolecular interactions. Intramolecular interaction refers to the migration of excitons along the conjugated backbone of a single polymer chain in the absence of any chain-to-chain contact (rigid-rod structure), which dominates in solution, while the intermolecular interactions refer to the migration of excitons between closely spaced chromophores.[23,24]

The diffusion and the mobility of excitons can be determined by weak and strong electronic coupling, in which the coupling can occur through space via columbic coupling (dipole-dipole interaction) and through bonds via coupling between two p orbitals of the neighbored chain.[26]

The dissolved structure of conjugated polyelectrolytes prevent any chain folding, thus incoherent exciton hopping along the polymer chains is therefore expected to be the main exciton migration channel, while in aggregated structure, new pathways of energy transfer can be involved as the direct interchain transfer of energy to the nearest chain. Therefore, the intrachain processes induce slow energy transfer to the end moieties than the interchain one. The higher energy transfer in interchain processes can be attributed to the strong coupling between the two neighbor chains, and the lower energy transfer in the intrachain processes can be attributed to the weak interaction in which the energy transfer occurs through two steps with hopping along the conjugated chains as the rate-limiting step.[24,23, 26]

One of the factors that affects the degree of aggregation is the presence of surfactants, which could lead to a dramatic increase in the fluorescent quantum yield driven by the electrostatic and hydrophobic interactions between the surfactants and CPEs.[27] The presence of surfactants can enhance the photoluminescence quantum yield by eliminating the interchain quenching (non-emissive relaxation) that competes with the emissive interchain exciton relaxation and by increasing the surface to volume ratio of the conjugated polyelectrolytes.[27] Moreover, the photoluminescence quantum yield can be enhanced by inhibiting the folding of the polymer chain and hence reducing the conformational disorder and the number of kink defects that serve as non-emissive recombination sites and extending the length of the electron delocalization path.[27]

Danesh *et al.* have studied the effect of surfactant (cetyltrimethylammonium bromide (CTAB)) on the dynamic conformational transition of the water-soluble poly[3-(potassium-6- hexanoate)thiophene-2,5-diyl] (P3KHT).[28]P3KHT adopts a coil conformation in some organic solvents and undergoes conformational changes from coil to rod aggregates, and then to crystalline nanowires in other solvent[28]. As a result of P3KHT-CTAB complexation, a blue shift , absence of vibronic fine structure, and enhancement in the fluorescence intensity of P3KHT was obtained; this can be attributed to the breakup of the aggregates of P3KHT due to the incorporation of the long alkyl side chains and to the disruption of ring stacking by CTAB.[28]

Pinnock *et al.* have shown the effect of conformations on the photophysical properties of conjugated polymers. They studied the capabilities of poly(p-phenyleneethyny lenethienyleneethynylene) (PPETE) fluorescent conjugated polymers in sensing nickel and cobalt in both solution and solid states, where they aimed at showing the role of intermolecular interaction in chemosensing.[29]

They reported that PPETE has two absorption peaks in solution; the lower energy peak at 442 nm is due to π-π* transitions in the conjugated polymer backbone, and the higher energy peak at 330 nm is due to n-π* transition centered on the pendant terpyridyl ligand. Upon going from solution to solid state, the absorption peak was broadened and the lower energy peak was found to be shifted in the red direction, which is due to both the extended geometry of the conjugated polymer and the increase of inter-polymer interactions.[29]

Karam *et al.* have studied the photophysical properties of negatively charged conjugated polyelectrolyte system, poly[5-methoxy-2-(3-sulfopropoxy)-1,4-phenylene-vinylene] (MPS-PPV)) encapsulated in neutral and in negatively charged lipid vesicles at the single-molecule level, showing the effect of the polymer conformation on its photophysical properties.[30] They showed that MPS-PPV adopts a collapsed chain conformation within the negatively charged vesicles where it exists as freely diffusing polymer, whereas it adopts an extending conformation within neutral vesicles. In the first case, stepwise photobleaching in fluorescence intensity-time trajectories and emission from low-energy chromophores along the chain were observed, which is due to efficient energy migration over many chromophores of many polymer chains. In the second case, exponential decay of the intensity over time and a broad blue-shifted emission spectrum were observed, because the emission arises from the chromophores within the same isolated polymer chain.[30]

1.6 Conjugated polyelectrolytes for sensing applications:

Amplified fluorescence polymers (AFP) or super-quenching occurs due to a signal gain, which results from the interaction of the conjugated polymer with analytes. This signal amplification is due to the ability of a conjugated polymer to serve as a highly efficient transport medium for efficient transport of electronic excited states, thus amplification basically depends on the exciton mobility.[31]

Swager and his coworkers used fluorescence quenching mediated by electron transfer to understand energy migration and to exploit its amplified fluorescence-based sensory events in a conjugated polymer.[32] They modified a conjugated polymer with a quencher-receptor attached to every repeating unit.

Fluorophore sensitivity is typically quantified by a Stern-Volmer plot. For a typical Stern-Volmer experiment, incremental amounts of a quencher are added to a constant fluorophore concentration.

$$\frac{F_0}{F} = (1 + k_{sv}[Q]) \qquad \textbf{Equation 1.6}$$

$$\frac{\tau_0}{\tau} = \left(1 + k_q \tau_0 [Q]\right) \qquad \textbf{Equation 1.7}$$

Where F_0 is the fluorescence intensity in the absence of a quencher, F is the fluorescence intensity after adding the quencher, K_{sv} is the Stern-Volmer quenching constant or diffusional quenching constant, τ_0 is the life time in the absence of quencher, τ is the lifetime in the presence of quencher, and [Q] is the quencher concentration.[31]

A linear relationship between [Q] and F_0/F indicates a purely static or dynamic quenching, as well as the decrease in the lifetime as the concentration of the quencher increases, which indicates that the quenching is dynamic, whereas in static quenching the lifetime remains unchanged by changing the quencher concentration.[31]

A large k_{sv} indicates a highly sensitive fluorophore.

Quenching could either be due to the binding of the quencher to the polymer (static quenching) or due to the diffusion of the quencher to the excited state (dynamic quenching).[31]

$$\tau = \left(k_r + k_{nr} + k_q[Q]\right)^{-1}$$

Equation 1.8

Where k_r is the radiative decay rate, k_{nr} is the non-radiative decay rate, and k_q is the bimolecular rate constant of fluorescence quenching.[31]

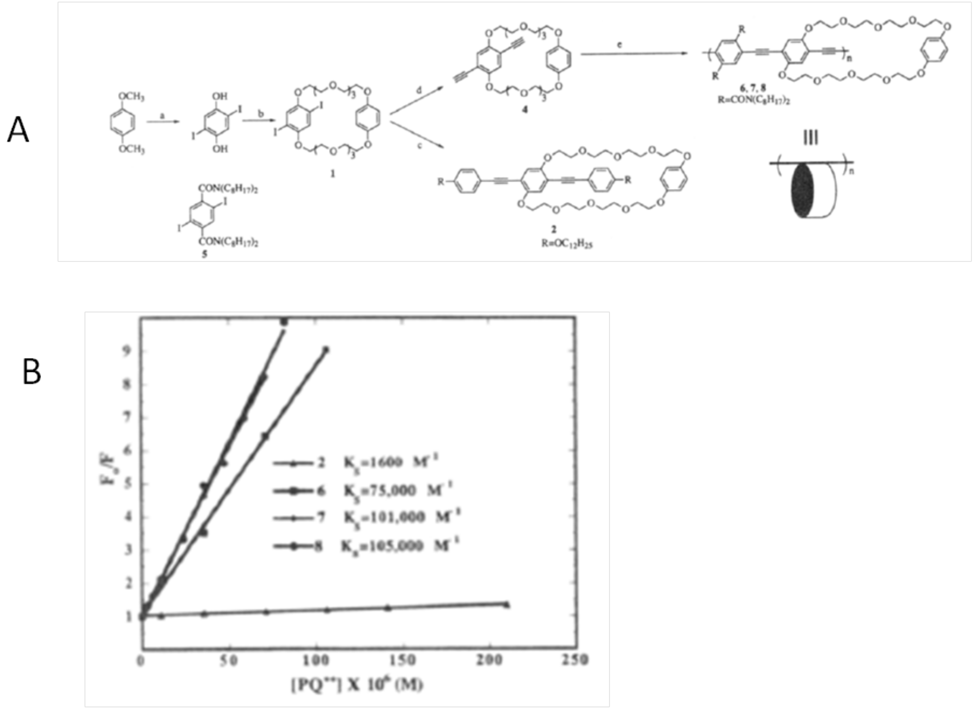

Figure 1.9: (A) synthetic scheme of 2 and 6-8. (B) Stem-Volmer plots of 2 and 6-8. (Reprinted with permission from Zhou *et al.*).[32]

In Swager's work (Figure 1.9), the monomer (**2**) quenching constant (K_{sv}) by paraquant was 1600 M^{-1}.[32] The polymer (**6**) showed a much higher quenching constant of 76000 M^{-1}. As the polymer size increased (**6-8**) the K_{sv} increased as well. The larger amplified quenching constant with increasing polymer size reflects that a single quencher bound to any of the repeating units can quench excitons formed along the polymer backbone.[32] Energy migration is faster than fluorescence decay so the excited state can sample every receptor in the polymer. Once the quencher is bound to the receptor, the excited state is immediately and quantitatively quenched. The result is an enhanced deactivation. Their results demonstrate a new principle for analyte detection via amplified fluorescence quenching upon energy migration in conjugated polymers.[32]

As such, CPEs have been implemented in single particle bio- and chemical assays.[18, 33,33b,33c] They were successfully used to detect specific oligonucleotides sequences,[18, 34] small molecules,[35] biomolecules[36] and discriminate between different bacteria strains.[37] Experimental approaches that utilize color or fluorescence intensity for chemosensing and biosensing applications have garnered great research interest and development. Generally, optical chemosensors consist of binding sites connected to a fluorophore, which acts as a signal source. Polymer-based fluorescence chemosensors have several important advantages over small organic compound-based chemosensors; these include signal amplification, high binding efficiency and recognition selectivity for specific analytes, in addition to ease of fabrication.[38]

In their tutorial review, Kim *et al*. showed the recent contribution of conjugated polymers for optical sensor applications by which their unique properties, such as their large number of absorbing units and their efficient inter- and intra chain energy transfer, make them a good optical material in highly sensitive chemical and biological sensors.[38]

Another example is organic fluorescent nanoparticles consisting of a highly fluorescent core, which is made up of poly(phenylene ethynylene) (PPE)-bearing pentiptycene units coated with hydrogels that display a reactive functional group; these were used by Cordovilla and Swager as an imaging probe for proteases. [39]

Furthermore, a study showing the importance of conjugated polymers in chemical sensing was performed by Childress *et al.* Using FRET method and conjugated polymer nanoparticles (donor) doped with rhodamine derivatives (acceptor), they developed an accurate method to detect mercury in aqueous solutions. The light harvesting capabilities of the conjugated polymer enhanced the fluorescence intensity of the rhodamine dye, thus allowing the detection of mercury at low concentrations (0.7ppb). The conjugated polymer nanoparticles showed a color change from green-yellow to orange-red when rhodamine bound to mercury.[40]

Additionally, Chang *et al.* have used conjugated polymer thin films, poly(p-phenylene vinylenes) (MEH-PPV and DP10-PPV) and a poly(dip- henylacetylene), that showed high fluorescence quenching sensitivities toward explosive compounds such as 2,4,6-trinitrotoluene (TNT) and 2,4- and 2,6-dinitrotoluene (DNTs).[41]

Im *et al.* prepared a hybrid system consisting of three films of gold nanoparticles and functionalized with five different conjugated polymer sensors array to detect organic vapors such as hexane, methanol, ethanol, toluene, and chloroform.[42]

Recently, Jeong *et al.* combined the tunable optical properties of conjugated polyelectrolytes with the specific binding characteristics of biomolecules to generate highly sensitive and selective sensing platforms for chemo- and biosensing applications.[43]

The high sensitivity and the biocompatibility of conjugated polyelectrolytes make them ideal candidates for sensing and for biological applications such as cell imaging. Their optical and electrical properties have also allowed them to be used in optoelectronic devices such as solar cells and light-emitting diodes.

1.7 Biocompatibility of conjugated polyelectrolyte

In vivo/vitro cell imaging and biological assays for advanced studying of biological systems relied heavily on spectroscopic approaches such as fluorescence microscopy, biosensors, versatile biological assays, and flow cytometry.[44]

However, these experimental approaches require materials with high absorptivity, high photostability, high sensitivity, high quantum yield, and low cytotoxicity.[45,44] As stated, earlier, QDs despite their unique photophysical properties, they show sever cytotoxicity towards cells and their fluorescence signal blinks.

Conjugated polymers exhibit several important characteristics where they have been considered as good fluorescent probes for biological imaging.[44]

Recent attempts were geared towards developing them into targeted fluorescent probes for cell imaging applications.[46] Moon and co-workers formulated an amine containing poly(p-phenylene ethynylene) (PPE) for imaging endothelial cells in a tissue model.[47] The particles showed good photostability and brightness with little to no cytotoxicity. The particles were also used to image various cells, including baby-hamster kidney (BHK) and BALB/C 3T3 (mouse embryonic fibroblast).[48] The conjugated polyelectrolytes showed good cell permeability and accumulates exclusively in the cytosol without any considerable inhibition of cell viability. Another similar report by Green *et al*. showed that CPEs are cell permeable with little to no cytotoxic effect.[49]

Moreover, Wang and co-workers designed amphiphilic lipid-modified cationic [poly(fluorenylene phenylene)(PFPL)] for cell imaging and transfection. Their system has two main features: the lipid, which serves as a side chain to provide the biocompatibility and to allow the entrance of the conjugated polymer to the cytoplasm, and the ammonium group, which interfaces with the gene to direct the PFPL for gene delivery. Cellular uptake of PFPL via endocytosis was observed which indicates that PFPL has little to no cytotoxicity. [45] Another example on the biocompatibility of conjugated polyelectrolytes for cell imaging application was reported by Wu *et al.*. PPE, PFPV, PFBT, and MEH-PPV conjugated polymer dots were used as fluid phase marker of pinocytosis in macrophages cells.[16] The images show that CP dots were successfully internalized by the cell and the fluorescent of the CP dots was observed in the cytoplasm, indicating that they crossed the cell membrane. CP dots showed no cytotoxicity under the loading concentration and the incubation time as well as they showed good stability in the cell growth medium.[16]

Thus, the biocompatibility of CPEs and their optoelectronic properties resulted in a great breakthrough in many biological and chemical applications.

1.8 Objectives:

Due to the wide range of applications of CPEs and the fact that they have a large extinction coefficient and high sensitivity, there is a pressing need to improve on their photophysical properties such as their photostability, brightness, and short lifetime.

Thus, in this work, we aim at improving the photophysical properties of the commercially available conjugated polyelectrolyte poly(5-methoxy-2-(3-sulfopropoxy)-1,4 phenylenevinylene) (MPS-PPV) by modifying the polymer microenvironment through complexing it with an amphiphilic polymer and by the means of metal enhanced phenomena through placing it in close proximity to conductive metallic nanoparticles.

CHAPTER 2

TUNING THE PHOTO-PHYSICAL PROPERTIES OF CONJUGATED POLYELECTROLYTES BY METAL ENHANCED FLUORESCENE

To answer the needs presented in the previous chapter, we aim in this project to enhance the photophysical properties of an anionic CPE by tuning its microenvironment. Placing it in close proximity to conductive metallic silver nano-particles enhances its emission intensity by a phenomenon known as metal enhanced fluorescence (MEF). Additionally, we aim at understanding the mechanism of the interaction between metallic nanoparticles and CPEs and the effect of different shapes and sizes of silver on this interaction. Our ultimate goal was to study the prepared structure at the ensemble and single molecular level.

2.1 Introduction:

Conjugated polymers attracted much of research interest and have been extensively studied due to their remarkable optical and electronic properties. They have been implemented in a great number of applications ranging from light emitting devices to chemical and biological sensing probes. However, these conjugated materials with π-conjugated backbone suffer from some limitations such as low quantum yield and low photostability. Therefore, great research efforts were employed to enhance their photo-physical properties and to modify their spectral properties. Conjugated polymers fluorescence has been enhanced using a variety of surfactants as detailed previously.

Another approach that opened a novel pathway in enhancing the optical and electronic properties of the fluorophore is the use of metallic nanoparticles, a phenomenon known as metal enhanced fluorescence.[50] The theory of fluorescence enhancement with metallic surfaces and particles dates back to 1911, when Selényi carried out the first experiment to examine the emission from a dye layer near an interface, i.e. a mirror.[51] [52] He observed a wide interference angle in the emitted fluorescence; this was attributed to the interference between the reflected rays from the interface and the direct rays from the dye layer.[51b] Investigating the behavior of fluorescent emitters above planar mirrors was continued by Drexhage and Kuhn in the 1960's.[52] Drexhage prepared and studied the photophysical properties of a single monolayer of cyanine dye molecules placed in a close proximity to the surface of silver using series of monolayers of fatty acid molecules .He found that the incident light interfered with the reflected light from the mirror to create a standing optical wave which is absorbed by the dye molecule and remitted as fluorescence. The intensity of fluorescence depends on its position to the standing wave field.[52-53] Despite the numerous works to unravel the mechanism by which the metallic surfaces influence the optical and the electronic properties of fluorescent molecules, it remains elusive.

This chapter will include the origination of (1) surface plasmonic resonance, (2) the effect of different size and shapes on the plasmonic resonance, (3) distance dependency of metallic nanoparticles on MEF phenomenon.

2.1.1 Surface Plasmon resonance (SPR)

Metal nanoparticles consist of a positively charged core and a cloud of mobile conduction electron on the surface. Upon illumination with electromagnetic radiation of wavelength larger than the particle size, the electromagnetic field induces coherent oscillation of surface electrons on nanoparticles which is known as surface plasmon resonance (SPR) (Figure 2.1). The electric field of the incoming radiation induces the formation of oscillating dipole in metal nanoparticles due to the movement of electrons between the positively charged core and the mobile electron cloud. This produces electromagnetic radiation in the far-field. The resonance condition is established when the frequency of incident photons matches the natural frequency of surface electrons oscillating against the restoring force of the positive nuclei.[54]

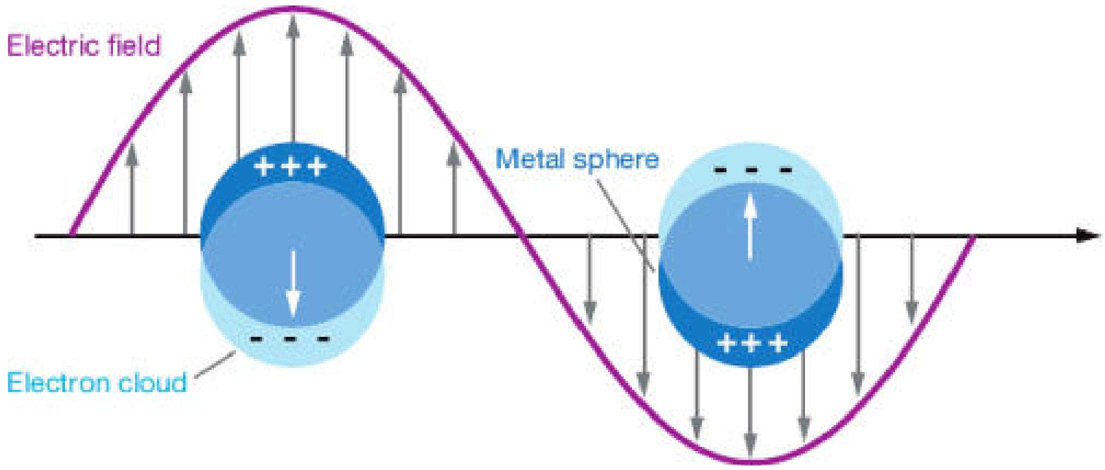

Figure 2.1: Surface Plasmon oscillation under the effect of electromagnetic field. (Reprinted with permission from Willets *et al.*).[54]

2.1.1.1 Size dependency of SPR

Nanoparticles are of special interest due to their unique set of properties especially their high surface-to-volume ratio which increases dramatically the number of surface atom, making these materials more reactive and more sensitive to the environment surrounding them. As it is shown in the Figure 2.2, when the dimension of the cube is lowered from 4 cm to 2 cm the surface area increases from 96 cm^2 to 192 cm^2, increasing the number of surface atoms.

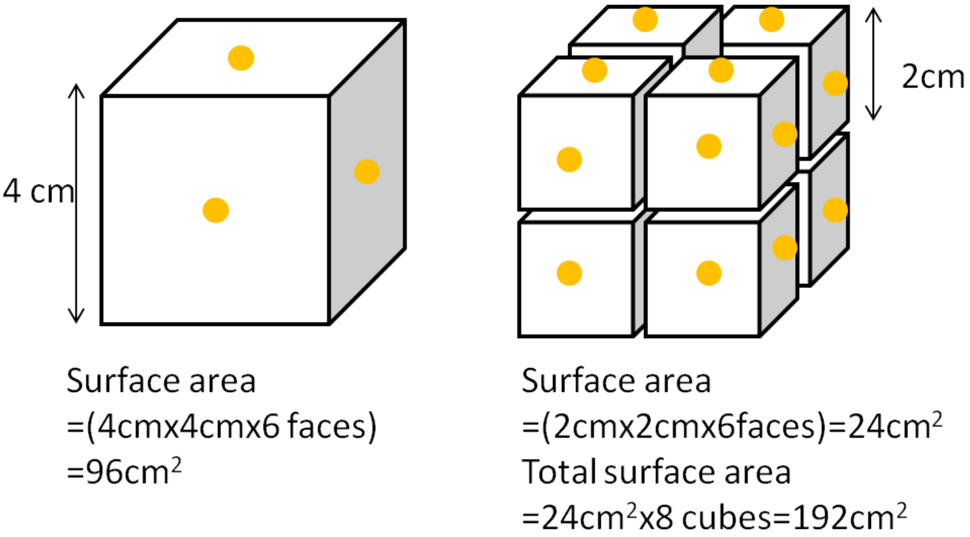

Figure 2.2: Schematically representing the increase in surface area and the number of exposed atoms upon changing the size of the particle.

The increase in the number of surface atoms might explain the changes in the electronic and optical properties as well as the oscillation frequency of nanoparticles upon a change in their size. The plasmon wavelength and the position of the absorption maximum are also influenced by the size and the shape of nanoparticles. Similar to an electron in a box, decreasing the dimension of the box will increase the energy separation between the adjacent levels. Reducing the size of nanoparticles will increase the energy level spacing between the completely filled valence band and the empty conduction band, blue shifting the position of the absorption maximum (Figure 2.3).[55]

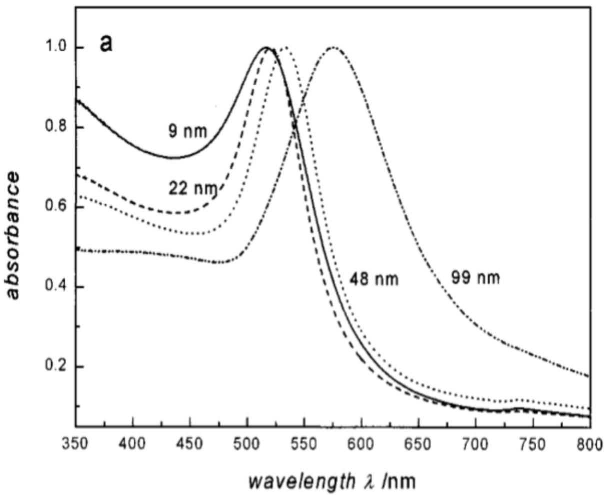

Figure 2.3: UV-Vis absorption spectra of 9, 22, 48, and 99 nm gold nanoparticles in water. All spectra are normalized at their absorption maxima, which are 517, 521, 533, and 575 nm, respectively. (Reprinted with permission from Link *et al.*).[55]

2.1.1.2 Shape dependency of SPR

The frequency and intensity of Plasmon resonance are determined by the dielectric properties of the metal, the dielectric constant of the medium, and the pattern of surface polarization. Changing the shape of the nanoparticles alters the surface polarization, which in turn changes the Plasmon resonance. Lu *et al.* have studied the effect of different shapes of silver nanoparticles of 40nm size on Localized Surface Plasmon Resonance (LSPR) (Figure 2.4).[56]

Increasing the corner sharpness and particles anisotropy shifts the dipole resonance peak to lower energy due to the accumulation of charges at the corner and to increased charge separation which lowers the restoring force of the oscillating electrons (as in cubic, tetrahedron and an octahedron shapes). It was also found that the intensity of the peak increases with the increase in particle symmetry (the case of triangular plate) as well that the number of peaks can be determined by the number of ways of nanostructure polarizing.[56,57]

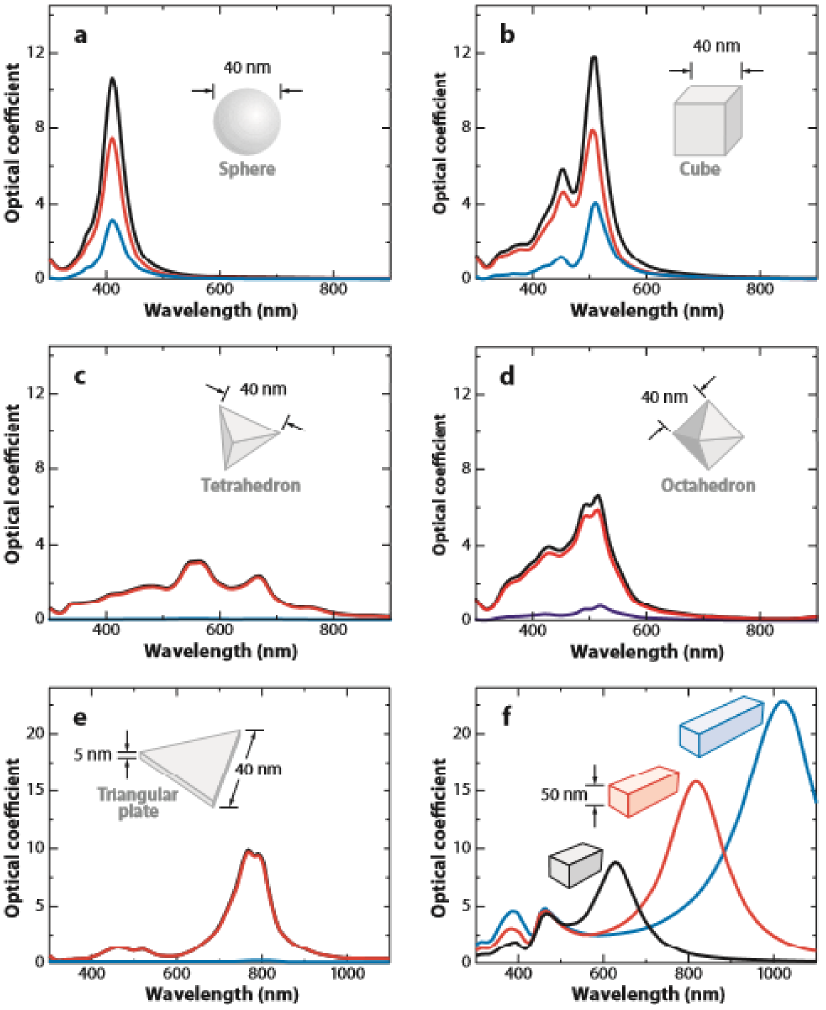

Figure 2.4: Extinction (black), absorption (red), and scattering (blue) spectra calculated for Ag nanoparticles of different shapes: (a) a sphere displaying a single dipole resonance peak and (b) a cube, (c) a tetrahedron, (d) an octahedron, and (e) a triangular plate. (f) Extinction spectra of rectangular bars with aspect ratios of 2(black), 3(red), and 4 (blue). (Reprinted With permission from Lu *et al*.).[56]

2.1.2 Metal enhanced fluorescence (MEF)

The radiative decay rate of the fluorophore can be increased or decreased with the presence of metal nanoparticles nearby. As illustrated in Figure 2.5, these effects can be described in terms of changes in the photonic mode density. Larger photonic mode density will provide more radiative decay pathways and larger radiative decay rate.[9,10]

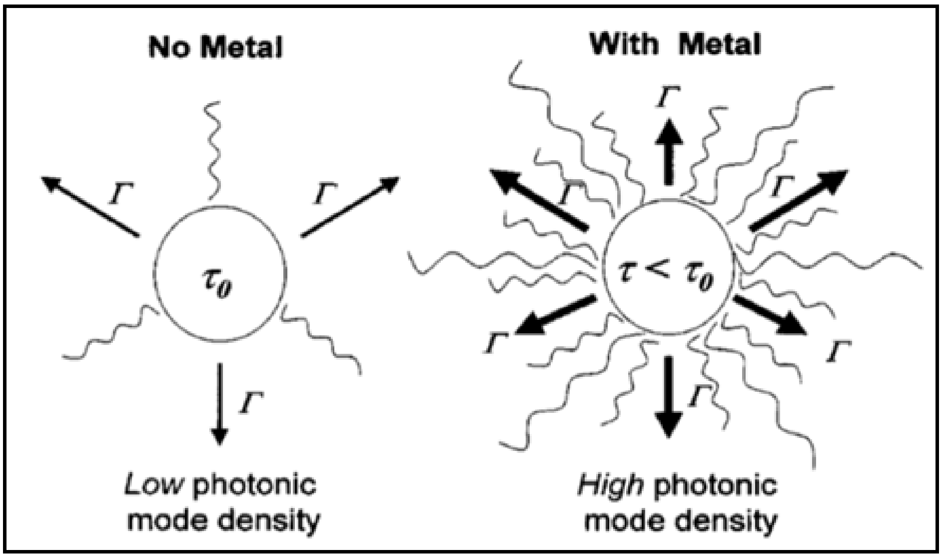

Figure 2.5: low and high photonic mode densities in the absence and presence of metal, respectively.(reprinted with permission from Geddes *et al.*).[10]

2.1.2.1 The mechanisms of fluorophore-metal nanoparticles interactions:

The mechanism by which the metallic NPs enhance the fluorescence is still controversial. In the absence of metallic nanoparticles, the fluorophore is characterized by three rates: the absorption rate, the radiative rate, and the non-radiative rate. In the presence of nanoparticles and upon light excitation the oscillation of electrons generates local electromagnetic field that changes the three characteristic rates of the fluorophore.[58]

Certain studies showed that the increase in the emission intensity is due to the enhancement of absorption rate as a result of increasing the local incident field by the metal on the fluorophore (E_m) which is known as “lightening rod effect”.[10] Other studies showed that the fluorescence enhancement is due to the increase of intrinsic radiative decay rate of the fluorophore (Γ_m).

However, metallic nanoparticles can enhance or quench the emission intensity of the fluorophore depending on the distance and the geometry of the metal; quenching is attributed to the energy transfer quenching (K_m) to the metal NPs which is distance dependent.[9,10]

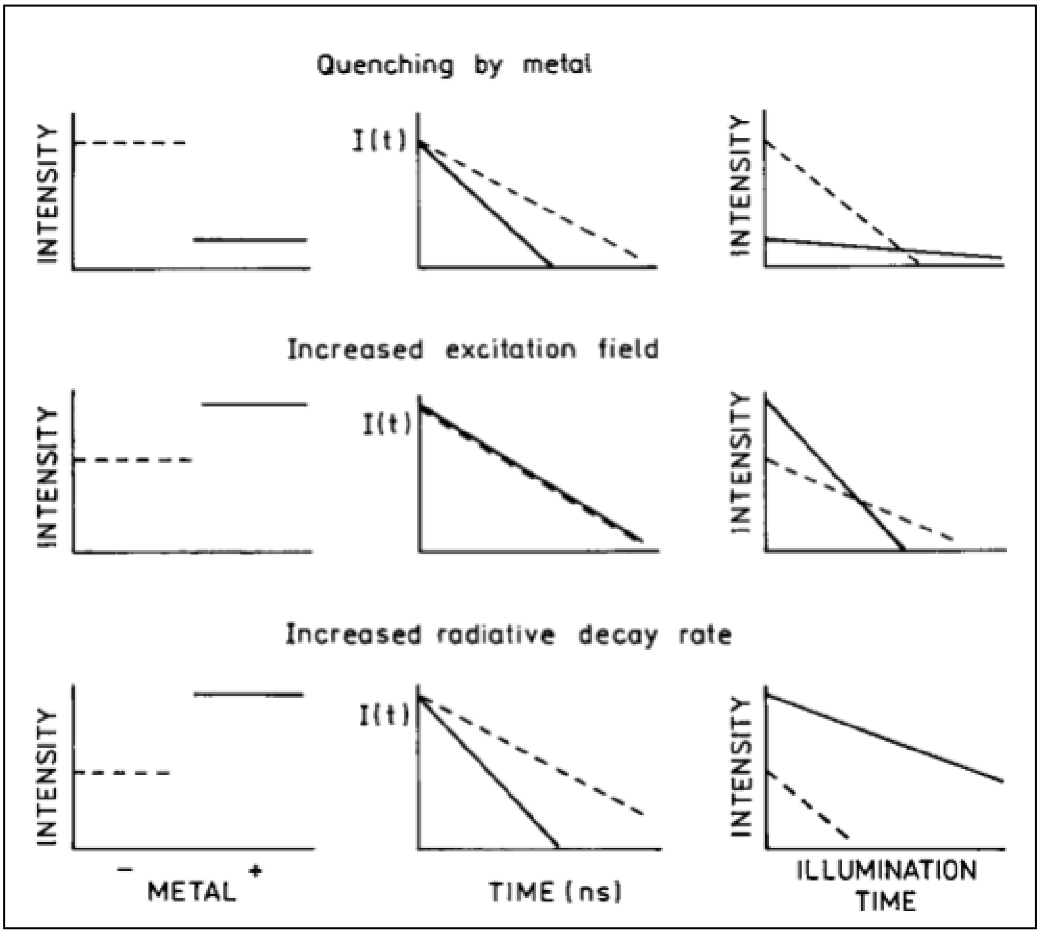

Figure 2.6: Effects of metal on the steady-state intensity, intensity decay, and photobleaching of a nearby fluorophore. From top to bottom the panels show quenching by the metal, the effect of an increased excitation field, and the effect of an increased radiative decay rate. The dashed lines indicate the absence of metal and the solid line indicates the presence of metal. (Reprinted with permission from Lakowicz *et al.*).[9]

The three mechanisms are summarized in Lakowicz's work (Figure 2.6). The top panels in Figure 2.6 show quenching in the emission intensity near the surface of the metal. The lifetime decrease enhances the photostability of the fluorophore and the quantum yield decreases which is defined as the number of emitted photons since the incident radiation is the same. (The number of emitted photons is equal to the integrated area for continuous illumination). The middle panels show the effect of concentrating the incident field by the metal, the fluorescence intensity increases, the lifetime remains the same, and the quantum yield is not affected much.

The lower panels show the effect of the increase of the radiative decay rate, the intensity increases, the lifetime decreases which will enhance the photostability, and the quantum yield increases dramatically. Thus based on this study the dominant mechanism is the increase of intrinsic radiative decay rate of the fluorophore (Γ_m).

To better understand the effect of metal NPs on the radiative decay rate of the fluorophore, we need to consider Jablonski diagram in the free space condition and with the presence of metallic nanoparticles.[9,10] The presence of a nearby metal (M) surface increases the radiative rate by the addition of a new rate Γ_m . In this case, the quantum yield (Q_m) and lifetime of the fluorophore (τ_m) near the metal surface would be given by:[9,10]

$$\phi_m = \frac{\Gamma+\Gamma_m}{\Gamma+\Gamma_m+k_{nr}} \qquad \textbf{Equation3.1}$$

$$\tau_m = \frac{1}{\Gamma+\Gamma_m+k_{nr}} \qquad \textbf{Equation3.2}$$

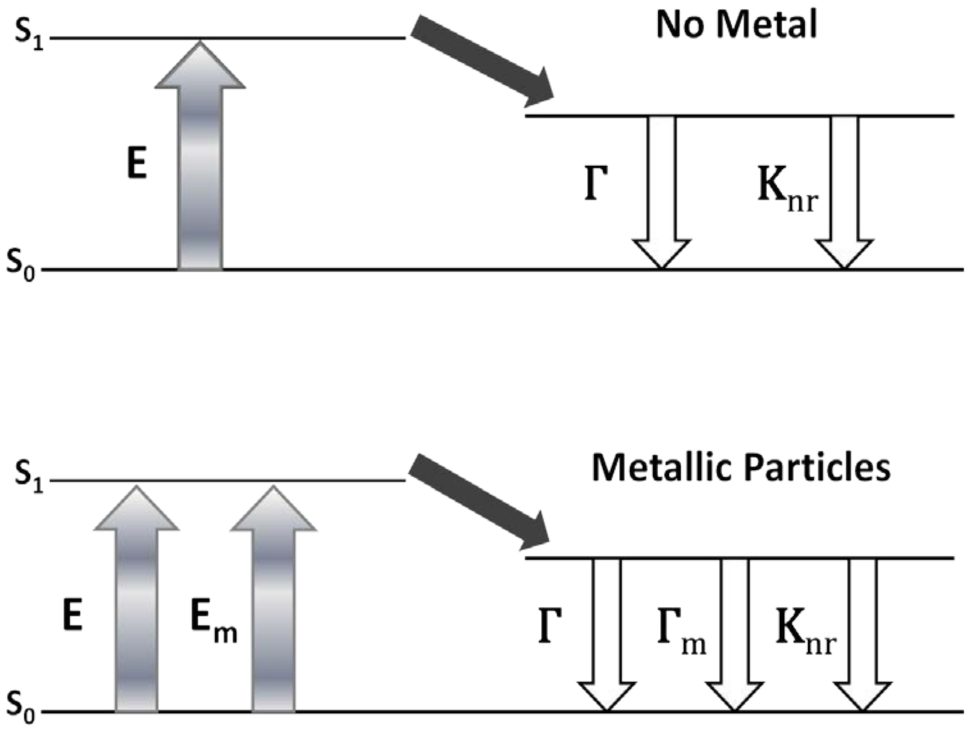

Figure 2.7: Classical Jablonski diagram for the free-space condition and the modified form in the presence of metallic particles, island or colloids. E-excitation, E_m-metal enhanced excitation rate, and Γ_m- radiative rate in the presence of metal.

2.1.2.2 The effect of metallic nanoparticles optical properties on the emission intensity of fluorophore

The optical properties of metallic colloids were first explained by Mie theory. According to Mie theory the extinction of metal nanoparticles is a combined effect of both absorbance and scattering. This theory shows that the absorption component of the extinction is due to the incident energy dissipation as heat which cannot radiate to the far filed, whereas the scattering component results from the far-field radiating plasmons.[55,59]

In 2004, Lakowicz *et al.* have reported that small colloids (<22nm) will result in quenching fluorescence rather than enhancement because the absorption components dominate the scattering component, while larger colloids are expected to enhance fluorescence because the scattering components dominate the absorption components.

Moreover, recent findings show that the overlap of multiple plasmons of nearby metal colloids even with small sizes would increase the intensity of the electromagnetic field in the overlapped region; this is known as plasmon coupling. A fluorophore trapped within a coupled plasmon its fluorescence can be enhanced due to two effects; it can feel the intensified electromagnetic field and have further increased probability for excitations, as well as radiate to the far field by coupling to the enhanced plasmon scattering. Therefore, metal-fluorophore aggregate can result in even greater fluorescence enhancements than single metal-fluorophore complexes and the metal particle size play a major role.[60]

2.1.2.3 Distance dependency of MEF

A study done by Sebastian Mackowski shows that the excitation rate and the quantum yield of the fluorophore depends on its distance to the metal nanoparticles. Figure 2.8 shows that increasing the distance between the fluorophore and the nanoparticles weaken the electromagnetic field felt by the fluorophore, which in turn exponentially decreases the excitation efficiency. However, the quantum yield starts to decrease when it reaches a distance shorter than 20nm due to a non-radiative energy transfer. Thus, the strongest Plasmon induced enhancement occurs for a distance between 10-30nm. At shorter distances the non-radiative energy transfer dominates and at longer distances the fluorophore barely feels the presence of metallic nanoparticles.[58]

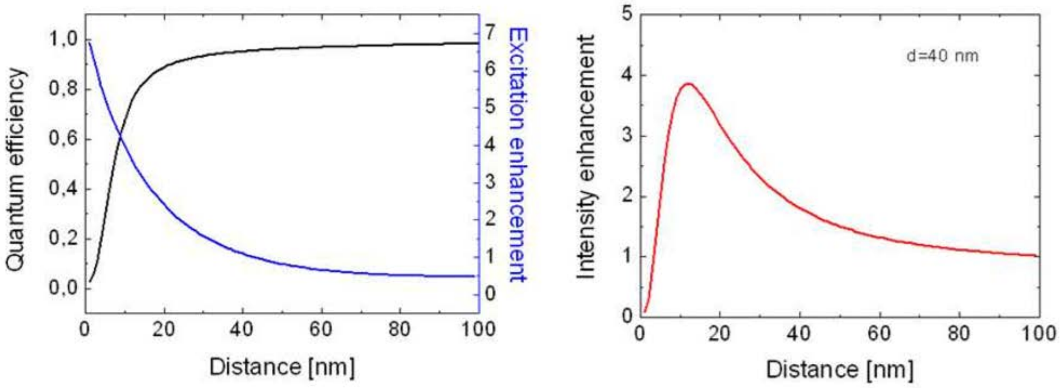

Figure 2.8: Dependence of the quantum yield and non-radiative fluorescence quenching upon the distance. Fluorescence intensity of a chromophore displayed as a function of the distance between the chromophore and spherical metallic nanoparticles with 40 nm diameter (Reprinted from Mackowski *et al*.).[61]

Based on what was presented earlier, we aimed to tune the photo-physical properties of conjugated polyelectrolyte by placing it near metal nanoparticles. In what follows, we present our research work which focus on (1) enhancing the photo-physical properties of conjugated polyelectrolyte (MPS-PPV) by placing it in a close proximity to a conductive surface of silver nanoparticles and (2) understanding the underlying mechanism of fluorescence enhancement at the single molecule level.

2.2 Experimental Section:

2.2.1 Materials:

The following were used in this study: poly[5-methoxy-2-(3-sulfopropoxy)-1,4-phenylenevinylene] potassium salt solution 0.25 wt. % in H_2O,MPS-PPV (Aldrich); Silver nitrate 99.9999% trace metals basis,$AgNO_3$ (Aldrich); Silver Nitrate meets analytical specification of Ph. Eur., BP, USP, 99.8-100.5% (Aldrich); Sodium citrate dehydrate ≥ 99%, $HOC(COONa)(CH_2COONa)_2.2H_2O$ (Aldrich); Glycerol,for molecular biology, ≥99.5% (Fisher BioReagents); Sodium borohydride granular, 99.99% trace metals basis, $NaBH_4$ (Aldrich); Tetraethyl orthosilicate reagent grade, 98%,$Si(OC_2H_5)_4$ (Aldrich);(3-Aminopropyl)trimethoxysilane97%,$H_2N(CH_2)_3Si(OCH_3)_3$ (Aldrich); Ammonium hydroxide, ACS reagent,28-30% solution in water ,NH_4OH (ACROS Organics); Sodium hydroxide puriss., meets analytical specification of Ph. Eur., BP, NF, E524, 98-100.5%, pellets, NaOH (Aldrich); 1,5-Pentanediol 96%, $OH(CH_2)_5OH$, (Aldrich); Copper(II) chloride, anhydrous Extra pure, 99%, $CuCl_2$ (ACROS); Potassium cyanide(KCN); Methylamine (CH_3NH_2); Ethanol (C_2H_5OH); Hydrochloric acid (HCl); Nitric acid (HNO3); Aqua-Regia (HNO_3:HCl 1:3 volume ratio) solution was used to clean glasswares for silver preparation; Double distilled water was used for cleaning; Deionized water (18µΩ-cm, Nanopure Diamond, CRSL, AUB) was used for solution preparations.

2.2.2 Preparation of silver nanoparticles of various sizes in 40% glycerol solution (Mono-dispersed method) (AgNPs)

2.2.2.1 Synthesis of silver nanoseeds

Silver nanoseeds were prepared using the Steinigeweg method. 50 mL of glycerol-water solution (40 vol% glycerol) was stirred in a 100 mL Erlenmeyer flask and heated to 95 °C. When the desired temperature was reached, 9 mg of $AgNO_3$ were added to the solvent followed by the addition of 1mL of 3% sodium citrate solution (1 minute later). The reaction mixture was stirred at 95°C for one hour. The prepared nanoseeds was then stored at 4°C.

2.2.2.2 Preparation of different sizes of silver nano-particles

AgNPs of different sizes were prepared by mixing138mL deionized water; 23 mL glycerol and 0.58 g of polyvinylpyrrolidone (PVP) together at room temperature in a 250 mL beaker. Different amounts of silver nanoseeds (30 nm) were then added as follows: 14.4 mL for 44.1 nm, 11.5 mL for 69.6 nm, 4.6 mL for 85.5 nm, and 2.6 mL for 98.4 nm. After 20 seconds, 290 µl of amine silver complex (20 mg silver nitrate in 1 mL water plus 220 µl ammonium hydroxide (30%) with 92 mL of 9.2 mg/92 mL ascorbic acid were added for 44.1 nm AgNPs. Whereas, 1.15 mL of amine silver complex (20 mg silver nitrate in 1 mL water plus 220 µl ammonium hydroxide (30%)) with 92 mL of 36.8 mg/92 mL ascorbic acid were added for 69.6 nm, 85.5 nm, and 98.4 nm.

The solutions were stirred at room temperature for one hour. After one hour, 6 g of PVP was added to the solution and the colloids were stored at 4 °C.

2.2.3 Preparation of nono-monodispersed silver nanoparticles free of glycerol

To 490 mL deionized water at 100 °C, 9 mg of $AgNO_3$ was added followed by dropwise addition of 10 mL 38.8 mM sodium citrate within 2 minutes. The reaction mixture was vigorously stirred for 1 hour. After which the reaction was allowed to cool to room temperature and the obtained silver colloids were stored at 4°C.

2.2.4 Preparation of cubic silver nanoparticles

2.2.4.1 Precursor preparation

Precursor A: 0.8 g of $CuCl_2$ was dissolved in 10 mL 1,5-pentadiol by sonication and vortexing at 10 minutes intervals.

Precursor B: 0.2 g of 29 K Mw PVP was suspended in 10 mL 1,5-pentadiol, vortexed and sonicated for another 30 minutes, the solution vortexed and sonicated every 10 minutes after the initial vortexing.

Precursor C: 120 mM $AgNO_3$ was prepared by suspending 0.2 g of $AgNO_3$ and 20 µl of precursor A in10 mL 1,5-pentadiol, the solution was sonicated for 60 minutes and vortexed every 10 min during sonication.

1 mL of the prepared precursor C was placed in ice-bath for 10 minutes.

2.2.4.2 Silver nano-cubes preparation

In 100 mL round bottom flask, 20 mL of 1,5-pentadiol was stirred and heated to 190 °C for 10 minutes, 500 µl of the cold precursor C was added to the solution followed by drop wise injection of 250 µl precursor B. 10 mL of room temperature precursor C was added by injecting 500 µl of the precursor C every minutes and injecting 250 µl of precursor B every 30 seconds. When finished adding the precursor solutions, the color changed to creamy green, the solution kept for additional 5 minutes at 190 °C and then allowed to cool to room temperature.

2.2.4.3 Silver nano-cubic octahedral preparation

Precursor D: 0.4 g of $AgNO_3$ was suspended in 10 mL 1,5-pentadiol with 40 µl of precursor A.

Silver cubic octahedral nanoparticles were prepared by placing the previously prepared silver cubic nanoparticles (**section 2.4.2**) in 100 mL round bottom flask and heating the solution at 190 °C. followed by the addition of precursor D and precursor B in the same way used to prepare silver nanocubes (**section 2.4.2**).When finished adding the precursor solutions to the cubic nanoparticles solution, the reaction allowed to proceed for additional 20-25 minutes at 190 °C and the reaction stopped when the color changed from creamy green to creamy yellow.

2.2.5 Coating silver nanoparticles (AgNPs) with different thicknesses of thin silica layer (SiO_2)

Silver nanoparticles were coated with a thin silica shell following a modified stöber method:

200 mL ethanol and 50 mL of silver nanoparticles were placed in 500 mL Erlenmeyer flask, followed by the addition of 4.3 mL ammonium hydroxide (NH_4OH).

Different amount of 10 mM of Tetraethylorthosilicate (TEOS) prepared in ethanol (2.5 mL, 5 mL, 10 mL, or 15 mL) were then added at a rate of addition of 2.5 mL/hour using a syringe pump. The reaction mixture was gently stirred at 500 rpm for 24 hours.

2.2.6 Modifying the surface of silica with APTS (3-Aminopropyl)trimethoxy silane)

5 mL of AgNPs-SiO_2 solution was centrifuged at 10000 rpm, re-suspended in 2 mL DI-water and added to 8 mL ethanol, various amount of ATPS (50 µl, 1 mL, 1.5 mL, and 2 mL) was then added to the solution. The mixture was stirred for one hour and then centrifuged at 10000 rpm and washed with DI-water.

2.2.7 Dissolution of AgNPs from SiO_2 core shell

20 μl of 1M KCN solution is added to 1 mL AgNPs-SiO_2-APTS solution, the solution is stirred for 1 hr to ensure the total dissolution of Ag from the core shell; the yellow color disappears immediately after adding KCN solution.

2.2.8 Absorption and emission measurement

Steady-state fluorescence spectroscopic measurement was carried out using a JASCO, V-570 UV/VIS/NIR Spectrophotometer. Absorption spectra were recorded using JASCO, V-570 UV/VIS/NIR Spectrophotometer in double-beam mode. For all steady-state absorption and emission experiments, the solutions were placed in 1 cm x 1 cm quartz cuvettes.

For emission experiment the total volume of the solution was kept constant with a quantity equal to 3 mL.

The blank solution: consist of 1480 μl of ethanol, 1480 μl of water, and 40 μl of MPS-PPV

The analyzed solution: consist of 1000 μl ethanol, 1000 μl water, 40 μl MPSPPV, and 960 μl analyte

Our measurements took place under the following conditions:
Excitation wavelength= 450nm, excitation slit=5nm, emission wave length from 470nm to 650nm, and emission slit=10nm.

2.3 Results and discussion

We chose silver nanoparticles as the metal of choice. First, they exhibit the highest plasmon excitation efficiency among other metals thus inducing the highest metal enhanced fluorescence.[62] Second, the plasmon resonance of silver can be tuned to any wavelength in the visible region simply by preparing different sizes or shapes of silver nanoparticles. This allows tuning the plasmon resonance of silver nanoparticles to 450nm which overlaps with the absorption maximum of the anionic conjugated polyelectrolyte of interest to us (MPS-PPV; Figure 2.9, Figure 2.10) and hence enhance the local incident field and maximize the spectral overlap with the absorbance spectrum of poly[5-methoxy-2-(3-sulfopropoxy)-1,4phenylenevinylene MPS-PPV.[62,63] Chen *et al.* demonstrated the importance of spectral overlap between the plasmonic resonance of the nanoparticles and the fluorescence intensity.[63] They have used 3 fluorescent dyes (Alexa Fluor 488, Alexa fluor 532, and Rhodamine Red) attached at a fixed distance from single silver nanoprism using DNA as biological linker. They have reported that the maximum fluorescence from Alexa Fluor 488, Alexa 532, and Rhodamine Red were observed when coupled to silver nanoparticles with LSPR at ~505nm, ~525nm, and ~570nm respectively.[63] As a result, the brightest fluorescent for the three dyes is observed when they are attached to nanoparticles with localized surface plasmon resonance (LSPR) that matches their absorption maximum or with LSPR peak between their absorption and emission maxima.[63]

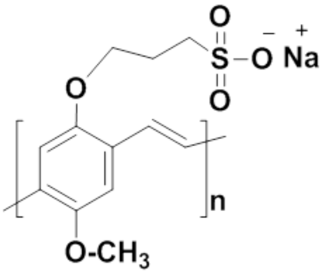

Figure 2.9: Chemical structure of poly[5-methoxy-2-(3-sulfopropoxy)-1,4-phenylenevinylene (MPS-PPV).

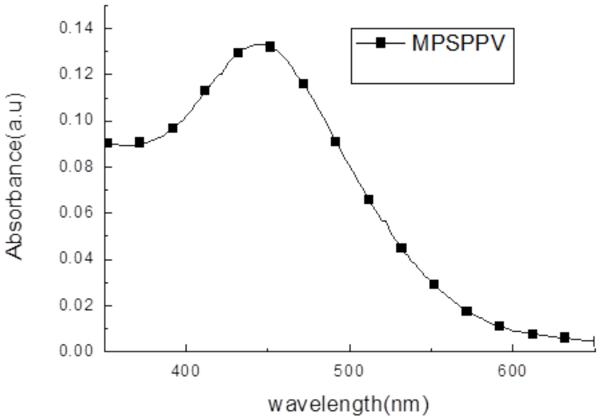

Figure 2.10: UV-Vis absorbance spectrum of MPS-PPV in DI-water

The strength of the electromagnetic field and the position of the plasmons depend also on the size and the shape of the metal. Increasing the size of the nanoparticles shifts the plasmonic resonance to the red region with scattering component dominates over the absorption component, and hence enhances the fluorescence. In addition, silver nanoparticles with sharp edges will have stronger electromagnetic field compared to smooth surfaces due to the accumulation of charges at the edges of the nanostructure and hence will have a larger LSPR.[55,57,56]

To search for the best overlap between the absorption maximum of MPS-PPV and the plasmonic resonance of silver nanoparticles we prepared different sizes (30nm, 44.1nm, 69.6nm, 85.5nm, and 98.4nm) and shapes (spherical, and cubic octahedral) of silver nanoparticles.

Silver nanoparticles of various sizes and shapes were synthesized by the reduction of a silver salt ($AgNO_3$) to form colloidal silver. There is a number of different techniques to synthesize Ag NPs. For our study, silver nanospheres were synthesized by two different methods; the first method is the monodispersed method introduced by Steinigeweg *et al.*, in this method the monodispersed silver nanoparticles are prepared by the reduction of $AgNO_3$ with trisodium citrate dihydrate at high temperature in aqueous solution containing 40% glycerol. The silver nanoparticles prepared by Steinigeweg *et al.* method were used as seeds to mediate the synthesis of different sizes of silver nanoparticles.[64]

The second method was introduced by Turkevich *et al*; in this method silver nanoparticles were prepared by reducing silver nitrate with the mild reducing agent sodium citrate.[65]

As we mentioned earlier in the introduction, the distance between the metal and the fluorophore is very crucial in metal enhancement fluorescence. A fluorophore placed at a very short distance to the metal undergoes a non radiative energy transfer resulting in quenching its fluorescence intensity. Whereas a fluorophore placed at a long distance from the metal barely feels the electromagnetic effect of the nanoparticles. Therefore, to achieve the highest metal enhanced fluorescence effect and to optimize the distance between the particles and the fluorophore, silver nanoparticles were coated with SiO_2 layer which serve as a spacer shell between the fluorophore and the metallic nanoparticles.[58] Different SiO_2 thicknesses were prepared to optimize the distance between the metal and the fluorophore so that the MPS-PPV will experience the near field Plasmon of AgNPs.

Silver nanoparticles were coated with SiO_2 by following modified Stöber method. An amorphous layer of SiO_2 is deposited on the surface of AgNPs by hydrolysis/condensation reaction of tetraethylorthosilicate (TEOS) in the presence of a base, ammonia, to catalyze the hydrolysis step.[66]

In what follows, we will summarize our findings and discuss our results in terms of fluorescence enhancement of conjugated polyelectrolytes.

2.3.1 Synthesis and characterization of AgNPs with different sizes and shapes:

We prepared monodispersed silver nanoparticles to rule out any MEF shape and size effect. Monodispersed silver nanoparticles were prepared by reducing silver nitrate with sodium citrate in 40% glycerol-water solution. The highly viscous glycerol increases the monodispersity by decreasing the reduction and/or nucleation speed. As seen in Figure 2.11, the maximum absorption peak of the prepared Ag nanoseeds is at 411 nm with full width at half maximum (FWHM) of 77 ± 0.59, calculated using the single fitting peak function in origin. The relatively small FWHM value reflects the monodispersity of the prepared silver colloids. The absorption maximum is however short from our 450nm target.[64]

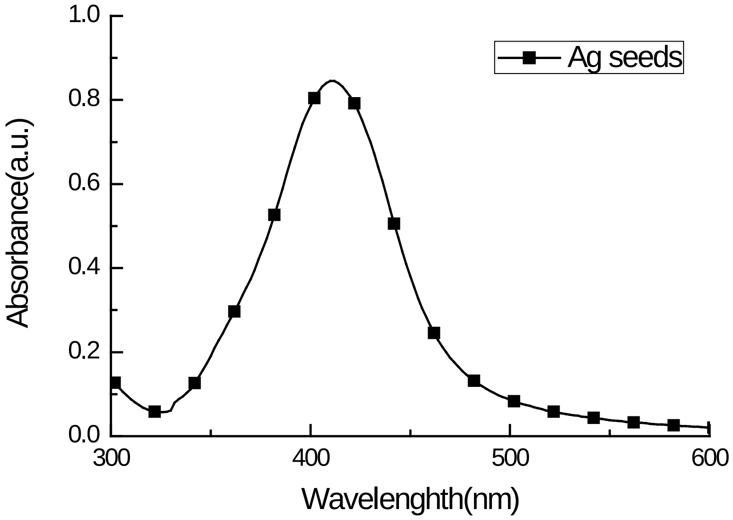

Figure 2.11: Absorption spectrum of Ag nanoseeds with an average size 30nm prepared in glycerol/water solution.

Given that increasing the particle size shifts the maximum absorption to the red region, we prepared different sizes of AgNPs (44.1 nm, 69.6 nm, 85.5 nm, and 98.4 nm) by using Steinigeweg *et al.* method. The particles were prepared by mixing different amount of Ag-nanoseeds with silver diamine complex (Ag $(NH_3)_2)^+$ followed by the addition of ascorbic acid as a mild reducing agent. To stabilize the big nanoparticles, PVP was added at the final step.[64]

As it is shown in Figure 2.12, the absorption maximum of the prepared particles red shifts as the size of AgNPs increases. Indeed, AgNPs with an average size of 44.1 nm have a absorption maximum at 435 nm, whereas NPs with an average size of 98.4 nm have two maxima at 420 nm and 525 nm. These results also show that with increasing the particle size the monodispersity decreases, evident by the FWHM and the appearance of a new peak.[64] The absorption maximum and the FWHM of the prepared nanoparticles are summarized in the Table 2.1.

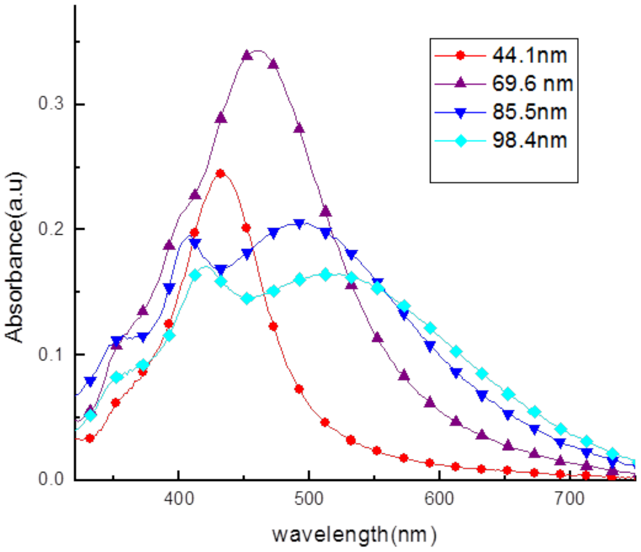

Figure 2.12: Absorption spectra of AgNPs with average sizes 44.1 nm (●), 69.6 nm (▲), 85.5 nm (▼), and 98.4 nm (◆) nm in glycerol/water solution.

Table 2.1: Absorption maximum and the full width at high maximum (FWHM) for silver nanoparticles of different sizes.

Ag-nanoparticles	Absorption maximum	FWHM
44.1nm NPs	435nm	93 ± 1.28
69.6nm NPs	460nm	147 ± 1.34
85.5nm NPs	408nm and 497nm	257 ± 3.23
98.4nm NPs	420nm and 525nm	290 ± 4.88

Plasmon resonance is not only dependent on the size of metallic nanoparticles and the distance between the metal and the fluorophore, but also on the geometry of the nanoparticles. As mentioned in the introduction, nanoparticles with sharp corners have a higher localized plasmonic resonance. We were interested in exploring the fundamental photophysics of different shapes on enhancing the fluorescence intensity of MPS-PPV at both ensemble and molecular levels. We synthesized cubic octahedron silver nanoparticles following a method introduced by Tao *et al.* In this method cubic nanoparticles were used as nanoseeds for cubic octahedral synthesis. First, Cubic nanoparticles were prepared in 1,5-pentadiol solution by using silver nitrate and copper chloride mixed together as the first precursor and PVP as a second precursor. The two precursors were then injected simultaneously every 30 second to a hot 1,5-pentadiol (190 ˚C) solution. Second, cubic octahedron was prepared following the same procedure as the cubic but with cubic nanoparticles as seeds but at longer time (120 min). The obtained particles were characterized with UV-Vis spectrophotometer and SEM.[67]

Figure 2.13 shows SEM images for perfect cubic octahedron geometry with a small portion of rods. The obtained absorption spectrum of cubic octahedron nanoparticles shows similar features to the one reported by Tao *et al.* where we got 2 peaks one between 350 nm-600 nm and another one at 800 nm (Figure 2.14).[67] Tao *et al.* have reported that the appearance of several peaks is due to several localized surface Plasmon modes. The peaks between 350 nm-600 nm are due to higher order mode which is the hexapolar localized surface Plasmon modes at the corners and the edges of the cubic octahedron. Whereas the resonance at 800 nm is due to the quadrupolar localized surface Plasmon modes.[67]

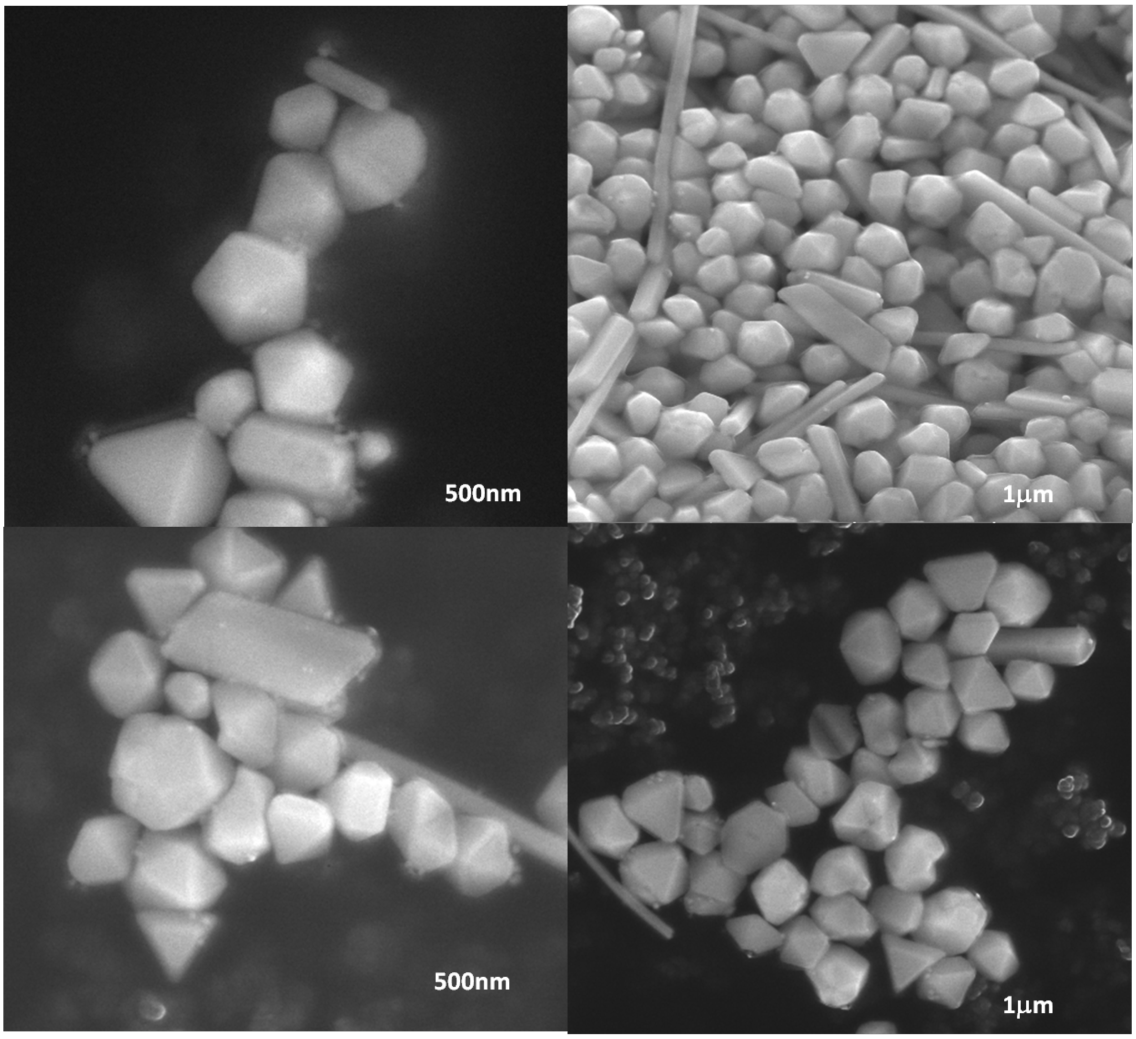

Figure 2.13: SEM images of cubic octahedron silver nanoparticles prepared by mixing silver nitrate cobalt chloride and PVP in hot 1,5-pentadiol solution.

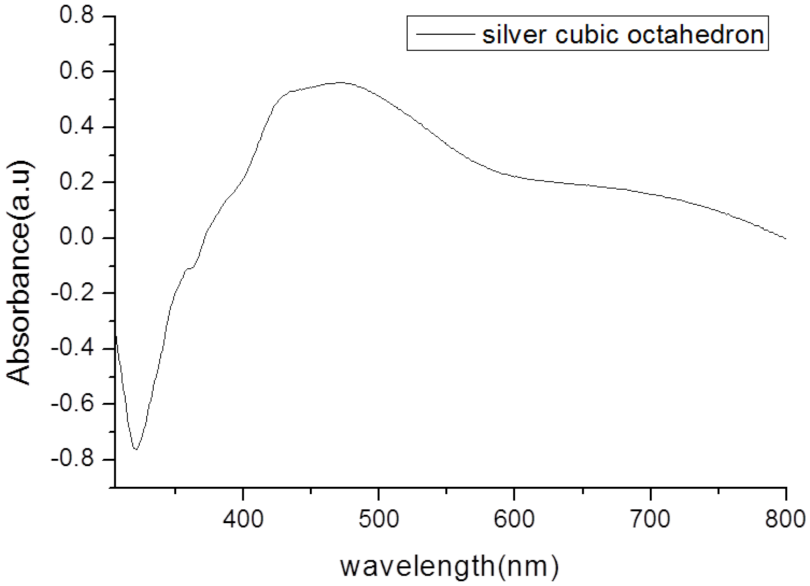

Figure 2.14: Absorption spectrum of cubic octahedron silver nanoparticles with absorption maximum at 463.5 nm prepared by mixing silver nitrate cobalt chloride and PVP in hot 1,5-pentadiol solution.

So far we have successfully prepared silver nanoparticles with different sizes and shapes. In the next section, we will study the effect of silver nanoparticles on the emission intensity of MPS-PPV. We decided to first focus on the spherical silver nanoparticles since it is the simplest system. AgNPs with an average size 44.1 nm and absorption maximum of 435 nm were selected to study their effect on the emission intensity of MPS-PPV since they have the best overlap with the absorption maximum of MPS-PPV (438 nm-451 nm).

2.3.2 Studying the effect of monodispersed AgNPs on the emission intensity of MPS-PPV:

We studied the effect of the prepared silver nanoparticles on MPS-PPV before coating them with SiO_2. AgNPs with an average size 44.1 nm were centrifuged at 9000 rpm and resuspended in DI-water. The resuspended particles were then added to a solution of DI-water containing 40 μl of MPS-PPV and the emission intensity was then recorded. As it is shown in Figure 2.15, the emission intensity of MPS-PPV was increased by 4.25 folds contrary to the expected quenching in the emission intensity of fluorophore by a non-radiative energy transfer mechanism due to the short distance to the silver nanoparticles. We hypothesize that the enhancement might be due to the spacing introduced by the nanoparticle capping agent. To ensure that the enhancement is due to MEF effect, we did a control experiment where 20 μl of 1M KCN were added to a 1 mL AgNPs solution to etch the Ag core. The samples was centrifuged and resuspended in 1 mL DI-water. The particles were added to a solution of DI-water containing 40 μl of MPS-PPV and the emission intensity was then recorded: 5.3 folds enhancement was obtained (Figure 2.15).

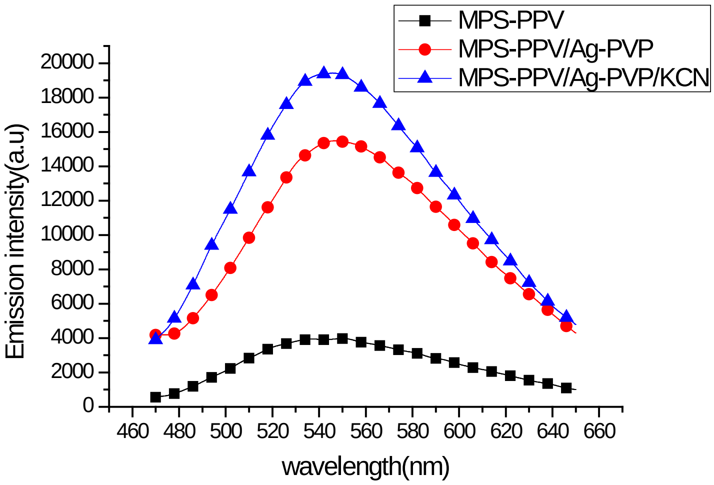

Figure 2.15: Fluorescence emission of MPS-PPV (■) MPS-PPV doped with AgNPs of an average size 44.1 nm (●), and MPS-PPV doped with AgNPs/KCN (▲) in DI-water containing 40 µl MPSPPV. The solutions were excited at 450nm and emission intensities were collected between 470 nm and 650 nm.

Based on the control experiment, we can conclude that the silver nanoparticles did not contribute to the fluorescence enhancement of MPS-PPV. The slight relative increase in the fluorescence after the silver core degradation is due to the disappearance of non radiative energy transfer at a short distance to the silver nanoparticles.

To investigate the source of the fluorescence enhancement, we added polyvinylpyrrolidone (PVP), the surfactant used as capping agent in the silver nanoparticles synthesis, to a solution of MPS-PPV. The fluorescence emission was enhanced by ~ 20 folds (Figure 2.16). This came as a surprise to us since many previously reported metal enhanced fluorescence based on silver nanoparticles have utilized PVP as a capping agent.[68] For instance, Liang *et al*, have used silver nanocube coated with 6mL of 147mM PVP as stabilizing agent. Multilayers of PDDA and PSS polyelectrolytes were used a as a spacer to enhance the fluorescence intensity of the cationic conjugated polyelectrolyte poly [9,9-bis(6'-(N,N,N-trimethylammonium) hexyl)-fluorenyldivinylene-alt-4,7-(2,1,3-benzothiadiazole)dibromide](PFVBT).[68] They have reported that fluorescence intensity of PFVBT was enhanced greatly (by ~ 10 folds) by silver nanocubes.[68] Consequently, we decided to focus on silver nanoparticles lacking PVP. The seed nanoparticles with an average diameter of 30 nm and absorption maximum of 411 nm were next tested for their lack of PVP.

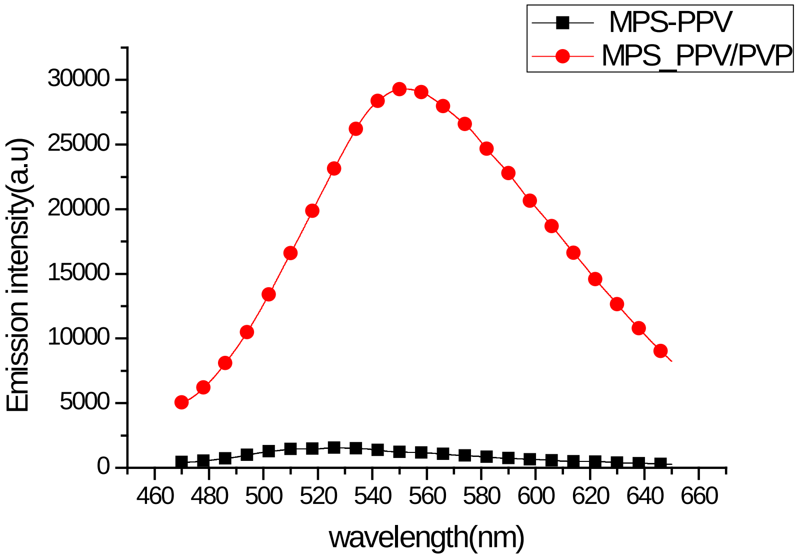

Figure 2.16: Emission intensity of 40 μl MPS-PPV (■) and MPS-PPV with 55K polyvinylpyrrolidone (PVP) (●) upon excitation at 450nm in 10 mM HEPES buffer pH=7.3 and 150 mM NaCl.

The AgNPs were coated with thin silica spacer to protect the conjugated polyelectrolyte from collisional quenching due to the non-radiative energy transfer. Following modified Stöber method, the prepared nanoparticles were purified by centrifugation at 10000rpm and mixed with ethanol followed by the addition of ammonia with different amount of 10mM Tetraethylorthosilicate TEOS. SiO_2 spacer shell was grown on AgNPs first by the hydrolysis of TEOS into $Si(OH)_4$ and then the condensation of $Si(OH)_4$ into SiO_2 in ethanol-water solution. The formation mechanism of SiO_2 is represented in the Figure 2.17 and Figure 2.18 illustrates the coating of AgNPs with SiO_2.[69]

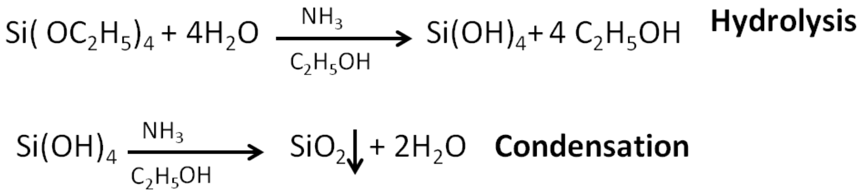

$$Si(OC_2H_5)_4 + 4H_2O \xrightarrow[C_2H_5OH]{NH_3} Si(OH)_4 + 4\ C_2H_5OH \quad \textbf{Hydrolysis}$$

$$Si(OH)_4 \xrightarrow[C_2H_5OH]{NH_3} SiO_2\downarrow + 2H_2O \quad \textbf{Condensation}$$

Figure 2.17: Particle formation and growth mechanism of silica shell in ethanol-DI water solution.

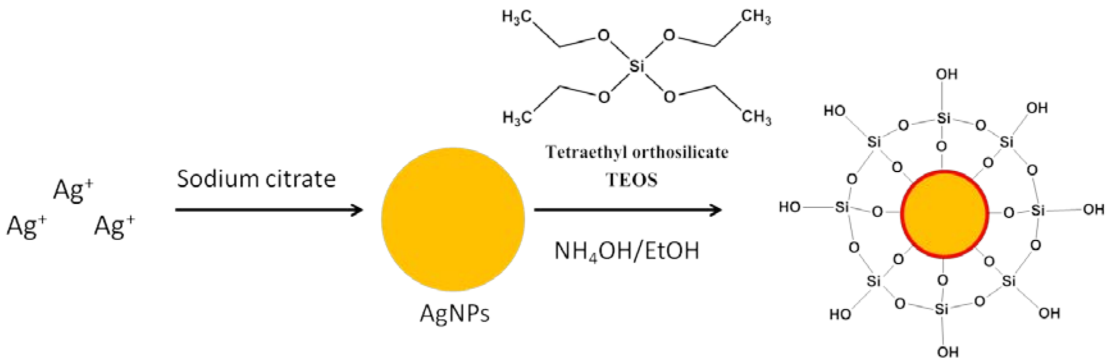

Figure 2.18: Simplified scheme of coating silver nanoparticles with SiO_2.

After coating the silver nanoparticles with SiO_2 using 400 µl of 10mM TEOS, the absorbance spectrum of the obtained AgNPs-SiO_2 was measured and transmission electron microscopy (TEM) images were acquired for AgNPs coated with SiO_2 to determine the exact size of the prepared nanoparticles and the exact thickness of SiO_2 shell.

Figure 2.19 Shows the absorption spectra of AgNPs and AgNPs coated with SiO_2. The absorption maximum shifted by 15nm to the red region upon coating the particles with SiO_2. The TEM images show that the prepared silver nanoseeds are monodispersed and uniformly coated with SiO_2 shell Figure 2.20**.**

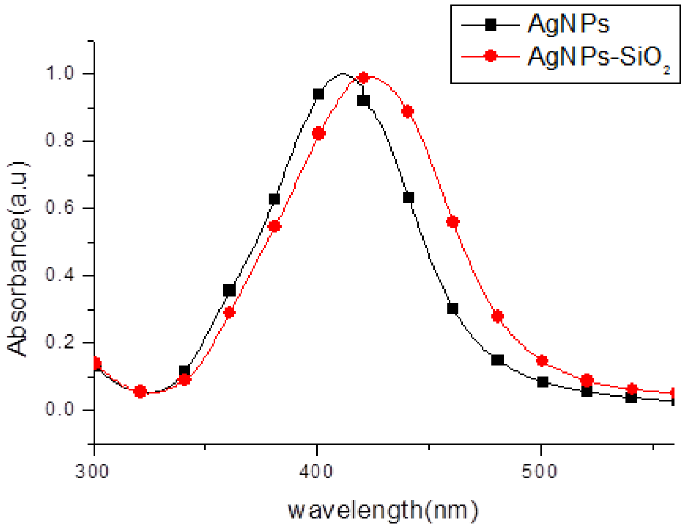

Figure 2.19: Absorption spectrum of AgNPs with an average size 30 nm (■) and the absorption spectrum of AgNPs coated with 400 µl 10mM TEOS (●).

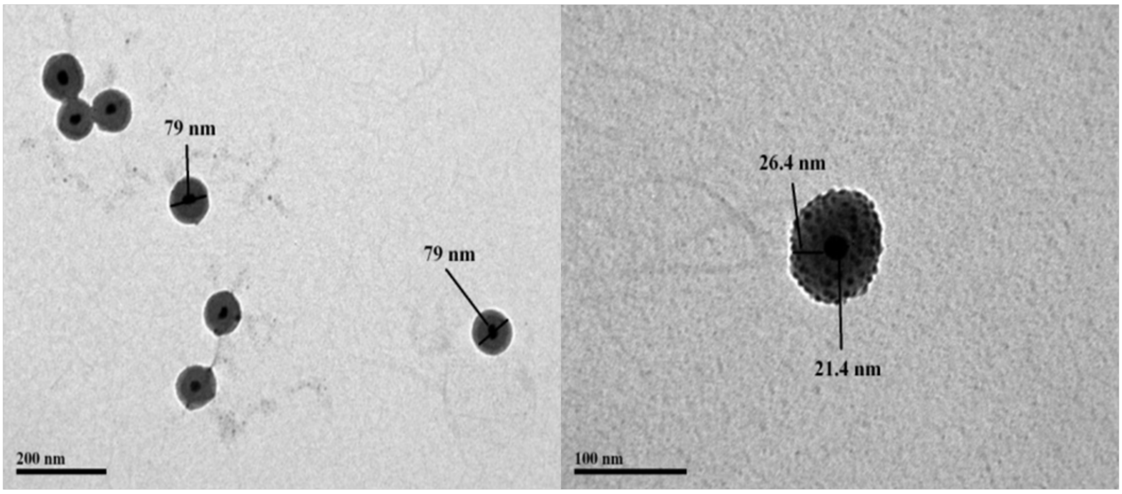

Figure 2.20: TEM images of Ag nanoseeds coated with SiO_2 shell spacer using modified stober method with 400 µl of 10mM TEOS in ethanol-water solution.

Up to this point, we have prepared monodispersed nanoparticles uniformly coated with SiO_2 thin shell. In the next section, we will study the effect of the obtained AgNPs coated with silica on the emission spectrum of MPS-PPV.

The isolated silanol groups deposited on the surface of AgNPs have a pKa value of 4.9.[70] To minimize the negative surface charges and potential repulsion interaction between the silver nanoparticles and the anionic conjugated polyelectrolyte (MPS-PPV), we performed our experiments at pH=5.[71] As it is shown in Figure 2.21, a quenching in the emission intensity of MPS-PPV was obtained upon adding AgNPs coated with SiO_2 to a solution of acetic acid at pH=5 containing 40 µl MPS-PPV. Figure 2.22shows the emission intensity of MPS-PPV in presence of silica where quenching was also obtained. The quenching could be due to the formation of aggregated MPS-PPV on the surface of SiO_2, which in turn will increase the possibility of trapping the exciton in the non-emissive trapping sites.

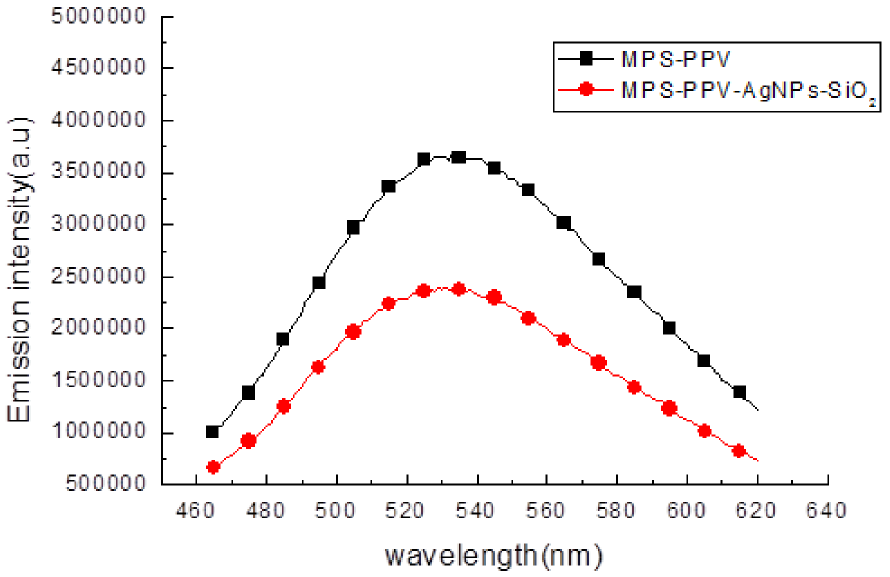

Figure 2.21: Fluorescence emission of MPS-PPV MPS-PPV (■) and MPS-PPV doped with AgNPs-SiO_2 (●) in acetic acid solution containing 40µl MPSPPV at pH=5. The solutions were excited at 450 nm and emission intensities were collected between 470 nm and 650 nm.

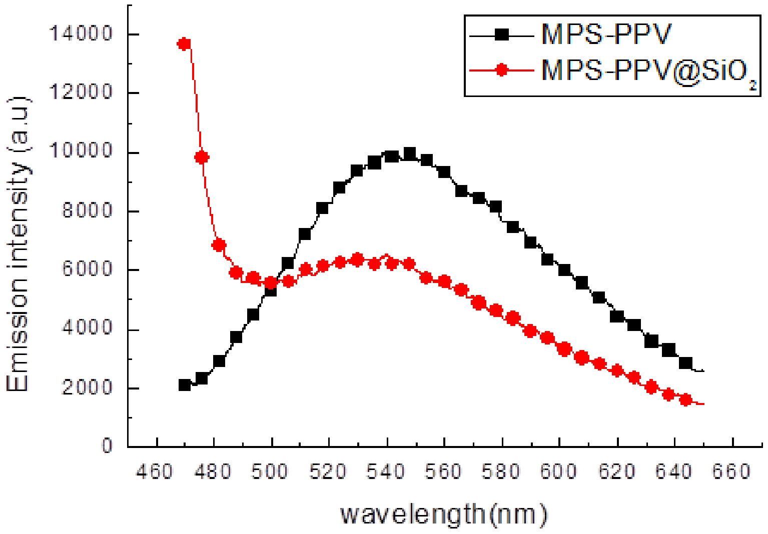

Figure 2.22: Fluorescence emission of MPS-PPV (■) and MPS-PPV doped with SiO_2 (●) in acetic acid solution containing 40 µl MPSPPV at pH=5. The solutions were excited at 450 nm and emission intensities were collected between 470nm and 650nm.

In order to increase the electrostatic attraction between the anionic MPS-PPV and AgNPs, SiO_2 surface was modified with 3-aminopropyltrimethoxysilane (APTS) to functionalize the surface with primary amine. Primary amine has a pKa value of 9.2 which at neutral pH renders the SiO_2 surface positively charged, and thus maximizing the attraction between AgNPs and MPS-PPV.[69] Figure 2.23 illustrates the modification of silica surface with APTS.[69]

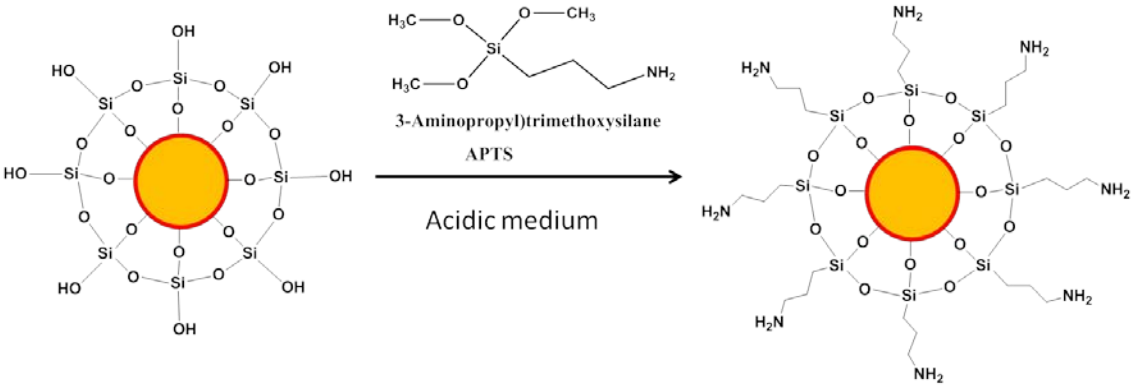

Figure 2.23: Scheme illustrates the modification of silica surface with APTS to functionalize it with primary amine which become positively charged under acidic conditions.

TEM images show the size of AgNPs and the thickness of SiO_2 shell allowing us to calculate the exact amount of APTS needed to modify the surface of SiO_2.

AgNPs coated with SiO_2 (400µl of 10mM TEOS) were modified with 1µl of APTS. The fluorescence intensity of MPS-PPV doped with the prepared AgNPs-SiO_2-APTS was measured (Figure 2.24).

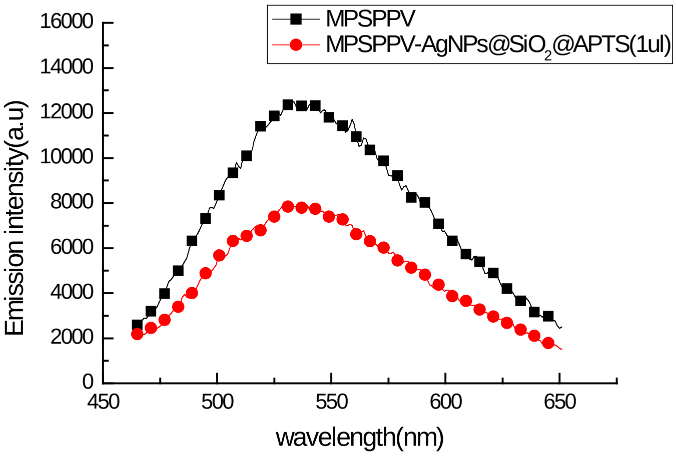

Figure 2.24: Fluorescence emission of MPS-PPV (■) and MPS-PPV doped with AgNPs-SiO_2-APTS (1 µl) (●) in acetic acid solution containing 40 µl MPSPPV at pH=5. The solutions were excited at 450nm and emission intensities were collected between 470 nm and 650 nm.

As it is shown in Figure 2.24, the prepared silver nanoparticles coated with 10 mM TEOS and modified with 1 μl APTS induced quenching instead of enhancement on the emission intensity of MPS-PPV which could be due the small size of the prepared nanoparticles. The TEM images show that the average size of the prepared silver nanoparticles is 21 nm. The extinction of small size silver colloids have absorption component dominant over their scattering components. This results in quenching the emission intensity of the fluorophore rather than enhancing it due to the dissipation of incident energy as heat instead of intensifying the incident energy.

As a summary for this section, monodispersed AgNPs with an average size 21 nm did not enhance the emission intensity of MPS-PPV. The result agrees with the Lakowicz report which stated that silver colloids with an average size less than 22 nm will quench the emission intensity because the dominant extinction component is the absorption which will dissipate the incident radiation as heat.[55,60] Unfortunately, the effect of silver nanoparticles of different shapes on the emission intensity of MPS-PPV was not pursued further since PVP is widely used in controlling the silver nanoparticles shape. We did explore few photochemical driven methods reported to control the shape of silver nanoparticles. Our attempts however failed to reproduce those results. We therefore decided to focus on preparing spherical silver nanoparticles capped with small molecules.

2.3.3 Synthesis of non-monodispersedand AgNPs:

Since we were not able to achieve any enhancement on the emission intensity of MPS-PPV using the monodispersed method, we decided to prepare silver nanoparticles with another approach free from PVP. In the new approach, silver nanoparticles were prepared following Turkevich's method, in which silver nitrate ($AgNO_3$) is reduced by trisodium citrate at boiling temperatures.[65]

Figure 2.25 shows the absorption spectrum of AgNPs reduced by sodium citrate without glycerol; the obtained particles have a maximum Plasmon resonance at 421 nm with FWHM of 103 ±1.42. Compared to the silver nanoseeds prepared in glycerol, the obtained AgNPs are more red shifted and have larger FWHM indicating that they are less monodispersed.

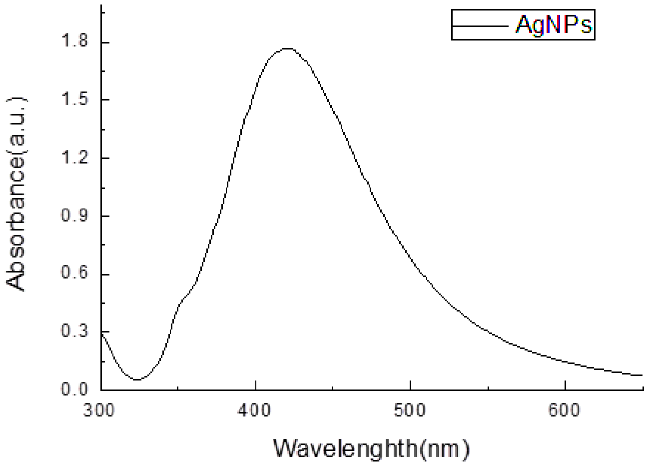

Figure 2.25: Absorption spectrum of AgNPs prepared with sodium citrated in DI-water.

2.3.4 *Studying the effect of non-monodispersed nanoparticlesAgNPs on the emission intensity of MPS-PPV:*

We varied the SiO_2 thicknesses by using different volumes of the 10mM TEOS (2.5 mL and 5 mL).

The effect of coated AgNPs with modified silica surface on the emission intensity of MPS-PPV was then studied.

As it shown in Figure 2.26, the emission intensity of MPS-PPV was successfully enhanced by ~ 2.8 folds in the presence of AgNPs-SiO_2-APTS. To achieve maximum enhancement, we titrated the MPS-PPV with AgNPs-SiO_2-APTS solution prepared with 5 mL (10 mM) TEOS and subsequently modified with APTS (Figure 2.27). In this experiment, we made sure that the final volume remained constant to ensure that the dilution effect does not interfere with our results.

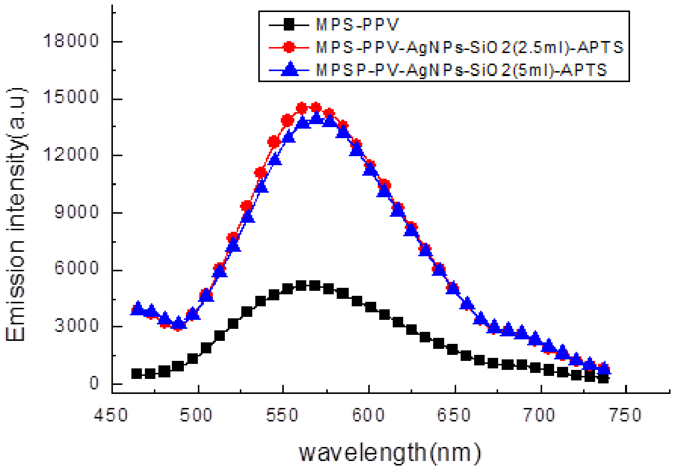

Figure 2.26: Fluorescence emission of MPS-PPV (■), MPS-PPV doped with AgNPs-SiO_2 (2 mL of 10mM TEOS)-APTS (●), and AgNPs- SiO_2 (5 mL of 10mM TEOS)-APTS (▲) in 2460 µl DI-water containing 40µl MPSPPV. The solutions were excited at 450 nm and emission intensities were collected between 470 nm and 650 nm

Figure 2.27 shows the emission intensity of MPS-PPV after the incremental addition of AgNPs-SiO_2-APTS where maximum enhancement was obtained with 2500 µl AgNPs-SiO_2-APTS. As such, the optimized particles concentrations were subsequently used in the following experiments.

Next, we focused on optimizing the concentration of APTS needed to modify the total surface of SiO_2 shell. Coated AgNPs were modified with different APTS concentrations. The Fluorescence intensity of MPS-PPV doped with AgNPs-SiO_2-APTS was then measured (Figure 2.28).

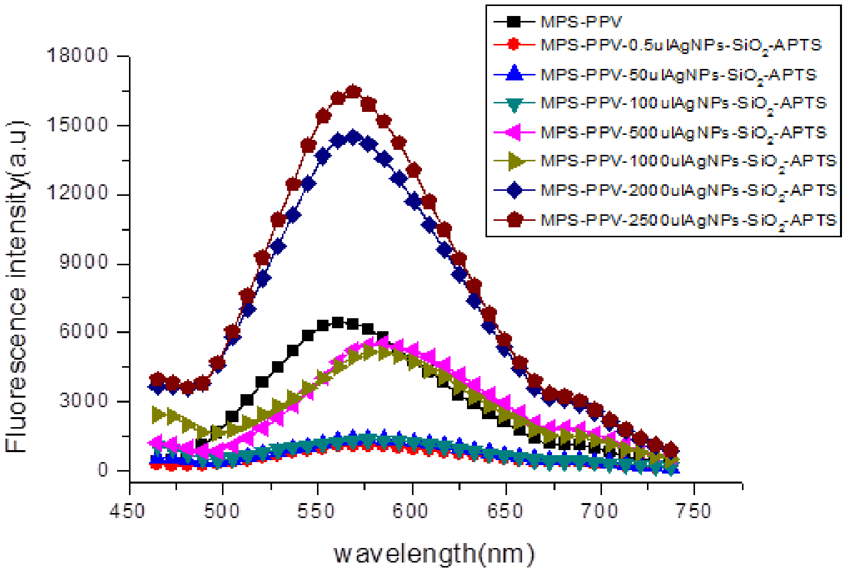

Figure 2.27: Fluorescence emission of MPS-PPV (■), and MPS-PPV doped with AgNPs- SiO_2 -APTS of different concentrations (0.5 µl, 50 µl, 100 µl, 500 µl, 1000 µl, 2000 µl, and 2500 µl) all in DI-water containing 40 µl MPSPPV and with total volume 3 mL. The solutions were excited at 450 nm and emission intensities were collected between 470 nm and 650 nm.

The fluorescence measurements in Figure 2.28 show that the emission intensity of MPS-PPV increased by a factor of 3.5 when modified with 8.6×10^{-6} M APTS with a trend of increased enhancement between 3×10^{-7} M and 8.6×10^{-6} M of added APTS. The results revealed that the optimized APTS concentration is far from the theoretical previously calculated value. It might stem from the coupling efficiency or even the fact that the multilayer condensation of APTS creates more dense surface charges.

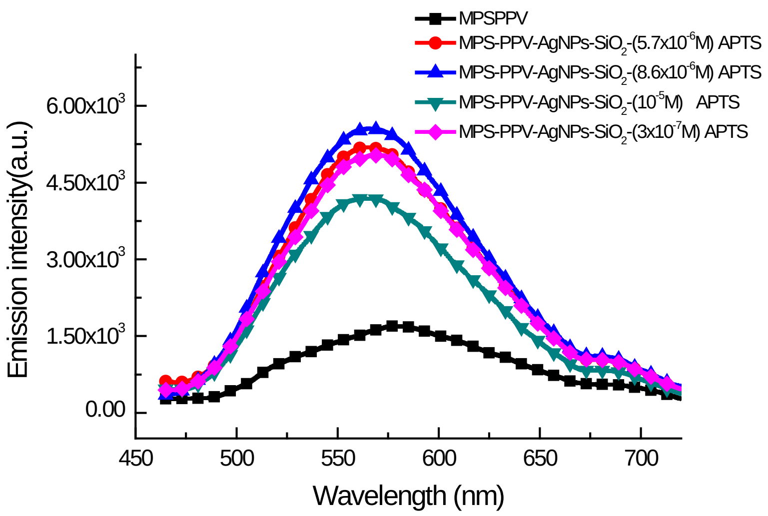

Figure 2.28: Fluorescence emission of MPS-PPV (■), MPS-PPV doped with AgNPs-SiO$_2$ -APTS of 5mL TEOS concentration and different APTS concentrations (3x10^{-7}M 5.7x10^{-6} M, 8.6x10^{-6} M, and 10^{-5}M).

2.3.4.1 Control experiments:

To ensure that silver nanoparticles induced the fluorescence enhancement of MPS-PPV, potassium cyanide was used to dissolve silver particles. The dissolution of AgNPs was confirmed by the disappearance of the absorption spectra after the addition of KCN (Figure 2.29 A). The emission intensity of MPS-PPV doped with AgNPs coated with modified silica surface was then measured in the presence and absence of KCN. Figure 2.29 B shows the emission intensity of MPS-PPV after the addition of AgNPs-SiO2-APTS and after the removal of silver. The obtained quenching in the emission intensity after the removal of AgNPs confirms that the 3.5 folds enhancement was due to the metal enhanced fluorescence induced by silver nanoparticles.

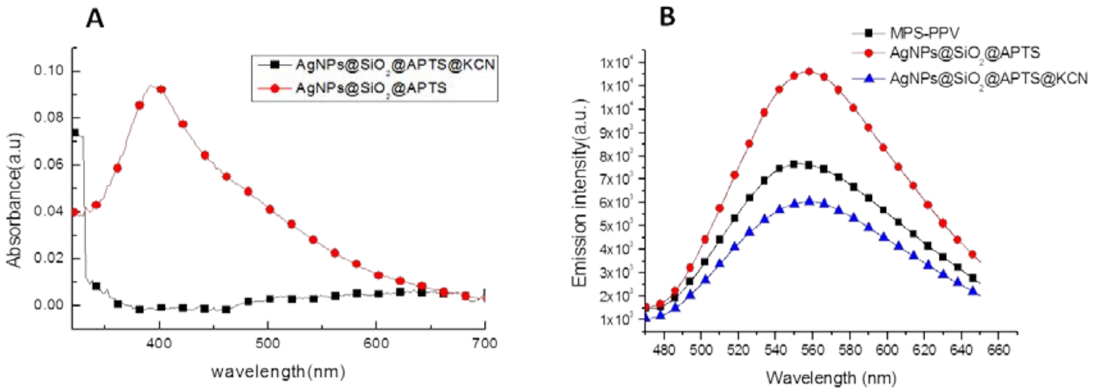

Figure 2.29: (A) Absorption spectra of AgNPs-SiO$_2$-APTS (●) and AgNPs-SiO$_2$-APTS with KCN (■). (B) Emission intensity of MPS-PPV (■), MPS-PPV doped with AgNPs-SiO$_2$-APTS (●), and MPS-PPV doped with AgNPs-SiO$_2$-APTS- KCN (▲).

After all the modifications and optimizations, the fluorescence enhancement was still very little compared to previously reported values. Silver nanoparticles prepared by Turkviech method are known to have an average size of 22 nm. But they tend to form aggregates since sodium citrate is a very mild stabilizing agent, these characteristics may allow explaining why we obtained enhancement with these nanoparticles when compared to slightly bigger and monodispersed particles. First of all, the scattering components of the extinction of colloids with average size greater than 22 nm will dominate the absorption component which will allow the particles to radiate in the far field and thus enhance the emission intensity of the fluorophore. In addition, AgNPs forming aggregates will induce the overlap of multiple plasmons, known as Plasmon coupling. This plasmonic overlap nearby Ag colloids would strongly intensify the electromagnetic field in the overlapped region. A fluorophore trapped within a coupled plasmon can be enhanced due to two effects: the fluorophore can feel the intensified electromagnetic field and have further increased probability for excitations, it can also radiate to the far field by coupling to the enhanced plasmon scattering.[60,55]

2.4 Conclusion

3.5 folds enhancement on the emission intensity of MPS-PPV was achieved in the presence of metallic silver colloid coated with SiO_2 to optimize the distance between the metal surface and the conjugated polyelectrolyte. The emission intensity of MPS-PPV enhanced due to the intensified electromagnetic field induced by Plasmon coupling of the aggregated silver colloids. PVP is known to control the shape and the size as well as to stabilize the metallic colloid. However the presence of PVP as a capping agent induces the enhancement of MPS-PPV intensity instead of silver. Thus we were not able to study the effect of different sizes and shapes on the photo-physical properties of MPS-PPV without PVP. The objectives that were placed forward at the beginning of this project were to understand the metal enhancement phenomena effect on the exciton migration in conjugated polyelectrolytes. The reported enhancement is shy from the theoretical expected enhancement (10-1000 folds) to allow any meaningful and systematic study of the system at the single and ensemble level.

Future plans include the grafting of conjugated polyelectrolytes onto the silica surface and/or the preparation of positively charged polymers that would adsorb onto the negatively charged silica surface.

CHAPTER 3

TUNING THE PHOTO-PHYSICAL OF MPS-PPV VIA POLYMER COMPLEXATION

In the previous chapter, we studied the effect of silver nano-particles on tuning the photo-physical properties of MPS-PPV which allowed us to achieve a 3.5 folds enhancement on the emission intensity of the MPS-PPV. The control experiments that we conducted revealed to us the effect of polyvinylpyrrolidone (PVP) on the photophysical properties of MPS-PPV.

In this chapter, we explored these effects at both ensemble and single molecule level.

3.1 Introduction:

The fluorescence emission of CPEs originates from individual chromophores believed to be delimited by twists that breaks the $\pi-\pi$ orbitals delocalization and creates multiple emissive sites. (Each chromophore is estimated to be between 6 to10 monomer repeat units). As such, polymer photophysics strongly correlates with its backbone conformation and its solvated state.[72] It dictates the energy transfer efficiency between neighboring chromophores. For instance, in water, conjugated polyelectrolytes adopt a highly coiled conformation to minimize the interaction between its hydrophobic backbone and the nonpolar solvent. The collapsed state induces stresses along the backbone leading to the formation of kinks and defective sites, which can serve as trapping and nonradiative recombination sites. The aggregated state also results in the formation of shorter chromophores and long range ordered and highly packed chains thus favoring efficient interchain or through-space energy transfer, which strongly compete with radiative emission processes.[24] The combined effects result in low quantum yield and overall mediocre photophysical properties in water as compared to other nonpolar solvents. (Figure 3.1).[24]

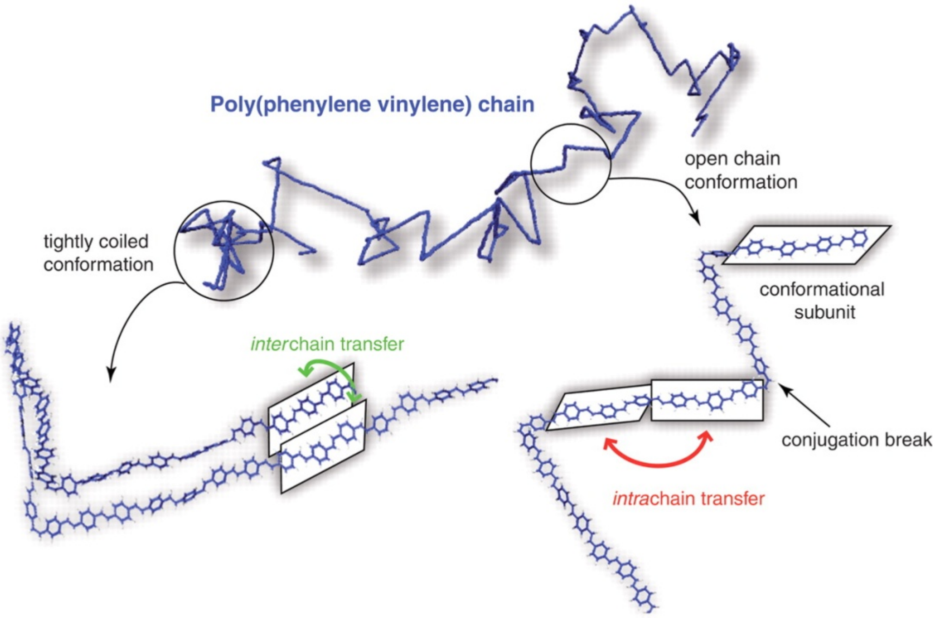

Figure 3.1: Conformational disorder in a conjugated polymer chain defines subunits which act as a single chromophore. (Reprinted with permission from Collini *et al.*).[73]

Specifically, recent single molecule studies demonstrated this direct correlation between the polymer conformation/solvation state and its spectroscopic properties.[30] When anionic conjugated polyelectrolyte, poly [5-methoxy-2-(3-sulfopropoxy)-1,4-phenylene-vinylene] (MPS-PPV), is encapsulated in negatively charged liposomes, it exists as a freely diffusing yet as a collapsed state. Discrete emission levels and on-off single-step transitions were observed in the intensity-time trajectories.[74] This quantized behavior reflects the efficient exciton transport in highly folded single PPV molecules to localized fluorescence quenching defects formed in the PPV backbone (oxidation, kinks etc). In marked contrast, fluorescence intensity-time trajectories from extended PPV chains embedded within lipid membranes showed an exponential decrease in intensity over time. This behavior is characteristic of the photobleaching of a collection of independent chromophores.[74] When compared to the folded structure, the later showed brighter intensities and better photostability.

Building on the knowledge gained from steady state fluorescence experiments and single molecule studies, surfactants and other polyelectrolytes were used to facilitate CPEs solubility and favor backbone de-aggregation.[17, 75,75b] In return, these structures provided a single molecule sensing capabilities to detect a membrane bound molecules,[76] and were developed into assays to probe enzymatic activity.[33b, 77]

For instance, when lipid vesicles were prepared in the presence of conjugated polyelectrolytes, the polymer backbone was readily dissolved in the hydrophobic core and its photoluminescence substantially increased.[75b] Indeed, MPS-PPV fluorescence intensity increased by 10 folds when complexed to zwitterionic lipid dioleoyl-phosphatidylcholine (DOPC) and its spectroscopic properties were tuned in the presence of mono or divalent cations.[17] The divalent cations (Ca^{2+}) binds to the zwitterionic lipids to confer on them cationic properties and hence promoting both electrostatic and hydrophobic interactions between the anionic polymer and the lipid. This resulted in 10 folds enhancement in the emission intensity of MPS-PPV at 1:1 molar ratio of DOPC:MPS-PPV. However, the monovalent cation (Na^{+}) promotes only hydrophobic interaction between the polymer and the lipid; large excess of lipid was required to achieve complete binding and 10 folds enhancement in the emission intensity of MPS-PPV. This complexed structure provided single molecule sensing capabilities to detect a membrane bound molecule, the liposome encapsulated MPS-PPV allowed the detection of the (DiD) embedded in the lipid membrane through Förster resonance energy transfer from the donor dye MPS-PPV to the membrane embedded acceptor dye (DiD).[76] Liu *et al.* exploited the enhanced photophysical properties upon heparin binding to conjugated polyelectrolytes to develop a specific biosensor assay that lights up upon detection of small amounts of heparin.[78] Shanze *et al.* developed a turnoff assay to probe the enzymatic activity of phospholipase C (PLC) based on the reversible interaction between phosphatidylcholine and conjugated polyelectrolyte (CPE). The addition of phospholipids to the CPE leads to the formation CPE-lipid complex due to both electrostatic and hydrophobic interactions. As a result of these interactions the emission intensity of CPE increased and blue-shifted. Incubation of the complex with PLC enzyme lowered the fluorescence intensity (turnoff) because of the catalytic hydrolysis of the zwitterionic head groups of phosphatidylcholine from the hydrophobic tail which resulted in disrupting the amphiphilic structure of the lipid and hence disrupting the CPE-lipid complex.[33b, 77]

This approach, however useful, limited the application of the enhanced CPEs to the presence of specific surfactants. New strategies to deaggregate the CPE backbone have emerged by deliberately engineering the polymer side chains and its backbone.[79] PPE-based conjugated polyelectrolytes were modified with dendritic poly(benzyl ether) terminated with carboxylic acid groups as side chains. With each dendrimer generation, the backbone charge density increased, resulting in its de-aggregation and subsequently an increase in the reported fluorescence quantum yield.[80] Recently, a more surgical approach was reported. Even in the absence of bulky or highly charged side groups, conjugated polyelectrolyte polymers were reported to be exhibit a quantum yield of approximately 25%. The absence of oxygen atom on the phenylene ring decreased the tendency of the polymer to aggregate in water resulted in increasing the fluorescence quantum yield by lowering the exciton quenching sites, however, in the presence of oxygen the conjugated polyelectrolyte exhibit a lower quantum yield of approximately 5% due to the formation of aggregates. These results were supported by fluorescence quenching with methyl viologen; the quenching efficiency in the presence of oxygen was 70 times more efficient than in the absence of oxygen due to the formation of aggregates which provides more quenching sites for the quencher.[81]

Polymer photostability is another major area where conjugated polyelectrolytes immensely suffer. Due to its conjugated backbone, CPEs are prone to the destructive effect of singlet oxygen.[82] Surfactants were extensively used to shield the conjugated backbone from oxygen. [83] Recently, Liu *et al.* have reported on the healing effect of β-mercaptoethanol, a known antioxidant, after CPE photodegreadation.[84]

Organic conjugated polymers, specifically polyfluorene and poly(phenylene vinylene) derivatives, were prepared into small fluorescent nanoparticles .[16] These particles showed high photostability and were used in bioimaging applications.[16, 85] However, they are at a disadvantage in long-term bioimaging applications, given their hydrophobic nature. Particles with hydrophilic surface groups are more desired for this type of applications given their improved solubility and lack to aggregate over time.

Consequently, there exists a major challenge to improve CPEs fluorescent efficiency and photostability while increasing their functionality. Previous attempts introduced stringent conditions that often narrowed the CPE spectrum of applications. In this work, we report a straightforward, simple, and general approach to increase the fluorescence quantum yield and, most importantly, enhance the photostability of a commercially available conjugated polyelectrolyte. Polyvinylpyrrolidone, an amphiphilic polymer, was used as a scaffold to extend the polymer backbone which resulted in a 23 folds increase in quantum efficiency. The amphiphilic macromolecule could be easily modified with biological molecules for added functionality.[86] Single molecule studies revealed the emission of a remarkable number of photons per nanohybrid particle. On average, 10^9 photons were emitted when the fluorescent signal was only 18% down from its initial intensity. All traces showed no sign of blinking during our experiment time window. The prepared hybrid particles were estimated to be in the range of few nanometers in diameters (ca. hydrodynamic 20nm). In this chapter, we will address fundamental questions such as how is PVP protecting the vulnerable CPE from photodegradation and how is it enhancing its photophysical properties? Our findings are significant, as they present a new and straightforward approach to prepare bright and highly photostable fluorescent conjugated polyelectrolytes.

3.2 Experimental section:

3.2.1 Materials:

The following were used in this study: Poly[5-methoxy-2-(3-sulfopropoxy)-1,4-phenylenevinylene] potassium salt solution 0.25 wt. % in H_2O,MPS-PPV (Aldrich); Sodium hydroxide puriss., meets analytical specification of Ph. Eur., BP, NF, E524, 98-100.5%, pellets, NaOH (Aldrich);Methyl viologen dichloride hydrate, 98%,MV^{2+}, $C_{12}H_{14}Cl_2N_2.xH_2O$ (ACROS Organics); Polyvinylpyrrolidone, average mol wt 360000,PVP$(C_6H_9NO)_n$ (Aldrich); Polyvinylpyrrolidone, average mol wt 55000,PVP$(C_6H_9NO)_n$ (Aldrich);Polyvinylpyrrolidone, average mol wt 10000,PVP$(C_6H_9NO)_n$ (Aldrich); Polyvinylpyrrolidone, average mol wt 1,30000,PVP$(C_6H_9NO)_n$ (Aldrich); Double distilled water was used for cleaning;

Deionized water (18µΩ-cm, Nanopure Diamond, CRSL, AUB) was used for solution preparations.

3.2.2 *Emission enhancement of MPS-PPV with different Mw PVP (Polyvinylpyrrolidone) solutions*

3.2.2.1 Studying the effect of PVP on the emission intensity of MPS-PPV

3.2.2.1.1 Titration of MPS-PPV with different PVP molecular weights:

As reference sample: 40 µl of 1.6×10^{-4}M MPS-PPV was suspended in 2mL 10 mM HEPES (150 mM NaCl at pH=7.35).

Analyzed samples were prepared by suspending 40 µl of MPS-PPV in 10 mM HEPES (150 mM NaCl at pH=7.35) and then titrated with incremental amount of 0.015 M of 10K PVP, 1.818×10^{-3} M of 55K PVP, 3.25×10^{-4} M of 360K PVP , and 8.13×10^{-5} M of 1300K PVP, separately until a saturation in the emission intensity was reached. The fluorescence intensity was measured after each addition.

3.2.2.2 Quenching the emission intensity of MPS-PPV with methyl viologen (MV^{2+})

MV^{2+} with concentration ranges from 0.1 M to 6.5 M were used for the below quenching experiments.

3.2.2.2.1 Quenching the emission intensity of MPS-PPV-PVP with MV^{2+}

In separate 3 mL quartz cell, 2 mL of 5×10^{-4} M 10K PVP in HEPES (10mM, pH=7.3), 2 mL of 5×10^{-4} M 55K PVP in HEPES (10mM, pH=7.3), 2 mL of 5×10^{-5} M 360K PVP in HEPES (10mM, pH=7.3), and 5×10^{-5} M 1300K PVP in HEPES (10mM, pH=7.3) were mixed with 40μl of 1.6×10^{-4} M MPS-PPV. MV^{2+} of different concentrations (0.1 M, 1 M, and 6.5 M) was incrementally added to each cell until no more quenching was obtained; the emission intensity was measured after each addition.

3.2.3 Absorption and emission measurement

Steady-state fluorescence spectroscopic measurement was carried out using a JASCO, V-570 UV/VIS/NIR Spectrophotometer. Absorption spectra were recorded JASCO, V-570 UV/VIS/NIR Spectrophotometer double-beam mode. For all steady-state absorption and emission experiments, the solutions were placed in 1 cm x 1 cm quartz cuvettes.

For emission experiment:

The reference solution: consist of 2mL HEPES, and 40μl of1.6×10^{-4}M MPS-PPV

The analyzed solution: consist of 2mL HEPES, 40μl of 1.6×10^{-4}M MPSPPV, and different amount of PVP solution

Our measurements took place under the following conditions: Excitation wavelength= 450nm, excitation slit=5nm, emission wave length from 470nm to 650nm, and emission slit=10nm

3.2.4 Single molecule experiment

Sample preparation: glass coverslips were cleaned in a piranha solution (15: 5 mL H_2SO_4:H_2O_2) for 1 hour. Flow chambers were prepared with a predrilled polycarbonate film (GraceBio) with an adhesive gasket which was assembled on top of the cleaned surface yielding a chamber with a total volume of 10 μL. Nano-hybrid particles in the concentration range of 10^{-9} M were injected into the chamber. All experiments were run under a constant flow of an oxygen scavenger solution consisting of β-mercaptoethanol 1% v/v, β-D (+) glucose 3% w/v, glucose oxidase 0.1 mg/mL, and catalase 0.02 mg/mL. Solutions were 10 mM in HEPES buffer pH 7.3 and 150 mM in NaCl. All experiments were conducted at room temperature (22-23 °C).

3.2.5 Confocal imaging

The experimental setup consisted of an Olympus IX-71 inverted microscope operated in a confocal form and provided with a closed-loop sample scanning stage (Nano LP100, Mad City Labs, Madison, WI) used for imaging and sample positioning. Samples were excited continuously employing the 488 nm from output from an Ar^+ laser. The circularly polarized laser beam was introduced via a single mode fiber optic and directed by a dichroic beam splitter (z488rdc DCLP, Chroma, Rockingham, VT) to the sample via a high numerical aperture (NA = 1.40) oil immersion objective (Olympus U PLAN SAPO 100X). Fluorescence emission was collected through the same objective and then directed to an avalanche photodiode detector (PerkinElmer Optoelectronics SPCM-AQR-14, Vaudreuil, Quebec, Canada). The emission was cleaned from any residual laser excitation by an HQ500LP (from Chroma, Rockingham, VT). Images consisting of 256 by 256 pixels were acquired by collecting the intensity for 1 ms at each pixel. Intensity-time trajectories were recorded at 1 ms dwell time by positioning the stage on a single vesicle. A home built LabView routine was used for data acquisition and stage positioning. A National Instruments NI-PCI-6602 board was used as a counter board.

3.3 Results and discussion

Our strategy was to search for an amphiphilic macromolecule that would de-aggregate conjugated polyelectrolyte backbone through strong and stable complexation/interactions contacts. Consequently, this will allow us to efficiently dissolve the polymer backbone, and enhances its water solubility and photophysical properties. The macromolecules, in addition, should be readily modified to indirectly introduce chemical functionality to existing conjugated polyelectrolytes. In this study, we picked polyvinylpyrrolidone (PVP) (Figure 3.2); PVP has been widely used to biomimetic systems to prepare biocompatible nanoparticles, drug delivery vehicles and passivate biomaterial surfaces. It is considered a safe material and has been approved by FDA for many medical uses. PVP could be also prepared with a terminal primary amine or a carboxylic acid group where it becomes easy to introduce specific biomolecules or small molecules using standard NHS/EDC chemistry.[86] This in turn adds an array of functionality and potential applications to the prepared hybrid structure while avoiding the complexity that accompanies CPEs chemical modifications. Its amphiphilic nature would dissolve and extend conjugated polyelectrolyte backbone.

The conjugated polyelectrolytes of choice was the anionic poly[5-methoxy-2-(3-sulfopropoxy)-1,4phenylenevinylene] (MPS-PPV) (Figure 3.2). It is commercially available and has been extensively used as a platform for biosensing schemes and its photophysical properties has been studied at the ensemble and single molecule levels.[87]

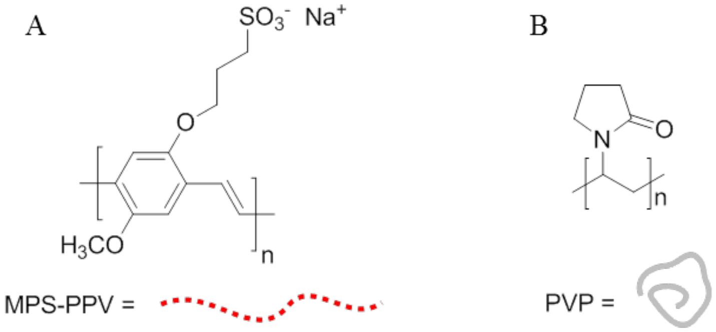

Figure 3.2: Chemical structures and the respective graphical representations of (A) the anionic conjugated polyelectrolyte poly[5-methoxy-2-(3-sulfopropoxy)-1,4phenylenevinylene] potassium (MPS-PPV) and (B) the amphiphilic polymer Polyvinylpyrrolidone (PVP).

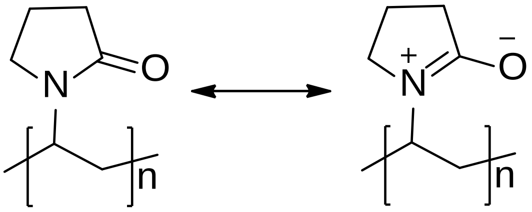

Figure 3.3: Resonance structures of a pyrrolidone ring in PVP polymers; this resonating structure gives PVP its amphiphilic properties.

The presence of the highly polar amide group and the apolar methylene group in the backbone of the PVP contribute to the amphiphilic properties of the polymer. The hydrophilic part consists of an amide group which facilitates the solubility of PVP in water due to the formation of hydrogen bond between the amide group and water molecules.[88] While, the hydrophobic part consist of methylene group which facilitate the interaction with other hydrophobic molecules, in our specific case the conjugated polyelectrolyte backbone, minimizes its contact with water (Figure 3.3).[88]

To probe the interactions between the conjugated polyelectrolyte and the amphiphilic polymer, we monitored changes in MPS-PPV spectroscopic properties with and without PVP. The addition of PVP to an MPS-PPV induced a 20 nm red shift in the absorption maximum concomitant with a slight increase in its absorbance (Figure 3.4). The absorbance spectrum revealed the transformation of the blue species (short chromophores) into a new red species (extended chromophores).

Next, we followed the changes in MPS-PPV fluorescence emission when adding incremental amounts of the amphiphilic polymer (PVP). The enhancement was calculated as the ratio of the maximum emission intensity recorded after each addition of PVP to that of the pristine $1.6x10^{-4}$M MPS-PPV maximum intensity. The results are summarized in (Figure 3.5). A 23-fold increase in fluorescence enhancement is observed followed by a plateau at approximately $5x10^{-5}$ M PVP polymer concentration (Figure 3.5). The enhancement is ascribed to the de-aggregation of the conjugated polymer backbone upon PVP complexation. As a result, the isolated chains inhibit efficient interchain coupling suppressing therefore self-quenching pathways. This strong interaction is believed to be driven by a combination of hydrophobic contacts between the two polymer backbones, and by favorable entropy changes upon the release of interfacial water molecules. The photoluminescence quantum yield of the hybrid structure was calculated to be equal to 23%. The brightness (given by the product of the extinction coefficient and the quantum yield over 1000) of the prepared hybrid structure was found to be equal to 420, which is significantly larger than most organic fluorescent dyes (typical values range between 0.5 and 90) .[89] Limited brightness of conventional dyes often results in low signal-to-background and is considered a major hurdle in sensing and single molecule fluorescence experiments.

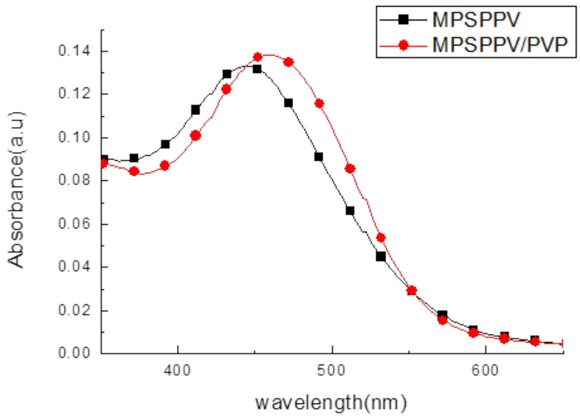

Figure 3.4: Absorption spectra of pristine 1.6x10^{-4}M MPS-PPV and upon addition of PVP (Mw=55K) at 150:1 monomer ratio in HEPES at pH=7.35

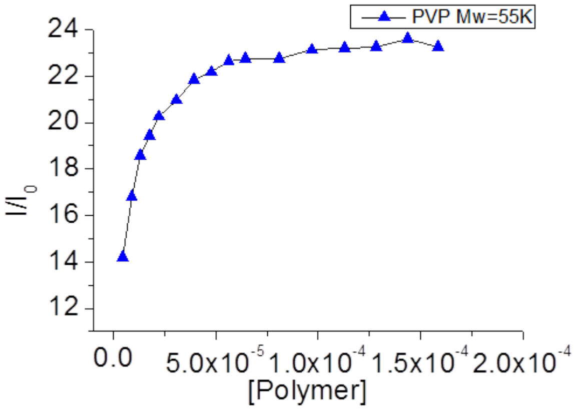

Figure 3.5: Fluorescence emission enhancement of 1.6x10^{-4}M MPS-PPV upon addition of incremental amount of PVP (Mw=55K). The fluorescence ratio was calculated by dividing the maximum intensity after each addition to the maximum fluorescence emission of pristine MPS-PPV upon excitation at 450nm in 10 mM HEPES buffer pH=7.3 and 150 mM NaCl and emission spectra were acquired upon excitation at 450nm.

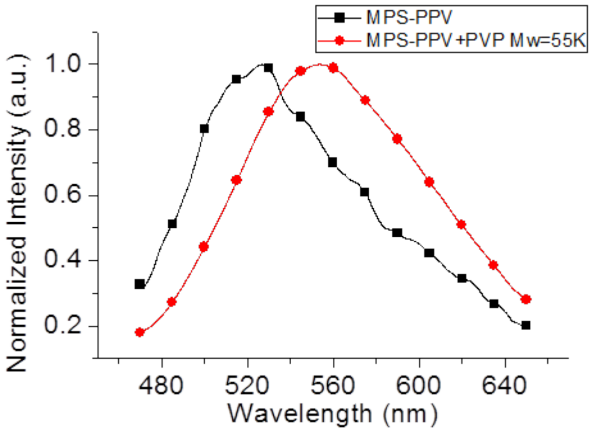

Figure 3.6: Normalized fluorescence intensity of pristine 1.6x10^{-4}M MPS-PPV and MPS-PPV/PVP (Mw=55K) mixtures. All measurements were done in 10 mM HEPES buffer pH=7.3 and 150 mM NaCl and emission spectra were acquired upon excitation at 450nm

Contrary to previously reported results where a blue shift in the fluorescence emission was observed upon conjugated polyelectrolyte de-aggregation , our results show a dramatic red shift (ca. 520 to 550 nm) (Figure 3.6) thus revealing a slightly different interaction mechanism. Previous reports argued that upon polymer backbone de-aggregation , exciton funneling to lower energy sites (red chromophores) and quenching sites is dramatically inhibited. As such, fluorescence enhancement is often accompanied with a blue shift in the emission spectrum. In 2000 , Chen *et al.* have studied the effect of dodecyltrimethylammonium bromide (DTA) surfactant on the photo-physical properties of MPS-PPV where they reported an increase in the emission intensity of MPS-PPV and a slight blue shift in the emission wavelength.[90] Similarly, In 2003 Abe *et al.* have reported an increase in the emission intensity of MPS-PPV and blue shift in the emission maximum upon studying the effect of neutral (PEG), cationic (PDDA), and anionic (PAA) polyelectrolytes on the photo-physical properties of MPS-PPV.[91] Malhotra *et al.* also reported that the emission maximum of

MPS-PPV is slightly blue shifted upon adding (DOTAP) surfactant in 1:8 MPS-PPV:surfactant ratios.[92] The presence of surfactant extended the chain of MPS-PPV and inhibited the folding of the polymer which resulted in lowering the conformational disorder of the polymer and lowering the kink defects that serve as non radiative trapping sites as well as lowering the interchain charge transfer that compete with the radiative emission process, these effects allowed the exciton to be transferred to high energetic chromophore without being trapped in nonemissive sites which results in both enhancement and blue shift in the emission peak of the polymer, these effects are illustrated in (Figure 3.7).[90,91,92]

In our specific case, while the previous hypothesis still applies, it is reasonable to assume that the red shift is due to the increase in chromophore conjugation length, a phenomena that is observed with increasing oligomer conjugation length. We speculate that upon PVP complexation, MPS-PPV chromophore length increases and interchain energy transfer to quenching sites, as expected and previously reported, is reduced leading to a fluorescence enhancement and a red shift in the fluorescence emission. This conclusion is also evident by the red shift in the absorbance spectra as discussed earlier. Similar red shift was reported when CPE backbone extension was induced by a third generation polypropylenimine hexadecamine dendrimer.[75a] The red shift add an additional 30 nm to the MPS-PPV pristine solution Stokes shift thus making the hybrid structure more appealing to a variety of imaging applications.

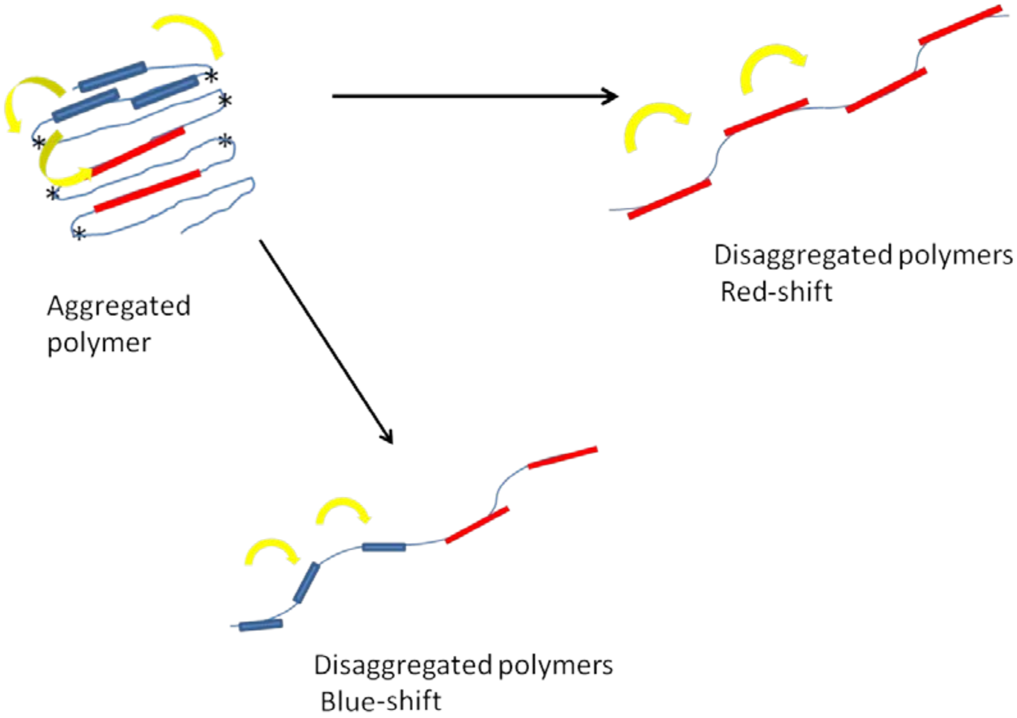

Figure 3.7: Scheme illustrating the effect of extending the polymer chain by deaggregating the folded polymer which may red or blue shift the emission peak of the polymer depending on the type of interaction between the polymer and the additive (surfactant, lipids …)

The large Stokes shift recorded of approximately 100 nm is important for imaging applications. The existence of Stokes shift plays an important role in fluorescence imaging. It enables the use of optical filters to separate the excitation wavelength from the emitted photons, improving dramatically the signal-to-background ratio. The large stokes shift is needed to minimize the background fluorescence of biological molecule and to minimize spectral overlap between absorption and emission.[93]

Next, we examined the PVP molecular weight effect on the fluorescence enhancement intensity. To understand the PVP/CPE interaction, four different molecular weights were studied 10K, 55K, 360K and 1300K. The fluorescence enhancement of $1.6x10^{-4}$M MPS-PPV ranged between 21 and 23 fold among the different molecular weights with no apparent correlation. However, the higher the molecular weight, the smaller is the polymer concentration needed to reach fluorescence saturation (Figure 3.8). For instance, for the highest PVP molecular weight (1300K), the fluorescence signal plateaued after adding $1.75x10^{-6}$M (in polymer concentration). On the other hand, a 450 fold increase in polymer concentration was needed for the lowest PVP molecular weight (10K) to reach signal saturation (ca. $8x10^{-4}$ M) (Table 3.1).

Table 3.1: Table 3.1: PVP concentrations of various PVP molecular weights needed to reach the fluorescence saturation of $1.6x10^{-4}$M MPS-PPV.

Different PVP Molecular weight	Concentration of polymer at saturation point (M)
10K PVP	$8x10^{-4}$
55K PVP	$9.5x10^{-5}$
360K PVP	$1.38x10^{-5}$
1300K PVP	$1.75x10^{-6}$

This indirect correlation between the molecular weight of PVP and the saturation concentration might be explained by two interactions models; in the first model, MPS-PPV is wrapping the exterior of the PVP macromolecule spheres. As the molecular weight increases, the polymer hydrodynamic radius increases providing bigger surface area for MPS-PPV adsorption; this is explained by Einstein viscosity relation where the molecular weight of the polymer is directly proportional to their hydrodynamic radius (Equation 3.1).[94] This model was addressed by conducting dynamic light scattering measurement on different molecular weight of PVP. The second model consists of intimate interactions between the conjugated polyelectrolytes and the PVP backbone. With the high polymer molecular weight, the monomer repeats units per polymer increases providing higher contact surface. To address this question, we normalized the fluorescence emission by the monomer repeat unit concentration. Figure 3.8reveals that irrespective of the polymer molecular weights, all polymers saturates at the same PVP monomer concentration at a ratio of 150:1 (PVP:MPS-PPV). If the conjugated polymer was strictly adhering to the outer PVP sphere, the monomer ratio of PVP to MPS-PPV would increase with increasing PVP molecular weight. This finding, therefore, endorses the second proposed mechanism and reveals an intimate type of interaction between the backbones of both polymers. We speculate that this unique mode of interaction is the prime reason behind the improved photophysical properties reported herein.

$$R_h = \left(\frac{3[\eta]M}{10\pi N_A}\right)^{1/3} \qquad \textbf{Equation 3.1}$$

Einstein viscosity relation between molecular weight and hydrodynamic radius, where M is the polymer molecular weight (g/mol), N_A Avogadro’s number, η intrinsic viscosity of polymer solution (mL/g), and R_h is the hydrodynamic radius (cm).

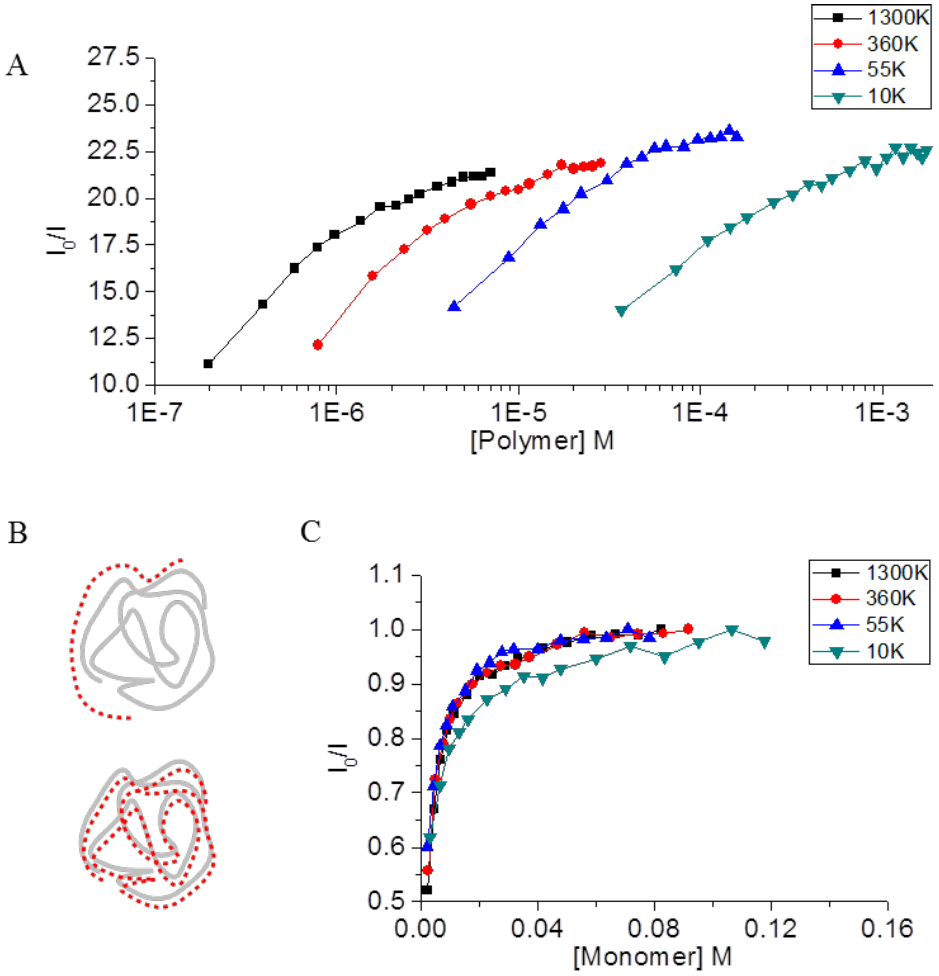

Figure 3.8: Titration of 1.6x10^{-4}M MPS-PPV with different PVP molecular weights. (A) Plots of the enhancement factor versus polymer concentration and (B) is the enhancement factor versus polymer monomer concentration. All measurements were done in 10 mM HEPES buffer pH=7.3 and 150 mM NaCl and emission spectra were acquired upon excitation at 450nm.

To further elucidate the mode of interaction between the two polymers, we performed a series of quenching experiments on the nanohybrid structure. We chose methyl viologen (MV^{2+}) as it has been shown to quench the fluorescence emission of MPS-PPV effectively. All PPV CPEs have a band gap of 2.4eV, thus light input of 2.4eV will promote an electron from the HOMO energy level of MPS-PPV to the LUMO energy level (Figure 3.9). The position of the LUMO level of MPS-PPV above the LUMO level the electron acceptor of MV^{2+} lead to a nonradiative photo-induced electron transfer from excited state MPS-PPV to the MV^{2+} thus showing a fluorescence quenching.[95],[96] First, MV^{2+} will electrostatically bind to excited state MPS-PPV and then an electron will be transferred to reduce MV^{2+} into ($MV^{+\cdot}$).The quenching reaction can be given as following[96]:

$$PPV \xrightarrow{h\nu} PPV^{*}$$

$$PPV^{*} + MV^{2+} \longrightarrow MV^{+\cdot}$$

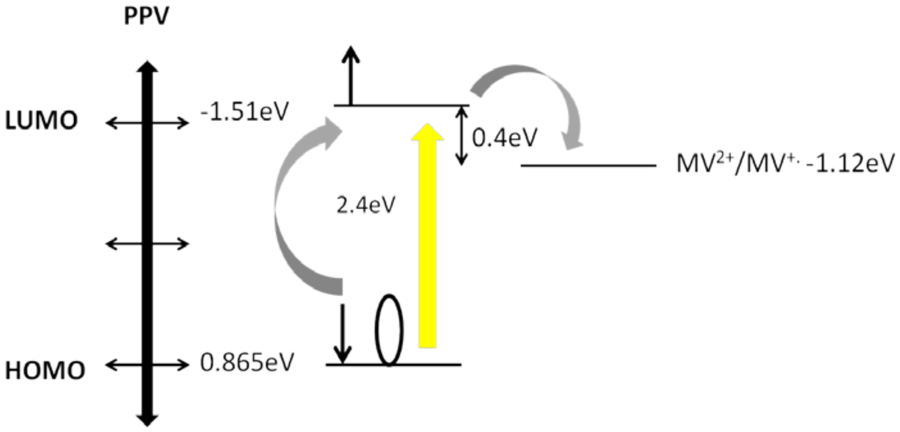

Figure 3.9: Photo-induced electron transfer from MPS-PPV to methyl viologen.

Figure 3.10 summarized the stern-volmer plots obtained for the different nanohybrid structures (PVP:MPS-PPV 150:1 monomer ratio). With the exception of PVP 10K, all particles showed an unquenchable fraction ($I_0/I= 1.2$) reflecting that 77% of the MPS-PPV is inaccessible to MV^{2+} and buried at the core of the amphiphilic molecule. Interesting enough, the PVP10K showed two quenching regimes and a lack of an unquenchable fraction. We hypothesized that the small polymer size of PVP10K is unable to interact with the entire MPS-PPV backbone thus exposing a substantial fraction of the conjugated polymer to quencher.

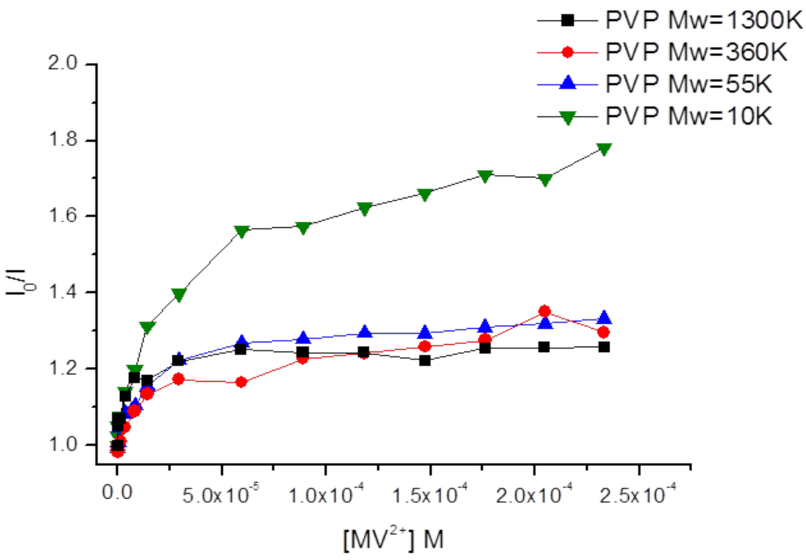

Figure 3.10: Fluorescence quenching upon adding increasing [MV^{2+}] to (■) an MPS−PPV solution 1.6x10^{-4} M in monomer units; (◊) (●). All experiments are done in 150 mM NaCl and 10 mM HEPES buffer solutions at pH=7.2. The lines connecting the experimental points are a visual aid.

To gain better molecular level understanding on the nanohybrid structure, we have performed light scattering experiments on MPS-PPV/PVP nanohybrid structure and PVP polymers. Particles size distribution of different Mw PVP and the obtained nanohybrid are summarized in Table 3.2 and Table 3.3, the results revealed an increase in the average hydrodynamic diameter when compared to PVP alone and a structure in the nanosize range ca. 15nm - 20 nm.

Table 3.2: Effective diameter and half-width of different Mw of PVP

Sample	Eff.Diameter(nm)	Half-width (nm)	Polydispersity	Baseline index
10K PVP	7.1	3.9	0.301	0
55K PVP	8.8	4.6	0.274	0
360K PVP	15.3	7.5	0.24	0
1300K PVP	16.2	8.2	0.265	0

Table 3.3: Effective diameter and half-width of different Mw of PVP/MPS-PPV

Sample	Eff.Diameter(nm)	Half-width (nm)	Polydispersity	Baseline index
10K PVP/MPS-PPV	8.2	4.7	0.329	0
55K PVP/MPS-PPV	16	8.5	0.286	0
360K PVP/MPS-PPV	19.6	9.9	0.258	0
1300K PVP/MPS-PPV	25.2	12.7	0.252	0

As mentioned earlier PVP has an amphiphilic property with hydrophobic backbone fragment greater than the hydrophilic part which will allow them to fold into a coil like structure that swell in some solvents and shrink in other solvents. When a monochromatic light hits small particles the light scatters in all direction (Rayleigh scattering). These particles will move due to the Brownian motion which depends on the particle size, particle density, temperature, and solution viscosity.[94] The motion of light emitting particles is characterized by the particle diffusion coefficient and the hydrodynamic diameter of the moving particles at absolute temperature T is defined by stokes- Einstein equation (Equation 3.2):

$$R_h = \frac{K_B\,T}{6\pi\eta D} \qquad \textbf{Equation 3.2}$$

Stoke-Einstein equation, where R_h is the hydrodynamic radius, η is the shear viscosity of the sample, K_B is the Boltzmann constant, and T is the absolute temperature

All the measurements were done with monochromatic light at 658 nm wavelength and 298 K and the particles were suspended in water which has a refractive index of 1.33 and a viscosity of 0.89 cp.

Based on all the previous results and the acquired molecular understanding of the interaction between MPS-PPV and PVP, we speculated that the intensity of the nanohybrid particles could be tuned by modifying the order of addition. When MPS-PPV is added to a solution of PVP, the amphiphilic macromolecules will compete to complex with the newly added MPS-PPV resulting in a homogenous distribution of CPEs among the nanohybrid particles (Sample 1) (Figure 3.11 B). However, When PVP is added to a solution of MPS-PPV, the first amphiphilic macromolecules will be exposed to a large amount of anionic CPEs. Consequently, each PVP polymer will scavenge multiple CPEs (Sample 2) (Figure 3.11 B). To verify our hypothesis, we examined the two samples at the single particle level. We therefore monitored individual nanohybrid fluorescence emission using a stage scanning inverted fluorescence microscope coupled to an Argon laser with an excitation at 488nm and a power of 53W.cm^{-2} measured coming out of the objective.

The emission was collected with a high numerical aperture objective and was directed to an avalanche photodiode detector (APD). All images showed diffraction-limited spots (*ca.* 300 nm in diameter) resulting from the emission of the nanohybrid particles (Figure 3.11 A). Fluorescence intensities were calculated for each particle and the intensity distributions are summarized in (Figure 3.11 C). When PVP is added to MPS-PPV, the average photo counts per particle were equal to 683 with a standard deviation of 147. The other order of addition yielded an average of photo counts per particle of 275 with a standard deviation of 91. As expected, the addition of PVP to a solution of MPS-PPV (rather than the addition of MPS-PPV to PVP) generates higher possibility of MPS-PPV encountering with multiple PVPs and the ensuing higher fluorescence emission of MPS-PPV/PVP hybrids. This result offers a simple way to tune the nanohybrid particle intensity.

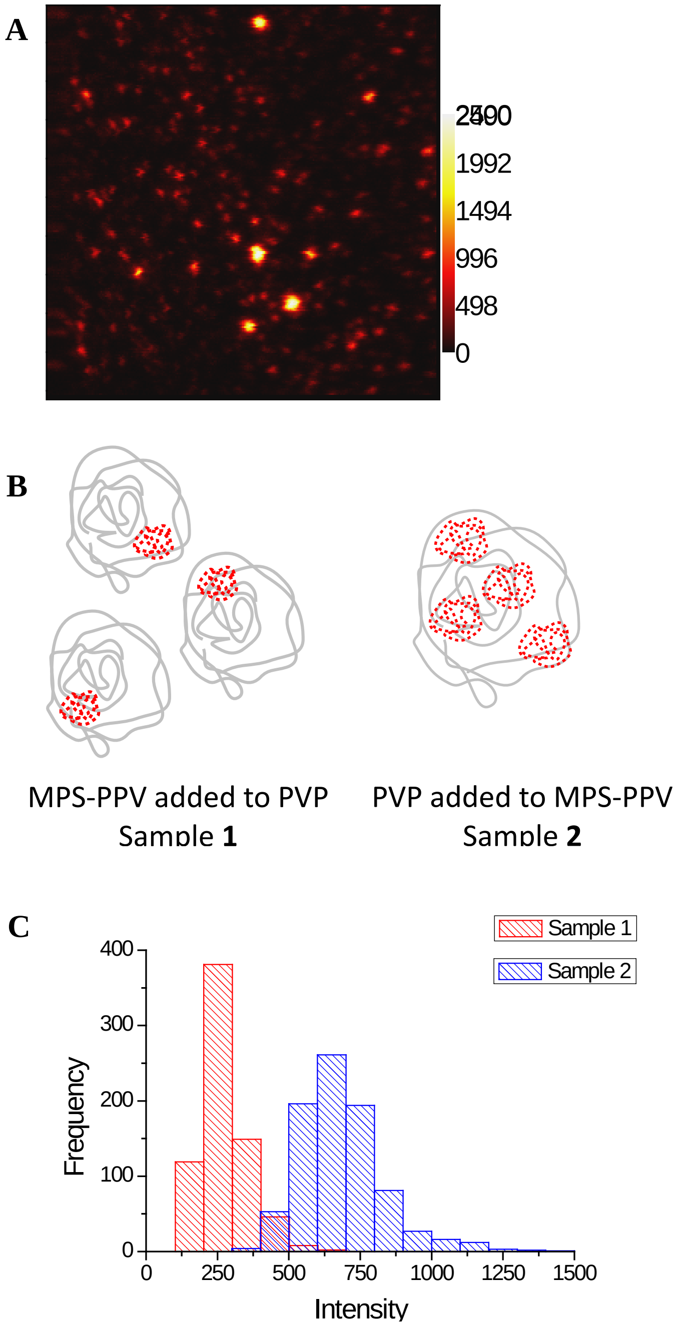

Figure 3.11: (A) 30x30 μm^2 fluorescence scanning confocal image of MPS-PPV-PVP nanohybrid particles acquired upon 488-nm excitation. The right bar illustrates the counts per millisecond per pixel. (B) Schematic illustration of MPS-PPV in complex with PVP based on the order of addition. (C) Intensity distribution histograms extracted from the single molecule images of sample 1 and sample 2.

We next focused our attention on evaluating the nanohybrid photostability. It was of great interest to us to prepare, in addition to a bright nanohybrid, a photostable particle that could be implemented in imaging applications and single molecule biosensing assays. Pristine conjugated polymer and nanohybrid solutions were subjected to continuous excitation at 450nm; MPS-PPV exhibited an exponential decay over time (20% of the original intensity was lost over 10^4 seconds) (Figure 3.12). In a marked contrast, the nanohybrid solution fluorescence intensity increased over the same time window by 18% (Figure 3.12). Nanohybrid particles prepared with different PVP molecular weights (10K and 360K in addition to 55K) was tested (Figure 3.13). Both high PVP molecular weight polymers (55K and 360K) showed similar photostability and an intensity increase of 6% within the first 4×10^3seconds. When compared to the smaller PVP molecular weight (10K), a smaller increase was observed (3%). The results reinforce the molecular level image proposed earlier where large PVP molecular weights protect the CPE from quenchers (MV^{2+}).

To explain why are we observing the increase in fluorescence intensity and how is PVP contributing to MPS-PPV photostability, we resorted to single molecule spectroscopy experiments.

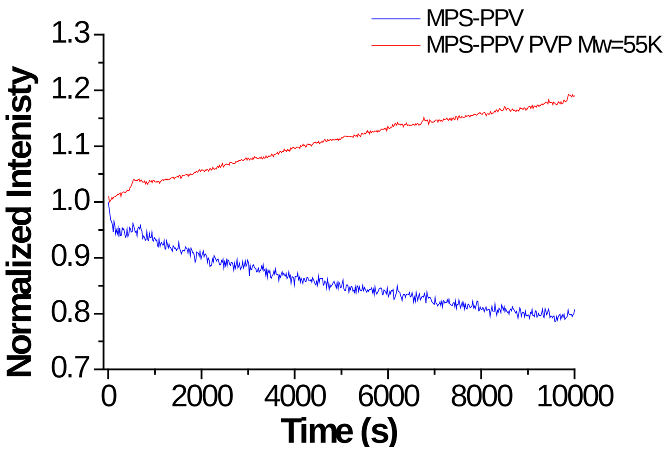

Figure 3.12: Intensity versus time trajectories of MPS-PPV and MPS-PPV_PVP (PVP:MPS-PPV 150:1 monomer ratio) nanohybrids upon 450 nm excitation.

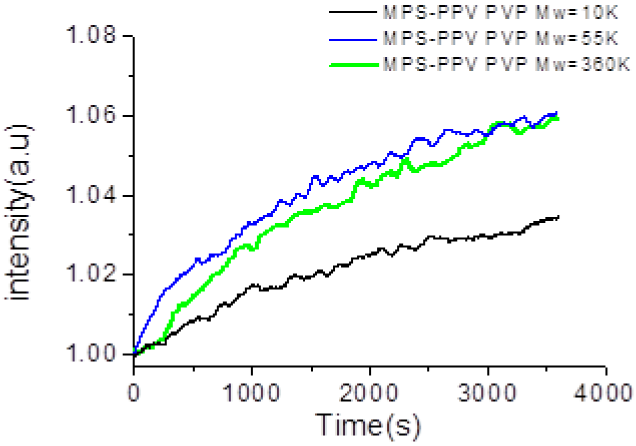

Figure 3.13: Intensity versus time trajectories of MPS-PPV-10K PVP(black) , MPS-PPV-55K PVP(blue) , and MPS-PPV-360K PVP(green) (PVP:MPS-PPV 150:1 monomer ratio) nanohybrids upon 450 nm excitation.

Intensity vs. time trajectories of single nanohybrid particles was acquired upon excitation at 488 nm (Figure 3.14). We could categorize the traces into three distinctive patterns (Figure 3.15). The majority (75% of all recorded traces) showed an increase in the intensity followed by a steady decrease (Figure 3.14 A). On average, the intensity increased to a value 1.8 times the initial value within 31 seconds. After 4 minutes of continuous excitation, we observed a small drop in intensity; 18% decrease from the original intensity.

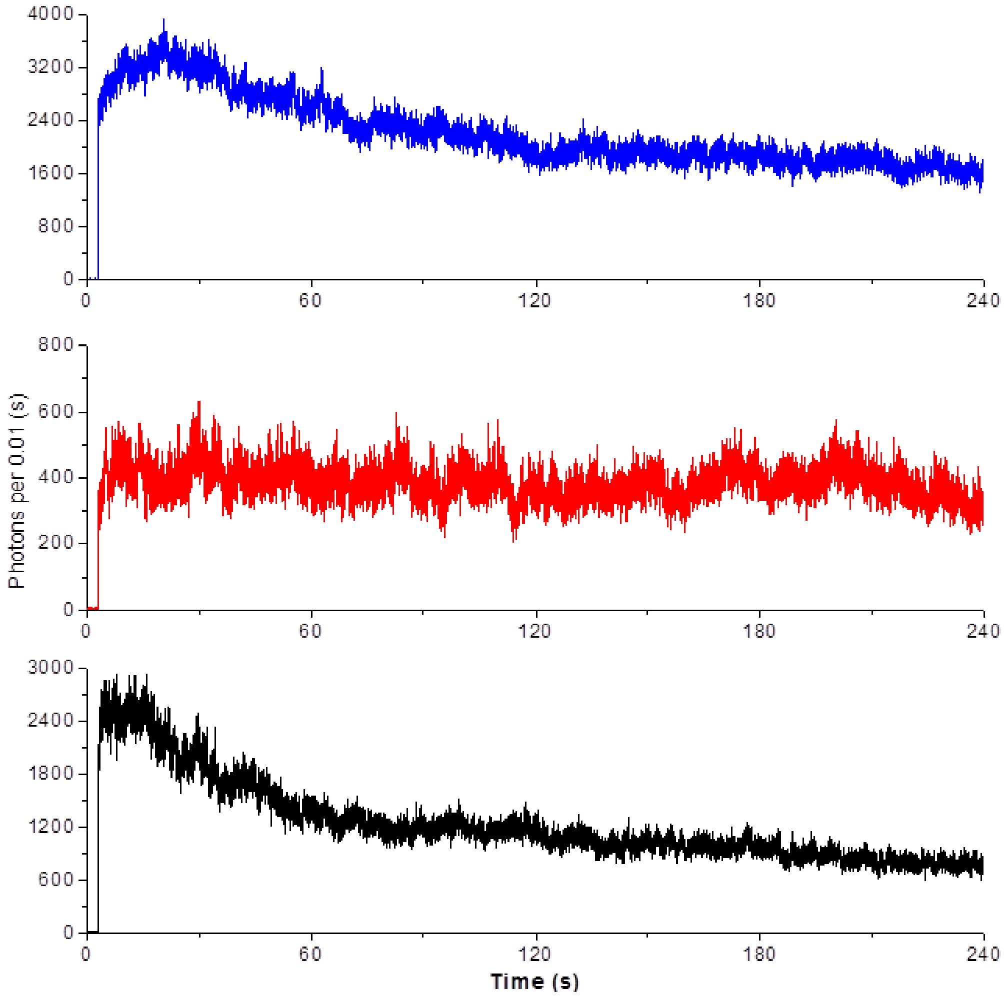

Figure 3.14: Intensity-time trajectories of the single particle nanohybrid acquired upon 488-nm excitation. The three traces represent the three different categories of the intensity change over time.

Similar pattern has been previously observed by McNeill *et al.* at the ensemble level when conjugated nanodots made of poly (2,5-di(3,7-dimethyloctyl)phenylene-1,4-ethynylene) (PPE) where continuously excited. The fluorescence intensity peaked at around 4 minutes. They reported a rapid increase in the fluorescence intensity followed by slow photobleaching upon light excitation of PPE. PPE showed two emission peaks one at 440nm and another at 480nm, the photo-bleaching kinetic measurement using time correlated single molecule counting techniques revealed that PPE has complex fluorescence decay kinetics where the 440nm emission peak showed single exponential decay kinetics while 480nm emission peaks showed bi-exponential decay kinetics.[16]

To explain this unique behavior, we tested few hypothesis; we first argued that this increase is due to conformation restructuring and energy minimization between the two polymers leadings to increased backbone extension /stabilization of the system over time. However, this hypothesis would not fit the observed pattern. Traces were sequentially acquired with time difference up to six hours between the first and the last one in some cases. The enhancement would always peak within the first 31 seconds of the measurement (Figure 3.16).

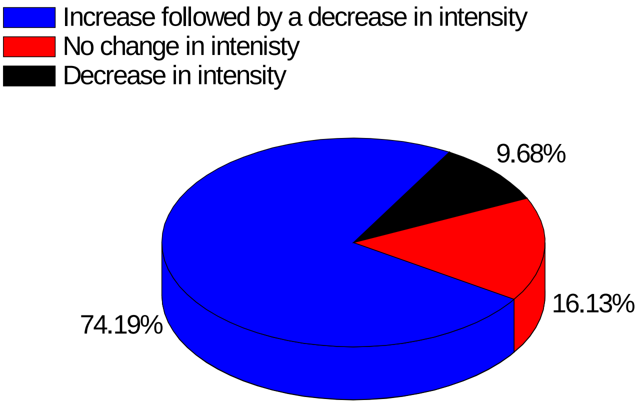

Figure 3.15: Statistical distribution of the intensity-time trajectories of the single particle nanohybrid.

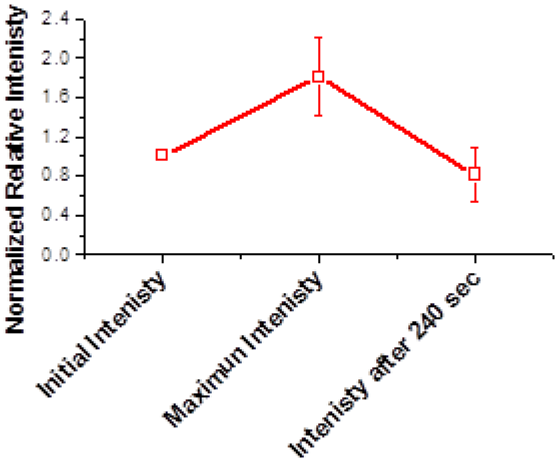

Figure 3.16: Average intensity changes of all the studied traces initially, after 30 and 240 seconds.

We then considered the probability that polymer restructuring is catalyzed by the thermal energy provided by the focused excitation beam. Indeed, a nanohybrid solution showed a 20% increase in fluorescence intensity after 5 minutes incubation at

35 °C. However, based on theoretical calculations reported by Hell *et al.* the temperature increases under our experimental conditions could not exceed 0.2-0.3 K.[97] In comparison to their model where water was irradiate with average power (Pav= 100mW) for 1 seconds and large apertures (1.2 NA) at 850nm, near IR which has higher induction, induces only 0.2 K increase in temperature due to local heating of linearly absorbed focused light; this small increase has no destructive role and will not induce focal heating.[97] However, our measurement was conducted at lower wavelength and with larger numerical apertures (1.4NA) where the temperature increase should be stronger due to the stronger axial focusing and higher axial heat dissipating and at lower wavelength, using their model with overestimating the temperature increase the induced focal heating did not exceed 0.2Kwhich indicates that the photon excitation with a high light intensity did not increase the temperature by linear absorption and thus focal heating could not explain this unusual increase in the intensity. In addition, the glass coverslip onto which the nanohybrid is deposited would act as efficient heat sink.

The inherited complex photophysics of the conjugated polyelectrolyte in addition to the strong backbone-backbone interaction with PVP might hold the answer to this unusual behavior. Conjugated polyelectrolytes, as stated earlier, could be described as a chain of connected multiple chromophores. In a highly concentrated solution of fluorophores, given the short distance between molecules, intermolecular Förster resonance energy transfer may occur leading to self-quenching. Over time, and upon photodegradation, the active fluorescent molecule concentration decreases leading to an increase in the fluorescence signal. In a similar fashion, photodegradation of the disaggregated and extended CPE in the nanohybrid particles reduces the number of emissive sites leading to chromophores “dilution” over time.

Of the remaining traces, 16 % showed no change in intensity and only 9% showed exponential photodegradation.

None of the traces showed a sign of blinking which is of high importance for real-time single particle tracking. To investigate in detail any underlying hidden dynamic or blinking, each single molecule fluorescence time trajectory was used to calculate the intensity autocorrelation function (Equation 3.3), autocorrelation function is given by the following equation:[98]

$$C(\hat{o}) = \frac{\langle I(t)I(t+\tau)\rangle}{\langle I(t)\rangle^2} - 1$$

Equation 3.3

Autocorrelation function where *I* is the intensity at time t.

We observed similar autocorrelation traces for all studied traces and therefore compiled them into one ensemble plot, (Figure 3.17). The function was fitted to a monoexponential decay function with a short lifetime of 24 ms. The correlation function amplitude is negligible.

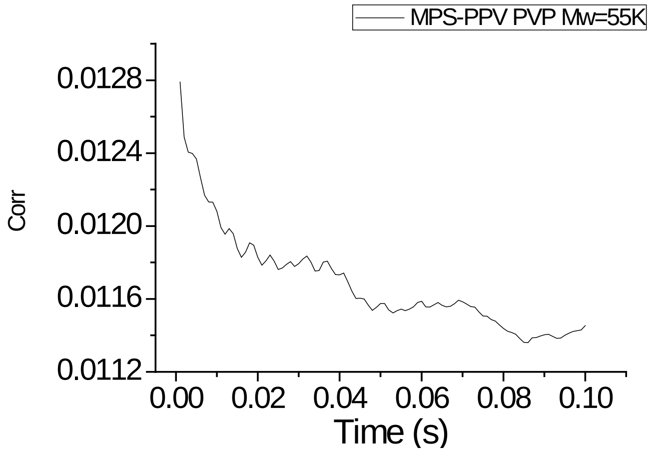

Figure 3.17: Auto-correlation of all single molecule traces.

The amount of photons emitted, on average, per trace within our experimental window (240s) was equal to 1.85 x10^9 (None of the recorded traces did completely photobleached, rather a 18% of the original intensity was lost on average). This amount of emitted photons is one the highest reported so far. When compared to other organic fluorophore, Cy5, for instance, would emit 6.5x10^5 photons before irreversible photobleaching and Alexa 633 around 9.3x10^6. Conjugated polymer dots prepared from conjugated polymers were reported to emit between 10^6 and 10^9 before complete irreversible photobleaching.

Photostability in general is attributed to the protection from molecular oxygen provided by surfactants.[83] However, in our specific case, PVP macromolecules are known to be oxygen permeable.[99]

In a recent single molecule study, Tian *et al.* showed that the collision between freely diffusing conjugated polymers lead to the simultaneous rupture of polymer chains.[100] The long chain of the polymer and the stiffness of the π-conjugated backbone create a bending stress at the contact point of the chains which in turn will catalyze the photochemical oxygen reaction at the contact point. These polymers undergo random thermal motion (Brownian motion), the collision between polymers and the existence of bending stress which catalyze the photo-oxidation and thus accelerates chain degradation by at least 20 times will induce the rupture of the polymer chain. In addition, chain bending was found to be also accentuated by prolonged polymer backbone interaction. This splitting is not a de-aggregation process for two reasons, first the aggregation process does not have an excited electronic state to induce a photo-degradation, second the degradation of the conjugated macromolecules was found to be dependent on oxygen concentration, finally, the collision between polymers should promote aggregation rather than dissociation.[100]

Based on the previously discussed molecular interaction, we believe that the intimate backbone interactions between PVP and the anionic conjugated polyelectrolyte is providing a protective shell against interchain impact and inhibiting prolonged backbone interactions thus increasing the photostability of the conjugated polyelectrolyte. It also explains why the short 10K PVP did not protect, as efficiently, the CPE from photodegradation.

3.4 Conclusion

We report herein a straightforward method to prepare photostable, bright and non-blinking nanohybrid particles by complexing conjugated polyelectrolytes with PVP. The fluorescence intensity can be easily tuned by changing the order of addition. By employing ensemble and single molecule spectroscopy methods, we unraveled the mode of interaction between the two polymers, quantified the amount of photon emitted per particle and explained the mechanism behind its photostability. The nanohybrid particles can prove instrumental in current state-of-the art single molecule tracking, bioimaging techniques and single molecules based sensing assays.

Given the challenges in preparing and modifying conjugated polyelectrolytes, the nanohybrid particles can be modified by preparing PVP with a terminal carboxylic acid or primary amine leading to an array of functionality and applications.

CHAPTER 4

THE EFFECT OF ANTIOXIDANTS ON ANIONIC CONJUGATED POLYELECTROLYTES PHOTOSTABILITY

The use of Conjugated polyelectrolyte in probing molecular interactions at single molecular level has received great attention due to their low cytotoxicity, high biocompatibility, and ease of bioconjugation.[101,102,103] Their wide application as a molecular probe for in vitro and in vivo protein and cell imaging, and as carrier and indicator for drug tracking and gene delivery, provide unprecedented understanding of biochemical and cellular processes.[103] However, Photobleaching and blinking represent the main limitations of modern fluorescence spectroscopy and imaging techniques.[84]

In our previous approach, we were able to enhance the photostability and the emission intensity of MPS-PPV through their complexation with PVP. Our hybrid system showed high brightness, large number of emitted photon, tunable nanosize, minimum photoblinking, and high photostability. These properties make this hybrid system a perfect candidate for cell imaging applications.[16] Although PVP protected the MPS-PPV from photobleaching, it is known to be oxygen permeable.

In this chapter, our aim is to further improve on the photostability of the MPS-PPV/PVP hybrid system by using antioxidants that scavenges the destructive singlet oxygen.

We will discuss the basic photophysical properties of fluorescence probe required for cell imaging and other biological applications at the single molecular level, the origin of photo-bleaching and photo-blinking, the mechanism by which the singlet oxygen decomposes the PPV polymers, the role of antioxidant in enhancing the photo-stability of fluorescence probes, and finally our preliminary findings on the effect of antioxidant in enhancing the photo-stability of MPS-PPV and MPS-PPV/PVP nanohybrid system.

4.1 Introduction:

The ultimate sensitivity of fluorescence single molecule spectroscopy and the need to acquire high quality images and data at very low molecular concentration requires a fluorescent probe with high brightness, high quantum yield, biocompatibility, large number of emitted photons for long time imaging and tracking application, and exceptional photostability to avoid photobleaching and photoblinking of the fluorophore.[104]

However, the emitted fluorescence of almost all fluorescence dyes fades gradually during the observation. This limits the application and the spread of single molecules techniques. To better solve this problem we need to go over the causes of photobleaching and some research approaches used to minimize this phenomenon which will allow us to better improve on the photostability of our nanohybrid system.

4.1.1 Photobleaching

Upon illumination, fluorescence molecule will be promoted from ground state to the singlet excited state. The absorbed energy will be dissipated by several processes such as fluorescence emission, internal conversion, and intersystem crossing to the triplet excited state. The life time of the triplet state is about 1000 time longer than the singlet state, thus the molecules spend more time in the triplet state before they reach the ground state which results in on-off switching in single molecule fluorescence intensity. This phenomenon is known as photo-blinking in which the excited fluorophore will be converted into transient dark state. The presence of molecular oxygen interacts with the triplet state dye and thus suppresses the photoblinking. However, the interaction between molecular oxygen and triplet state dye will generate singlet state oxygen which has a longer life time and higher energy than molecular oxygen. Singlet oxygen will react rapidly with the chemical groups of the dye to change them into oxidized form which is no longer fluorescent: this phenomenon is known as photo-bleaching in which the excited state fluorophore will be converted into irreversible (permanent) dark state. Molecular oxygen is not the source of only singlet oxygen but also other reactive oxygen species such as superoxide anion, hydroxyl radical, and hydrogen peroxide that lead to oxidative damage of the fluorescent molecule.[105,104,106]

4.1.2 Effect of oxygen scavenger and antioxidants in minimizing the photodegradation:

Current approaches for improving dye stability involve (1) the addition of enzymatic oxygen scavenger such as glucose oxidase and catalase in buffer solution which suppresses the photobleaching of the fluorophore and (2) the addition of chemical additives such as trolox ((±)-6-hydroxy-2,5,7,8- tetramethylchroman-2-carboxylic acid) or beta-mercaptoethanol which serves in minimizing the photo-blinking by quenching the triplet state.[107,74]

Liu *et al.* have studied the effect of different chemical additives, β-mercaptoethanol and ascorbic acid, in the presence and absence of enzymatic ground state oxygen scavenger (glucose oxidase, catalase, and β-D-(+)-glucose) on the emission intensity of MPS-PPV coated nanobeads. They found that β-mercaptoethanol and ascorbic acid can regenerate the photodamaged MPS-PPV by scavenging the nonoemissive traps, which is the dioxetanes formed upon the interaction of MPS-PPV with singlet oxygen formed along the polymer backbone. The emission intensity dropped upon the removal of β-mercaptoethanol, indicating that β-mercaptoethanol is acting as triplet state quencher. Additionally, the emission intensity of MPS-PPV increased by 3 folds with no photodamage upon the addition of β-mercaptoethanol in the presence of ground state oxygen scavenger, indicating that the addition of oxygen scavenger suppresses the photodamage of the polymer. However, the emission intensity remained the same upon the addition and the removal of ascorbic acid, indicating that the ascorbic acid has no role as triplet state quencher but rather it acts as singlet state oxygen scavenger.[84]

The combination of enzymatic oxygen scavenger and triplet state quencher suppresses the photo-bleaching and the photo-blinking of fluorescence dyes, allowing these dyes to be implemented in many single molecule fluorescence assays. However, the use of enzymatic oxygen scavenger limits the use of fluorescence dyes in in-vivo application and cell imaging. So our approach is to scavenge the singlet oxygen by using hydrophilic (L-ascorbic acid, vitamin C) and hydrophobic ((±)-α-Tocopherol (vitamin E)) antioxidants separately and together.

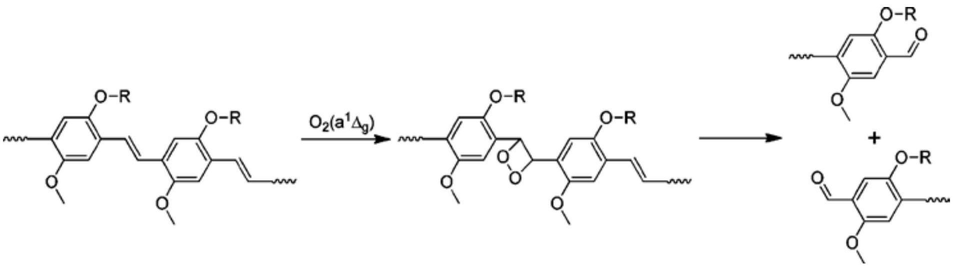

Figure 4.1: Mechanism of Single Oxygen Mediated Decomposition of PPV Polymers.(Reprinted with permission from Liu *et al.* [84])

As it is shown in Figure 4.1, the presence of singlet oxygen generated from the triplet excited state of the chromophore interacts with the vinyl group of PPV polymers. This cycloaddition will generate dioxetane which results in the cleavage of the polymer chain and the production of carbonyl defects.[84]

The presence of small antioxidants molecules such as vitamin E and/or vitamin C are able to interact completely with the reactive oxygen species (ROS) ($O_2^{\cdot -}$, $^{\cdot}OH$, H_2O_2) generated from the triplet state, inhibiting the photo-degradation of PPV conjugated polyelectrolyte.[108] Vitamin C is a water soluble antioxidant serving as the first defensive line to scavenge aqueous-phase ROS by very rapid electron transfer, and it lowers the rate of vitamin E degradation (oxidized form, i.e. tocopheroxyl radicals).Whereas VE is a hydrophobic antioxidant which interacts with hydrophobic backbone of MPS-PPV to terminate the chain reaction of polymer peroxidation and thus providing a protective layer for the polymer. Therefore, VE and VC can function together to scavenge the ROS present and hence protect the polymer from photodamaging.[109,108]

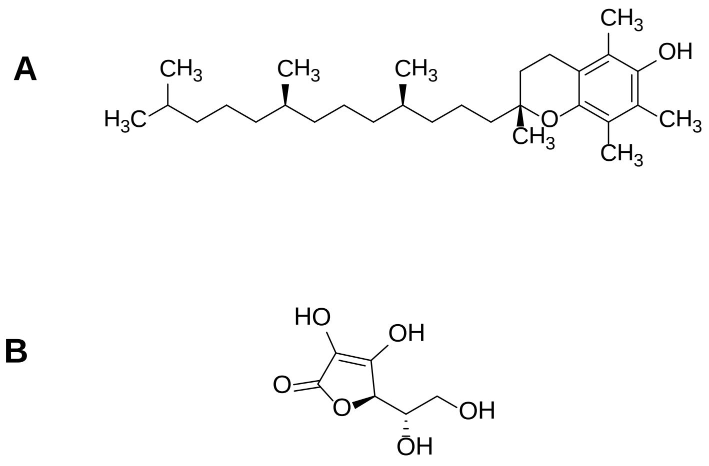

Figure 4.2: (A) Chemical structures of ((±)-α-Tocopherol (vitamin E) and (B) the chemical structure of L-Ascorbic acid (vitamin C).

Vitamin E or α-Tocopherol quenches singlet oxygen by both physical and chemical reaction with $k_q > k_{ox}$, making the quenching processes almost entirely physical. Physical quenching occurs through electron energy transfer from vitamin E to the singlet oxygen to regenerate the molecular oxygen where α-Tocopherol can deactivate about 120 $^1O_2$ molecules before being degraded, whereas chemical quenching occurs due to the interaction between $^1O_2$ and α-Tocopherol to generate various oxidation products(Figure 4.3).[110,111]

$^1O_2 + \alpha\text{- Toc} \xrightarrow{k_q} {}^3O_2 + \alpha\text{-Toc}$ **Physical quenching**

$^1O_2 + \alpha\text{- Toc} \xrightarrow{k_{ox\text{-}O}} {}^3O_2 + \alpha\text{-Toc} + \text{other oxidation products}$ **Chemical quenching**

Figure 4.3: physical and chemical quenching of singlet oxygen by vitamin E.[112,110]

Vitamin E and Vitamin C are considered chain breaking antioxidants where they act as radical scavengers to terminate the radical reactions. NiKi has studied the interaction between vitamin C and vitamin E during the oxidation of methyl linoleate. He found that when both antioxidants exist together the rate of consumption of vitamin C initially increases where vitamin E remains constant. After the complete depletion of vitamin C, the consumption of vitamin E starts. After the complete depletion of both antioxidants, the oxidation of methyl linoleate quickly starts (Figure 4.4). His study clearly shows that both antioxidants function as radical scavenger, however the presence of vitamin C with vitamin E will lengthen the inhibition period.[109]

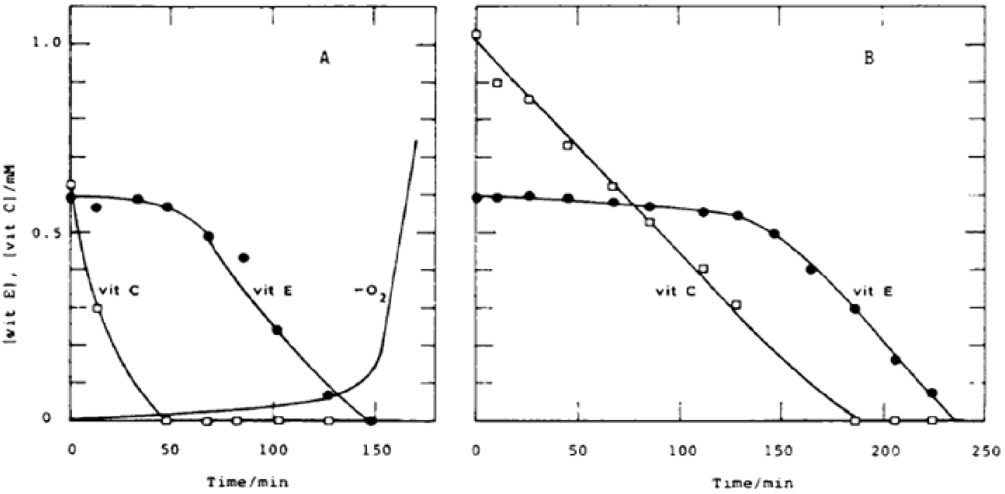

Figure 4.4: The consumption of vitamin E (●) and vitamin C (o) during the oxidation of methyl linoleate.((reprinted with permission from Niki *et al.*^{109})

4.2 Experimental setup:

4.2.1 Materials

The following were used in this study: Poly[5-methoxy-2-(3-sulfopropoxy)-1,4-phenylenevinylene] potassium salt solution 0.25 wt. % in H_2O,MPS-PPV (Aldrich); Silver nitrate 99.9999% trace metals basis,$AgNO_3$ (Aldrich); L-Ascorbic acid 99%,$C_6H_8O_6$ (Aldrich); Sodium hydroxide puriss., meets analytical specification of Ph. Eur., BP, NF, E524, 98-100.5%, pellets, NaOH(Aldrich); HEPES sodium salt ≥99.5% (titration),$C_8H_{17}N_2NaO_4S$(Aldrich); Polyvinylpyrrolidone, average mol wt 55000,PVP$(C_6H_9NO)n$ (Aldrich); (±)-α-Tocopherol (vitamin E); Ethanol (C_2H_5OH); Double distilled water was used for cleaning; Deionized water (18µΩ-cm, Nanopure Diamond, CRSL, AUB) was used for solution preparations.

4.2.2 Studying the effect of antioxidants on the photo-degradation of MPS-PPV in the presence and absence of PVP

4.2.2.1 Sample preparation:

Solution 1**:** 50 µl of (±)-α-Tocopherol (vitamin E, VE) and 2.5 g of 55K PVP were suspended in 25 mL DI-water; then 1 mL of VE/PVP solution was mixed with 20 µl of 1.6x10^{-4}M MPS-PPV, (MPS-PPV/PVP/VE).

Solution 2**:** 50 µl of (±)-α-Tocopherol (vitamin E, VE) and 0.625 g of 55K PVP were suspended in 6.25 mL DI-water.;then 1mL of VE/PVP solution was mixed with 20 µl of 1.6x10^{-4}M MPS-PPV, (MPS-PPV/PVP/VE).

Solution 3**:** 50 µl of (±)-α-Tocopherol (vitamin E, VE) and 0.25 g of 55K PVP were suspended in 2.5 mL DI-water; then 1 mL of VE/PVP was mixed with 20 µl MPS-PPV, (MPS-PPV/PVP/VE).

Solution 4: 104 µl of (±)-α-Tocopherol (vitamin E, VE) was suspended in 3.5 mL ethanol and 1.5 mL DI-water.

Solution 5: 0.4 g of L-Ascorbic acid (vitamin C, VC) was dissolved in 10 mL DI-water.

Solution 6: 80 µl of MPS-PPV was suspended in 4 mL 10 mM HEPES (150 mM NaCl, pH=7.35)

Solution 7: 40 µl of MPS-PPV was suspended in 2 mL 10 mM HEPES (150 mM NaCl, pH=7.35) followed by the addition of 200µl of 55K PVP (100 mg/mL), (MPS-PPV/PVP).

4.2.2.2 Preparation of analytes in 96 well plates

200 µl of solution 6 (MPS-PPV) was placed in 10 wells.

MPS-PPV was then mixed with different concentrations of vitamin E ($5.7x10^{-4}$M, $2.3x10^{-3}$ M, and $5.8x10^{-3}$ M), different concentrations of vitamin C ($1.2x10^{-3}$M, $4.5x10^{-3}$ M, and$1.2x10^{-2}$ M), and different ratios of vitamin E-Vitamin C mixture ($5.7x10^{-4}$ M V.E:$1.2x10^{-2}$ M V.C, $2.3x10^{-3}$ M V.E:$4.5x10^{-3}$ M V.C, and $5.8x10^{-3}$ M V.E:$1.2x10^{-2}$ M V.C) in different wells separately.

In another 10 wells 200µl MPS-PPV/PVP solutions were added and mixed

with different with different concentrations of vitamin E ($5.7x10^{-4}$ M, $2.3x10^{-3}$ M, and $5.8x10^{-3}$ M), different concentrations of vitamin C ($1.2x10^{-3}$ M, $4.5x10^{-3}$ M, and$1.2x10^{-2}$ M), and different ratios of vitamin E-Vitamin C mixture ($5.7x10^{-4}$ M V.E:$1.2x10^{-2}$ M V.C, $2.3x10^{-3}$ M V.E:$4.5x10^{-3}$ M V.C, and $5.8x10^{-3}$ M V.E:$1.2x10^{-2}$ M V.C) in different wells separately.

4.2.2.3 Photo-stability measurements of the analyte

The photo-stability of the above analytes (section 2.13.2) was measured by using Flouroskan Ascent F, the analytes were excited at 485nm and the emission was collected at 538nm, all the measurements were conducted at 25°C.

4.3 Results and discussion:

In what follows, we report our investigation on the photophysical effects of antioxidants on the anionic conjugated polyelectrolytes MPS-PPV.

Figure 4.5 shows the HOMO-LUMO energy diagram of MPS-PPV, Vitamin E, and Vitamin C (from left to right). No electron transfer can occur between MPS-PPV and Vitamin E/C since the HOMO of the former lies below the LUMO of either vitamin E or C, indicating that MPS-PPV cannot undergo quenching by electron transfer in the presence of both antioxidants. Therefore, both vitamins can be used to scavenge singlet oxygen with no fear of quenching the MPS-PPV.[113,114,115]

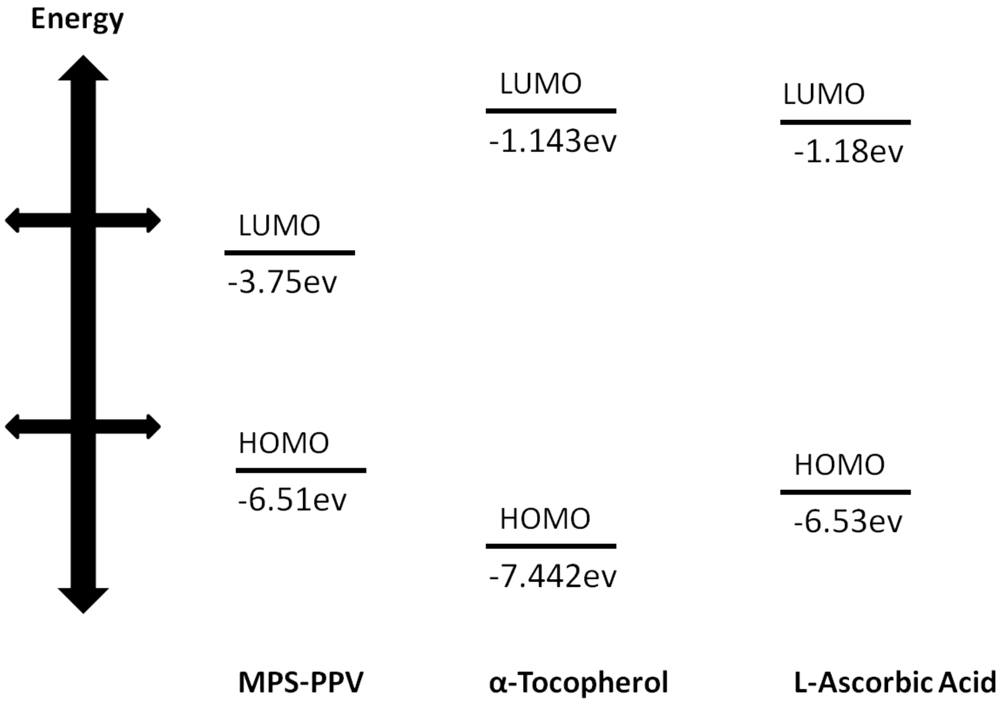

Figure 4.5: HOMO-LUMO Energy diagram of MPS-PPV, α-Tocopherol (Vitamin E), and L-Ascorbic Acid (Vitamin C).[113,114,115]

In our case, we studied the photostability of MPS-PPV and MPS-PPV/PVP in the presence of vitamin E, Vitamin C and their mixtures at different concentrations and ratios. Table 4.1 and Table 4.2 summarize the change in the initial emission intensity after 10000 counts excitation of MPS-PPV and MPS-PPV/PVP in the presence and absence of antioxidants.

Table 4.1: The effect of VE, VC, and VE/VC on the emission intensity of MPS-PPV in 10mM HEPES buffer solution (in 150mM NaCl) at pH=7

Sample	Initial intensity(I_0)	Final intensity (I)	(I/I_0)x100
MPS-PPV	115	96	83.2%
MPS-PPV/VE(5.7x10^{-4}M)	123	105	85.4%
MPS-PPV/VE(2.3x10^{-3}M)	152	137	90.11%
MPS-PPV/VE(5.8x10^{-3}M)	206	216	105%
MPS-PPV/VE(5.7x10^{-4}M) /VC(1.2x10^{-3}M)	122	106	87.12%
MPS-PPV/ VE(2.3x10^{-3}M) /VC(4.5x10^{-3}M)	141	152	107.37%
MPS-PPV/VE(5.8x10^{-3}M) /VC(1.2x10^{-2}M)	178	260	145.77%
MPS-PPV/VC(1.2x10^{-3}M)	148	133	89.74%
MPS-PPV/VC(4.5x10^{-3}M)	109	97	88.8%
MPS-PPV/VC(1.2x10^{-2}M)	100	91	91.5%

Table 4.2: The effect of VE, VC, and VE/VC on the emission intensity of MPS-PPV/PVP in 10mM HEPES buffer solution (in 150 mM NaCl) at pH=7.35)

Sample	Initial intensity(I_0)	Final intensity (I)	(I/I_0)x100
MPS-PPV/PVP	708	708	100%
MPS-PPV/PVP/VE(5.7x10^{-4}M)	693	705	101.72%
MPS-PPV/PVP/VE(2.3x10^{-3}M)	660	668	101.14%
MPS-PPV/PVP/VE(5.8x10^{-3}M)	648	661	102.05%
MPS-PPV/PVP/VE(5.7x10^{-4}M) /VC(1.2x10^{-3}M)	694	694	100%
MPS-PPV/PVP/VE(2.3x10^{-3}M) /VC(4.5x10^{-3}M)	641	686	106.96%
MPS-PPV/PVP/VE(5.8x10^{-3}M) /VC(1.2x10^{-2}M)	630	665	105.67%
MPS-PPV/PVP/VC(1.2x10^{-3}M)	689	684	99.24%
MPS-PPV/PVP/VC(4.5x10^{-3}M)	724	756	104.35%
MPS-PPV/PVP/VC(1.2x10^{-2}M)	684	697	101.9%

Figure 4.6 shows the emission intensity of MPS-PPV over time. The initial emission intensity of MPS-PPV dropped from 115.4 a.u after 10 seconds of excitation and reached 95a.u after 10000 seconds. As expected, MPS-PPV undergoes photo-degradation upon light excitation. The complexation of MPS-PPV with PVP enhanced its emission intensity and its photo-stability. As it is shown in Figure 4.7, the initial emission intensity of MPS-PPV dropped from 590 a.u to 582 a.u during the first 1000

seconds. However, of the course of the experiment, an increase in the fluorescence intensity is observed reaching 710 a.u after 10000 seconds.

To better enhance the photostability of MPS-PPV and to minimize the loss in the initial intensity different antioxidant systems were employed. We used different concentration of vitamin E as a hydrophobic antioxidant, different concentration of vitamin C as a hydrophilic antioxidant, and different concentration of VE/VC mixture. (The results are summarized in Table 4.1and Table 4.2).

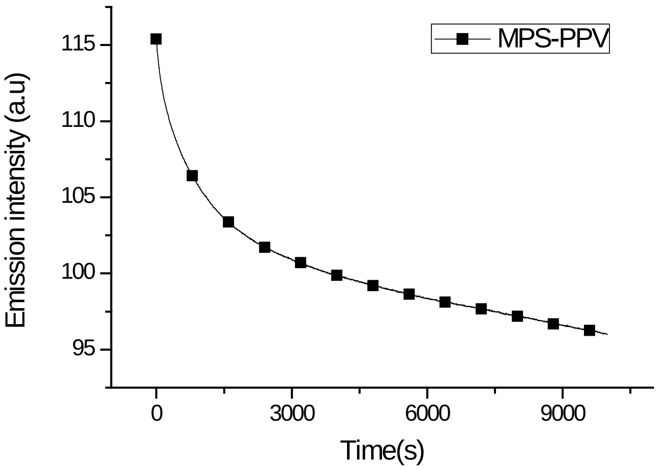

Figure 4.6: Emission intensity over time of MPS-PPV in 10 mM HEPES buffer pH=7.3 and 150 mM NaCl.

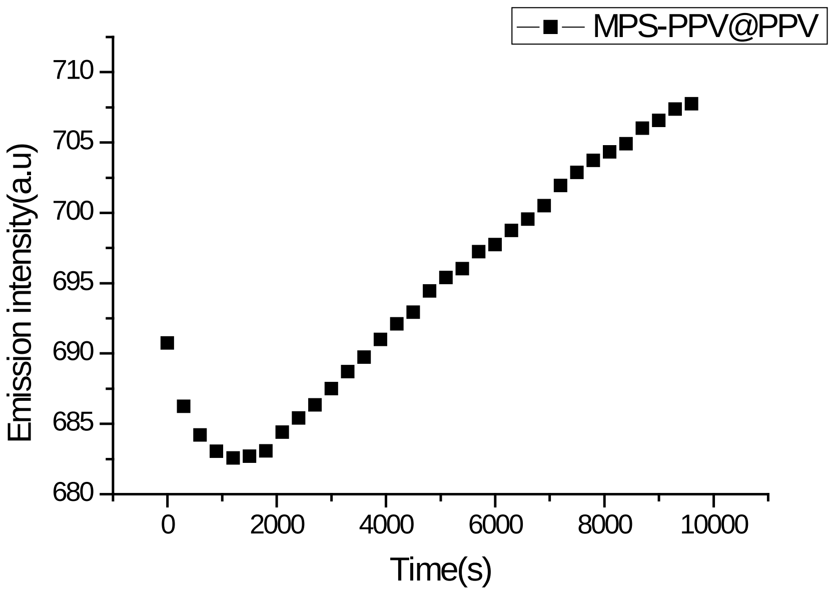

Figure 4.7: Emission intensity over time of MPS-PPV/PVP (0.2g/mL) in 10mM HEPES in 10 mM HEPES buffer pH=7.3 and 150 mM NaCl.

Figure 4.8 shows the photostability of MPS-PPV with different antioxidant. As it is shown, the emission intensity increases exponentially with $2.3x10^{-3}$ M vitamin E and $4.5x10^{-3}$ M vitamin C, and with $5.8x10^{-3}$ M VE and $1.2x10^{-2}$ M VC. When compared to pristine MPS-PPV, the initial intensity of MPS-PPV drops when $4.5x10^{-3}$ M and 1.2×10^{-2} M vitamin C were added (Table 4.1).

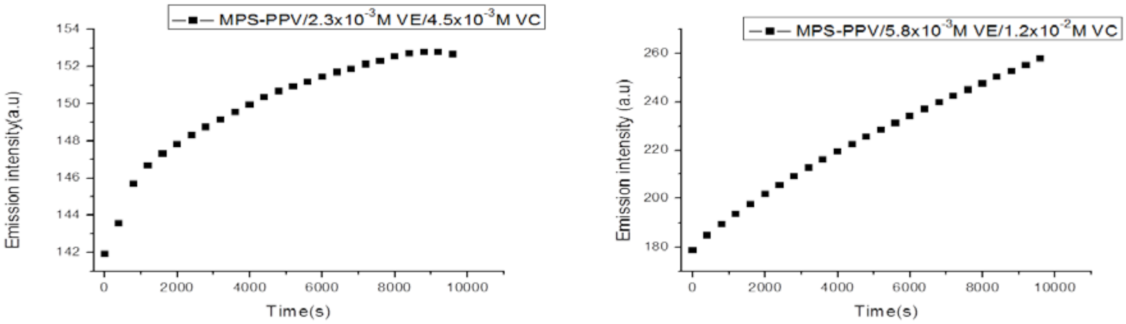

Figure 4.8: Emission intensity over time of MPS-PPV mixed with 2.3x10^{-3}M VE and 4.5x10^{-3}M of VC (Left) and 5.8x10^{-3}M VE and 1.2x10^{-2}M VC (right). The measurements were done in 10mM HEPES in 10 mM HEPES buffer pH=7.3 and 150 mM NaCl.

The effect of different antioxidant systems on the emission intensity and photostability of MPS-PPV/PVP complex was studied. As it is seen (Table 4.2), the initial intensity of MPS-PPV/PVP complex decreased upon adding the antioxidants (Figure 4.7).

Whereas, the emission intensity increases with the addition of antioxidants of 2.3 x10^{-3} M vitamin E with 4.5 x10^{-3} M vitamin C and 5.8 x10^{-3} M vitamin E with 1.2 x10^{-2} M vitamin C (Figure 4.9).

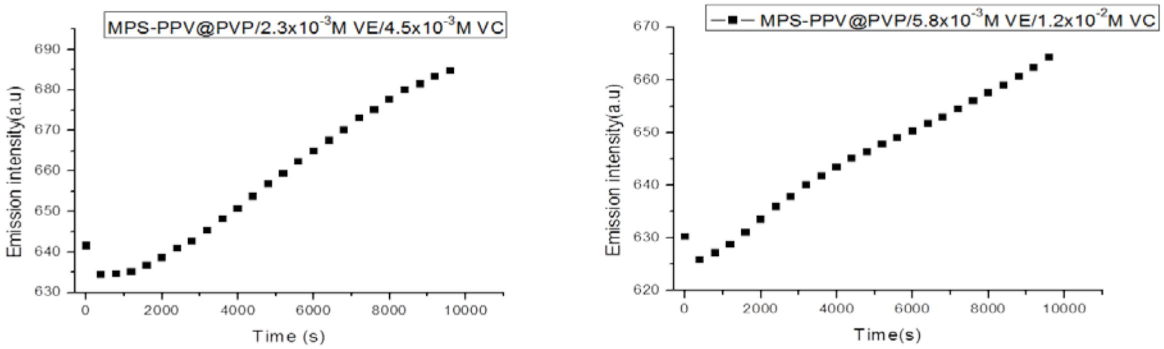

Figure 4.9: Emission intensity over time of MPS-PPV/PVP mixed with 2.3x10-3M VE and 4.5x10-3 M of VC (left) and 5.8x10-3M VE and 1.2x10-2 M VC (right). The measurements were done in 10 mM HEPES in 10 mM HEPES buffer pH=7.3 and 150 mM NaCl.

4.4 Conclusion:

The photostability of MPS-PPV was enhanced in the presence of 5.8x10^{-3}M of vitamin E, 2.3x10^{-3}M VE with 4.5x10^{-3}M VC, and 5.8x10^{-3}M VE with 1.2x10^{-2}M VC. The addition of antioxidants to the nanohybrid structure further enhanced the emission intensity and the photostability of MPS-PPV. Even though many more experiments are needed to optimize the fluorescence enhancement of conjugated polyelectrolytes in the presence of antioxidants, the results present a huge step forward towards enhancing the fluorescence of this class of polymers.

CHAPTER 5

CONCLUSION AND FUTURE WORK

In chapter 2, we investigated the effect of silver nanoparticles on the photo-physical properties of conjugated polyelectrolyte. We first prepared silver nanoparticles with Plasmon resonance that overlap with absorption maximum of MPS-PPV; the presence PVP as capping agent contribute to the enhancement of the emission intensity of the CPEs (MPS-PPV). AgNPs free of PVP and coated with amino functionalized silica surface was then prepared. Different enhancement parameters were optimized to achieve 3.5 folds increase in the emission intensity of MPS-PPV.

Preparing AgNPs in the absence of any stabilizing agent was very challenging; we were not able to prepare particles with different sizes and shapes in the absence of PVP which is known to control the shape of nanoparticles. Thus, more investigation should be done to synthesize metallic nanoparticles free from surfactants or capping agents due to their role in modifying the microenvironment of the conjugated polyelectrolyte.

Modifying the silica surface with APTS to render the surface of SiO_2 positively charged, which increases the electrostatic interaction with CPEs, was also very challenging. We are expecting to obtain higher fluorescence enhancement if cationic CPEs is employed which will allow us to skip the Silica modification step and to avoid losing AgNPs upon adding APTS.

In chapter 3, we investigated the effect of amphiphilic macromolecules (PVP) on the photophysical properties of CPEs (MPS-PPV).The effect of different molecular weight of PVP was studied. 23-folds enhancements on the emission intensity of MPS-PPV were obtained with different Mw PVP but with different concentrations. For instance, 23 folds enhancement was obtained with 1300K PVP at concentration $1.75x10^{-6}$ M and with 10K PVP at concentration $8x10^{-4}$M. The ensemble and single molecular spectroscopic methods allowed us to unravel the mode of interaction between PVP and MPS-PPV. In this chapter we were able to prepare very stable, bright, non photoblinking nanohybrid particles which can improve on bioimaging techniques and sensing assays.

This project provided a wealth of information on the interaction of two macromolecules that will have a concrete impact on the field of bioimaging. Our future prospective is to modify the biocompatible PVP with biological molecules in order to probe intracellular compartments and specific cellular membrane receptors.

In chapter 4, we investigated the effect of hydrophobic (vitamin E) and hydrophilic (vitamin C) on the photostability of pristine MPS-PPV and MPS-PPV-PVP nanohybrid system. The use of both antioxidants improved the photostability of MPS-PPV and the nanohybrid particles by removing singlet oxygen species. More investigation should be done to explore the effect of other antioxidants such as vitamin A, glutathione etc. we are aiming at studying the effect of the order of addition of both antioxidants where vitamin C is known to as first defense line and vitamin E is known as last defense line. Using antioxidants instead of oxygen scavenging systems will allow the implementation of these probes in Invivo imaging.

REFERENCES:

1. Bae, W.; Choi, M.-G.; Hyeon, C.; Shin, Y.-K.; Yoon, T.-Y., Real-Time Observation of Multiple-Protein Complex Formation with Single-Molecule FRET. *Journal of the American Chemical Society* **2013,** *135* (28), 10254-10257.

2. Phillip, Y.; Kiss, V.; Schreiber, G., Protein-binding dynamics imaged in a living cell. *Proceedings of the National Academy of Sciences* **2012,** *109* (5), 1461-1466.

3. (a) Ghosh, S. K.; Kim, P.; Zhang, X.-a.; Yun, S.-H.; Moore, A.; Lippard, S. J.; Medarova, Z., A Novel Imaging Approach for Early Detection of Prostate Cancer Based on Endogenous Zinc Sensing. *Cancer Research* **2010,** *70* (15), 6119-6127; (b) Shahzad, A.; Kohler, G.; Knapp, M.; Gaubitzer, E.; Puchinger, M.; Edetsberger, M., Emerging applications of fluorescence spectroscopy in medical microbiology field. *Journal of Translational Medicine* **2009,** *7* (1), 99.

4. Turro, N. J., Modern Molecular Photochemistry. **1991**.

5. Yildiz, A.; Tomishige, M.; Vale, R. D.; Selvin, P. R., Kinesin Walks Hand-Over-Hand. *Science* **2004,** *303* (5658), 676-678.

6. Grynkiewicz, G.; Poenie, M.; Tsien, R. Y., A new generation of Ca2+ indicators with greatly improved fluorescence properties. *Journal of Biological Chemistry* **1985,** *260* (6), 3440-3450.

7. Rasnik, I.; McKinney, S. A.; Ha, T., Nonblinking and long-lasting single-molecule fluorescence imaging. *Nat Meth* **2006,** *3* (11), 891-893.

8. Dempsey, G. T.; Bates, M.; Kowtoniuk, W. E.; Liu, D. R.; Tsien, R. Y.; Zhuang, X., Photoswitching Mechanism of Cyanine Dyes. *Journal of the American Chemical Society* **2009,** *131* (51), 18192-18193.

9. Lakowicz, J. R., Radiative Decay Engineering: Biophysical and Biomedical Applications. *Analytical biochemistry* **2001,** *298* (1), 1-24.

10. Geddes, C.; Lakowicz, J., Editorial: Metal-Enhanced Fluorescence. *Journal of Fluorescence* **2002,** *12* (2), 121-129.

11. (a) Kim, S.; Schroeder, C. M.; Xie, X. S., Single-Molecule Study of DNA Polymerization Activity of HIV-1 Reverse Transcriptase on DNA Templates. *Journal of Molecular Biology* **2010,** *395* (5), 995-1006; (b) Chan, Y.-H. M.; van Lengerich, B.; Boxer, S. G., Effects of linker sequences on vesicle fusion mediated by lipid-anchored DNA oligonucleotides. *Proceedings of the National Academy of Sciences* **2009,** *106* (4), 979-984; (c) Rothenberg, E.; Trakselis, M. A.; Bell, S. D.; Ha, T., MCM Forked Substrate Specificity Involves Dynamic Interaction with the 5′-Tail. *Journal of Biological Chemistry* **2007,** *282* (47), 34229-34234.

12. Liu, S.; Harada, B. T.; Miller, J. T.; Le Grice, S. F. J.; Zhuang, X., Initiation complex dynamics direct the transitions between distinct phases of early HIV reverse transcription. *Nature Structural & Molecular Biology* **2010,** *17* (12), 1453-60.

13. Schuler, B.; Lipman, E. A.; Eaton, W. A., Probing the free-energy surface for protein folding with single-molecule fluorescence spectroscopy. *Nature* **2002,** *419* (6908), 743-7.

14. Resch-Genger, U.; Grabolle, M.; Cavaliere-Jaricot, S.; Nitschke, R.; Nann, T., Quantum dots versus organic dyes as fluorescent labels. *Nat Meth* **2008,** *5* (9), 763-775.

15. Wu, X.; Liu, H.; Liu, J.; Haley, K. N.; Treadway, J. A.; Larson, J. P.; Ge, N.; Peale, F.; Bruchez, M. P., Immunofluorescent labeling of cancer marker Her2 and other cellular targets with semiconductor quantum dots. *Nat Biotech* **2003,** *21* (1), 41-46.

16. Wu, C.; Bull, B.; Szymanski, C.; Christensen, K.; McNeill, J., Multicolor Conjugated Polymer Dots for Biological Fluorescence Imaging. *ACS Nano* **2008,** *2* (11), 2415-2423.

17. Ngo, A. T.; Cosa, G., Assembly of Zwitterionic Phospholipid/Conjugated Polyelectrolyte Complexes: Structure and Photophysical Properties. *Langmuir* **2009,** *26* (9), 6746-6754.

18. Wang, D.; Gong, X.; Heeger, P. S.; Rininsland, F.; Bazan, G. C.; Heeger, A. J., Biosensors from conjugated polyelectrolyte complexes. *Proceedings of the National Academy of Sciences* **2002,** *99* (1), 49-53.

19. Ito, T.; Shirakawa, H.; Ikeda, S., Simultaneous polymerization and formation of polyacetylene film on the surface of concentrated soluble Ziegler-type catalyst solution. *Journal of Polymer Science Part A: Polymer Chemistry* **1996,** *34* (13), 2533-2542.

20. Saxman, A. M.; Liepins, R.; Aldissi, M., Polyacetylene: Its synthesis, doping and structure. *Progress in Polymer Science* **1985,** *11* (1–2), 57-89.

21. Shirakawa, H.; Louis, E. J.; MacDiarmid, A. G.; Chiang, C. K.; Heeger, A. J., Synthesis of electrically conducting organic polymers: halogen derivatives of polyacetylene, (CH). *Journal of the Chemical Society, Chemical Communications* **1977,** (16), 578-580.

22. Jiang, H.; Taranekar, P.; Reynolds, J. R.; Schanze, K. S., Conjugated Polyelectrolytes: Synthesis, Photophysics, and Applications. *Angewandte Chemie International Edition* **2009,** *48* (24), 4300-4316.

23. Beljonne, D.; Pourtois, G.; Silva, C.; Hennebicq, E.; Herz, L. M.; Friend, R. H.; Scholes, G. D.; Setayesh, S.; Müllen, K.; Brédas, J. L., Interchain vs. intrachain energy transfer in acceptor-capped conjugated polymers. *Proceedings of the National Academy of Sciences* **2002,** *99* (17), 10982-10987.

24. Hennebicq, E.; Pourtois, G.; Scholes, G. D.; Herz, L. M.; Russell, D. M.; Silva, C.; Setayesh, S.; Grimsdale, A. C.; Müllen, K.; Brédas, J.-L.; Beljonne, D., Exciton Migration in Rigid-Rod Conjugated Polymers: An Improved Förster Model. *Journal of the American Chemical Society* **2005,** *127* (13), 4744-4762.

25. Rochat, S.; Swager, T. M., Conjugated Amplifying Polymers for Optical Sensing Applications. *ACS applied materials & interfaces* **2013,** *5* (11), 4488-4502.

26. Singh, J.; Bittner, E. R.; Beljonne, D.; Scholes, G. D., Fluorescence depolarization in poly[2-methoxy-5-((2-ethylhexyl)oxy)-1,4-phenylenevinylene]: Sites versus eigenstates hopping. *The Journal of Chemical Physics* **2009,** *131* (19), -.

27. Al Attar, H. A.; Monkman, A. P., Effect of Surfactant on Water-Soluble Conjugated Polymer Used in Biosensor. *The Journal of Physical Chemistry B* **2007,** *111* (43), 12418-12426.

28. Danesh, C. D.; Starkweather, N. S.; Zhang, S., In Situ Study of Dynamic Conformational Transitions of a Water-Soluble Poly(3-hexylthiophene) Derivative by Surfactant Complexation. *The Journal of Physical Chemistry B* **2012,** *116* (42), 12887-12894.

29. Pinnock, S.; Malele, C.; Che, J.; Jones, W., Jr., The Role of Intermolecular Interactions in Solid State Fluorescent Conjugated Polymer Chemosensors. *J Fluoresc* **2012,** *22* (2), 583-589.

30. Karam, P.; Ngo, A. T.; Rouiller, I.; Cosa, G., Unraveling electronic energy transfer in single conjugated polyelectrolytes encapsulated in lipid vesicles. *Proceedings of the National Academy of Sciences* **2010**.

31. Thomas, S. W.; Joly, G. D.; Swager, T. M., Chemical Sensors Based on Amplifying Fluorescent Conjugated Polymers. *Chemical Reviews* **2007,** *107* (4), 1339-1386.

32. Zhou, Q.; Swager, T. M., Method for enhancing the sensitivity of fluorescent chemosensors: energy migration in conjugated polymers. *Journal of the American Chemical Society* **1995,** *117* (26), 7017-7018.

33. (a) Ogawa, K.; Chemburu, S.; Lopez, G. P.; Whitten, D. G.; Schanze, K. S., Conjugated polyelectrolyte-grafted silica microspheres. *Langmuir* **2007,** *23* (8), 4541-4548; (b) Chemburu, S.; Ji, E.; Casana, Y.; Wu, Y.; Buranda, T.; Schanze, K. S.; Lopez, G. P.; Whitten, D. G., Conjugated Polyelectrolyte Supported Bead Based Assays for Phospholipase A2 Activity†. *The Journal of Physical Chemistry B* **2008,** *112* (46), 14492-14499; (c) Achyuthan, K.; Bergstedt, T.; Chen, L.; Jones, R.; Kumaraswamy, S.; Kushon, S.; Ley, K.; Lu, L.; McBranch, D.; Mukundan, H., Fluorescence superquenching of conjugated polyelectrolytes: applications for biosensing and drug discovery. *Journal of Materials Chemistry* **2005,** *15* (27-28), 2648-2656.

34. (a) Gaylord, B. S.; Heeger, A. J.; Bazan, G. C., DNA detection using water-soluble conjugated polymers and peptide nucleic acid probes. *Proceedings of the*

National Academy of Sciences **2002,** *99* (17), 10954-10957; (b) Gaylord, B. S.; Heeger, A. J.; Bazan, G. C., DNA hybridization detection with water-soluble conjugated polymers and chromophore-labeled single-stranded DNA. *Journal of the American Chemical Society* **2003,** *125* (4), 896-900; (c) Liu, B.; Bazan, G. C., Homogeneous fluorescence-based DNA detection with water-soluble conjugated polymers. *Chemistry of materials* **2004,** *16* (23), 4467-4476.

35. Zhao, X.; Liu, Y.; Schanze, K. S., A conjugated polyelectrolyte-based fluorescence sensor for pyrophosphate. *Chemical Communications* **2007,** (28), 2914-2916.

36. Chen, L.; McBranch, D. W.; Wang, H.-L.; Helgeson, R.; Wudl, F.; Whitten, D. G., Highly sensitive biological and chemical sensors based on reversible fluorescence quenching in a conjugated polymer. *Proceedings of the National Academy of Sciences* **1999,** *96* (22), 12287-12292.

37. Duarte, A.; Chworos, A.; Flagan, S. F.; Hanrahan, G.; Bazan, G. C., Identification of Bacteria by Conjugated Oligoelectrolyte/Single-Stranded DNA Electrostatic Complexes. *Journal of the American Chemical Society* **2010,** *132* (36), 12562-12564.

38. Kim, H. N.; Guo, Z.; Zhu, W.; Yoon, J.; Tian, H., Recent progress on polymer-based fluorescent and colorimetric chemosensors. *Chemical Society reviews* **2011,** *40* (1), 79-93.

39. Cordovilla, C.; Swager, T. M., Strain Release in Organic Photonic Nanoparticles for Protease Sensing. *Journal of the American Chemical Society* **2012,** *134* (16), 6932-6935.

40. Childress, E. S.; Roberts, C. A.; Sherwood, D. Y.; LeGuyader, C. L. M.; Harbron, E. J., Ratiometric Fluorescence Detection of Mercury Ions in Water by Conjugated Polymer Nanoparticles. *Analytical Chemistry* **2012,** *84* (3), 1235-1239.

41. Chang, C.-P.; Chao, C.-Y.; Huang, J. H.; Li, A.-K.; Hsu, C.-S.; Lin, M.-S.; Hsieh, B. R.; Su, A.-C., Fluorescent conjugated polymer films as TNT chemosensors. *Synthetic Metals* **2004,** *144* (3), 297-301.

42. Im, J.; Sengupta, S. K.; Baruch, M. F.; Granz, C. D.; Ammu, S.; Manohar, S. K.; Whitten, J. E., A hybrid chemiresistive sensor system for the detection of organic vapors. *Sensors and Actuators B: Chemical* **2011,** *156* (2), 715-722.

43. Jeong, J.-E.; Woo, S.-J.; Le, V.; Choi, H.; Woo, H., Combination of conjugated polyelectrolytes and biomolecules: A new optical platform for highly sensitive and selective chemo- and biosensors. *Macromol. Res.* **2014,** *22* (5), 461-473.

44. Wu, C.; Schneider, T.; Zeigler, M.; Yu, J.; Schiro, P. G.; Burnham, D. R.; McNeill, J. D.; Chiu, D. T., Bioconjugation of Ultrabright Semiconducting Polymer Dots for Specific Cellular Targeting. *Journal of the American Chemical Society* **2010,** *132* (43), 15410-15417.

45. Feng, L.; Zhu, C.; Yuan, H.; Liu, L.; Lv, F.; Wang, S., Conjugated polymer nanoparticles: preparation, properties, functionalization and biological applications. *Chemical Society reviews* **2013,** *42* (16), 6620-6633.

46. Dalgarno, P. A.; Traina, C. A.; Penedo, J. C.; Bazan, G. C.; Samuel, I. D. W., Solution-Based Single Molecule Imaging of Surface-Immobilized Conjugated Polymers. *Journal of the American Chemical Society* **2013,** *135* (19), 7187-7193.

47. Rahim, N. A. A.; McDaniel, W.; Bardon, K.; Srinivasan, S.; Vickerman, V.; So, P. T. C.; Moon, J. H., Conjugated Polymer Nanoparticles for Two-Photon Imaging of Endothelial Cells in a Tissue Model. *Advanced Materials* **2009,** *21* (34), 3492-3496.

48. Moon, J. H.; McDaniel, W.; MacLean, P.; Hancock, L. F., Live-Cell-Permeable Poly(p-phenylene ethynylene). *Angewandte Chemie International Edition* **2007,** *46* (43), 8223-8225.

49. Howes, P.; Thorogate, R.; Green, M.; Jickells, S.; Daniel, B., Synthesis, characterisation and intracellular imaging of PEG capped BEHP-PPV nanospheres. *Chemical Communications* **2009,** (18), 2490-2492.

50. (a) Moskovits, M., Surface-enhanced spectroscopy. *Reviews of Modern Physics* **1985,** *57* (3), 783-826; (b) Lakowicz, J. R.; Malicka, J.; Gryczynski, I., Silver Particles Enhance Emission of Fluorescent DNA Oligomers. *BioTechniques* **2003,** *34* (1), 62-68.

51. (a) Selényi, P., Über Lichtzerstreuung im Raume Wienerscher Interferenzen und neue, diesen reziproke Interferenzerscheinungen. *Annalen der Physik* **1911,** *340* (8), 444-460; (b) Selényi, P., Wide-Angle Interferences and the Nature of the Elementary Light Sources. *Physical Review* **1939,** *56* (5), 477-479.

52. Andrew, P. Molecular fluorescence near metallic interfaces. University of Exeter, 1998.

53. Kuhn, H., Classical Aspects of Energy Transfer in Molecular Systems. *The Journal of Chemical Physics* **1970,** *53* (1), 101-108.

54. Willets, K. A.; Van Duyne, R. P., Localized surface plasmon resonance spectroscopy and sensing. *Annu. Rev. Phys. Chem.* **2007,** *58*, 267-297.

55. Link, S.; El-Sayed, M. A., Size and Temperature Dependence of the Plasmon Absorption of Colloidal Gold Nanoparticles. *The Journal of Physical Chemistry B* **1999,** *103* (21), 4212-4217.

56. Lu, X.; Rycenga, M.; Skrabalak, S. E.; Wiley, B.; Xia, Y., Chemical synthesis of novel plasmonic nanoparticles. *Annual review of physical chemistry* **2009,** *60*, 167-192.

57. Kelly, K. L.; Coronado, E.; Zhao, L. L.; Schatz, G. C., The Optical Properties of Metal Nanoparticles: The Influence of Size, Shape, and Dielectric Environment. *The Journal of Physical Chemistry B* **2002,** *107* (3), 668-677.

58. Mackowski, S., Metallic nanoparticles coupled with photosynthetic complexes. *Smart Nanoparticles Technology* **2012**, 3-28.

59. Noguez, C., Surface Plasmons on Metal Nanoparticles: The Influence of Shape and Physical Environment. *The Journal of Physical Chemistry C* **2007,** *111* (10), 3806-3819.

60. Lakowicz, J. R., Radiative decay engineering 5: metal-enhanced fluorescence and plasmon emission. *Analytical Biochemistry* **2005,** *337* (2), 171-194.

61. Mackowski, S., *Metallic nanoparticles coupled with photosynthetic complexes*. INTECH Open Access Publisher: 2012.

62. Evanoff, D. D.; Chumanov, G., Synthesis and Optical Properties of Silver Nanoparticles and Arrays. *ChemPhysChem* **2005,** *6* (7), 1221-1231.

63. Chen, Y.; Munechika, K.; Ginger, D. S., Dependence of Fluorescence Intensity on the Spectral Overlap between Fluorophores and Plasmon Resonant Single Silver Nanoparticles. *Nano Letters* **2007,** *7* (3), 690-696.

64. Steinigeweg, D.; Schlucker, S., Monodispersity and size control in the synthesis of 20-100 nm quasi-spherical silver nanoparticles by citrate and ascorbic acid reduction in glycerol-water mixtures. *Chemical Communications* **2012,** *48* (69), 8682-8684.

65. Gorup, L. F.; Longo, E.; Leite, E. R.; Camargo, E. R., Moderating effect of ammonia on particle growth and stability of quasi-monodisperse silver nanoparticles synthesized by the Turkevich method. *Journal of Colloid and Interface Science* **2011,** *360* (2), 355-358.

66. Lessard-Viger, M.; Rioux, M.; Rainville, L.; Boudreau, D., FRET Enhancement in Multilayer Core−Shell Nanoparticles. *Nano Letters* **2009,** *9* (8), 3066-3071.

67. Tao, A.; Sinsermsuksakul, P.; Yang, P., Polyhedral Silver Nanocrystals with Distinct Scattering Signatures. *Angewandte Chemie International Edition* **2006,** *45* (28), 4597-4601.

68. Liang, J.; Li, K.; Gurzadyan, G. G.; Lu, X.; Liu, B., Silver Nanocube-Enhanced Far-Red/Near-Infrared Fluorescence of Conjugated Polyelectrolyte for Cellular Imaging. *Langmuir* **2012,** *28* (31), 11302-11309.

69. Ung, T.; Liz-Marzán, L. M.; Mulvaney, P., Controlled Method for Silica Coating of Silver Colloids. Influence of Coating on the Rate of Chemical Reactions. *Langmuir* **1998,** *14* (14), 3740-3748.

70. Jal, P. K.; Patel, S.; Mishra, B. K., Chemical modification of silica surface by immobilization of functional groups for extractive concentration of metal ions. *Talanta* **2004,** *62* (5), 1005-1028.

71. Ahmed, S.; Madathingal, R. R.; Wunder, S. L.; Chen, Y.; Bothun, G., Hydration repulsion effects on the formation of supported lipid bilayers. *Soft Matter* **2011,** *7* (5), 1936-1947.

72. Huser, T.; Yan, M.; Rothberg, L. J., Single chain spectroscopy of conformational dependence of conjugated polymer photophysics. *Proceedings of the National Academy of Sciences* **2000,** *97* (21), 11187-11191.

73. Collini, E.; Scholes, G. D., Coherent Intrachain Energy Migration in a Conjugated Polymer at Room Temperature. *Science* **2009,** *323* (5912), 369-373.

74. Karam, P.; Ngo, A. T.; Rouiller, I.; Cosa, G., Unraveling electronic energy transfer in single conjugated polyelectrolytes encapsulated in lipid vesicles. *Proceedings of the National Academy of Sciences* **2010,** *107* (41), 17480-17485.

75. (a) Montano, G. A.; Dattelbaum, A. M.; Wang, H.-L.; Shreve, A. P., Enhanced photoluminescence from poly(phenylene vinylene) [ratio] dendrimer polyelectrolyte assemblies in solution. *Chemical Communications* **2004,** (21), 2490-2491; (b) Karam, P.; Hariri, A. A.; Calver, C. F.; Zhao, X.; Schanze, K. S.; Cosa, G., Interaction of Anionic Phenylene Ethynylene Polymers with Lipids: From Membrane Embedding to Liposome Fusion. *Langmuir* **2014,** *30* (35), 10704-10711.

76. Ngo, A. T.; Karam, P.; Fuller, E.; Burger, M.; Cosa, G., Liposome Encapsulation of Conjugated Polyelectrolytes: Toward a Liposome Beacon. *Journal of the American Chemical Society* **2008,** *130* (2), 457-459.

77. Liu, Y.; Ogawa, K.; Schanze, K. S., Conjugated Polyelectrolyte Based Real-Time Fluorescence Assay for Phospholipase C. *Analytical Chemistry* **2007,** *80* (1), 150-158.

78. Pu, K.-Y.; Liu, B., Conjugated Polyelectrolytes as Light-Up Macromolecular Probes for Heparin Sensing. *Advanced Functional Materials* **2009,** *19* (2), 277-284.

79. Lee, S. H.; Kömürlü, S.; Zhao, X.; Jiang, H.; Moriena, G.; Kleiman, V. D.; Schanze, K. S., Water-Soluble Conjugated Polyelectrolytes with Branched Polyionic Side Chains. *Macromolecules* **2011,** *44* (12), 4742-4751.

80. Jiang, D.-L.; Choi, C.-K.; Honda, K.; Li, W.-S.; Yuzawa, T.; Aida, T., Photosensitized Hydrogen Evolution from Water Using Conjugated Polymers Wrapped in Dendrimeric Electrolytes. *Journal of the American Chemical Society* **2004,** *126* (38), 12084-12089.

81. Koenen, J.-M.; Zhu, X.; Pan, Z.; Feng, F.; Yang, J.; Schanze, K. S., Enhanced Fluorescence Properties of Poly(phenylene ethynylene)-Conjugated Polyelectrolytes Designed to Avoid Aggregation. *ACS Macro Letters* **2014,** *3* (5), 405-409.

82. Scurlock, R. D.; Wang, B.; Ogilby, P. R.; Sheats, J. R.; Clough, R. L., Singlet Oxygen as a Reactive Intermediate in the Photodegradation of an Electroluminescent Polymer. *Journal of the American Chemical Society* **1995,** *117* (41), 10194-10202.

83. Dou, W.; Wang, C.; Wang, G.; Ma, Q.; Su, X., Enhance Effect of Surfactants on the Photoluminescence and Photostability of Water-Soluble Poly(phenylene ethynylene). *The Journal of Physical Chemistry B* **2008,** *112* (40), 12681-12685.

84. Liu, H.-W.; Ngo, A. T.; Cosa, G., Enhancing the Emissive Properties of Poly(p-phenylenevinylene)-Conjugated Polyelectrolyte-Coated SiO2 Nanoparticles. *Journal of the American Chemical Society* **2011,** *134* (3), 1648-1652.

85. Wu, C.; Szymanski, C.; Cain, Z.; McNeill, J., Conjugated Polymer Dots for Multiphoton Fluorescence Imaging. *Journal of the American Chemical Society* **2007,** *129* (43), 12904-12905.

86. (a) Lee, H. Y.; Seol, A. Y.; Jeong, K. H.; Kim, Y. J., Poly (vinyl pyrrolidone) conjugated lipid system for the hydrophobic drug delivery. *Macromolecular Research* **2007,** *15* (6), 547-552; (b) Kamada, H.; Tsutsumi, Y.; Yamamoto, Y.; Kihira, T.; Kaneda, Y.; Mu, Y.; Kodaira, H.; Tsunoda, S.-i.; Nakagawa, S.; Mayumi, T., Antitumor activity of tumor necrosis factor-α conjugated with polyvinylpyrrolidone on solid tumors in mice. *Cancer research* **2000,** *60* (22), 6416-6420.

87. Ngo, A. T.; Lau, K. L.; Quesnel, J. S.; Aboukhalil, R.; Cosa, G., Deposition of anionic conjugated poly(phenylenevinylene) onto silica nanoparticles via electrostatic interactions — Assembly and single-particle spectroscopy. *Canadian Journal of Chemistry* **2011,** *89* (3), 385-394.

88. Julinova, M.; Kupec, J.; Slavik, R.; Vaskova, M., Initiating Biodegradation of Polyvinylpyrrolidone in an Aqueous Aerobic Environment: Technical Note / Zainicjowanie Biodegradacji Poliwinylopirolidonu W Środowisku Wodno-Tlenowym: Notatki Techniczne. In *Ecological Chemistry and Engineering S*, 2013; Vol. 20, p 199.

89. Resch-Genger, U.; Grabolle, M.; Cavaliere-Jaricot, S.; Nitschke, R.; Nann, T., Quantum dots versus organic dyes as fluorescent labels. *Nature methods* **2008,** *5* (9), 763-775.

90. Chen, L.; Xu, S.; McBranch, D.; Whitten, D., Tuning the Properties of Conjugated Polyelectrolytes through Surfactant Complexation. *Journal of the American Chemical Society* **2000,** *122* (38), 9302-9303.

91. Abe, S.; Chen, L., Tuning the photophysical properties of an ionic conjugated polymer through interactions with conventional polyelectrolytes. *Journal of Polymer Science Part B: Polymer Physics* **2003,** *41* (14), 1676-1679.

92. Dalvi-Malhotra, J.; Chen, L., Enhanced Conjugated Polymer Fluorescence Quenching by Dipyridinium-Based Quenchers in the Presence of Surfactant. *The Journal of Physical Chemistry B* **2005,** *109* (9), 3873-3878.

93. Fernandez-Moreira, V.; Thorp-Greenwood, F. L.; Coogan, M. P., Application of d6 transition metal complexes in fluorescence cell imaging. *Chemical Communications* **2010,** *46* (2), 186-202.

94. Pavlov, G.; Korneeva, E.; Jumel, K.; Harding, S.; Meijer, E. W.; Peerlings, H. W. I.; Stoddart, J. F.; Nepogodiev, S., Hydrodynamic properties of carbohydrate-coated dendrimers. *Carbohydrate Polymers* **1999,** *38* (3), 195-202.

95. Bird, C. L.; Kuhn, A. T., Electrochemistry of the viologens. *Chemical Society Reviews* **1981,** *10* (1), 49-82.

96. Richter, M. M.; Fan, F.-R. F.; Klavetter, F.; Heeger, A. J.; Bard, A. J., Electrochemistry and electrogenerated chemiluminescence of films of the conjugated polymer 4-methoxy-(2-ethylhexoxyl)-2, 5-polyphenylenevinylene. *Chemical Physics Letters* **1994,** *226* (1), 115-120.

97. Schönle, A.; Hell, S. W., Heating by absorption in the focus of an objective lens. *Optics Letters* **1998,** *23* (5), 325-327.

98. Liu, H.-W.; Cosa, G.; Landes, C. F.; Zeng, Y.; Kovaleski, B. J.; Mullen, D. G.; Barany, G.; Musier-Forsyth, K.; Barbara, P. F., Single-Molecule FRET Studies of Important Intermediates in the Nucleocapsid-Protein-Chaperoned Minus-Strand Transfer Step in HIV-1 Reverse Transcription. *Biophysical Journal* **2005,** *89* (5), 3470-3479.

99. (a) Wichterlová, J.; Wichterle, K.; Michálek, J., Determination of permeability and diffusivity of oxygen in polymers by polarographic method with inert gas. *Polymer* **2005,** *46* (23), 9974-9986; (b) Hadassah, J.; Sehgal, P. K., A novel method to measure oxygen permeability and transmissibility of contact lenses. *Clinical and Experimental Optometry* **2006,** *89* (6), 374-380.

100. Tian, Y.; Kuzimenkova, M. V.; Xie, M.; Meyer, M.; Larsson, P.-O.; Scheblykin, I. G., Watching two conjugated polymer chains breaking each other when colliding in solution. *NPG Asia Mater* **2014,** *6*, e134.

101. Feng, G.; Ding, D.; Liu, B., Fluorescence bioimaging with conjugated polyelectrolytes. *Nanoscale* **2012,** *4* (20), 6150-6165.

102. Parthasarathy, A.; Ahn, H.-Y.; Belfield, K. D.; Schanze, K. S., Two-Photon Excited Fluorescence of a Conjugated Polyelectrolyte and Its Application in Cell Imaging. *ACS Applied Materials & Interfaces* **2010,** *2* (10), 2744-2748.

103. Feng, X.; Tang, Y.; Duan, X.; Liu, L.; Wang, S., Lipid-modified conjugated polymer nanoparticles for cell imaging and transfection. *Journal of Materials Chemistry* **2010,** *20* (7), 1312-1316.

104. Ha, T.; Tinnefeld, P., Photophysics of Fluorescence Probes for Single Molecule Biophysics and Super-Resolution Imaging. *Annual review of physical chemistry* **2012,** *63*, 595.

105. Diaspro, A.; Chirico, G.; Usai, C.; Ramoino, P.; Dobrucki, J., Photobleaching. In *Handbook of biological confocal microscopy*, Springer: 2006; pp 690-702.

106. Landry, M. P.; McCall, P. M.; Qi, Z.; Chemla, Y. R., Characterization of Photoactivated Singlet Oxygen Damage in Single-Molecule Optical Trap Experiments. *Biophysical Journal* **2009,** *97* (8), 2128-2136.

107. Aitken, C. E.; Marshall, R. A.; Puglisi, J. D., An Oxygen Scavenging System for Improvement of Dye Stability in Single-Molecule Fluorescence Experiments. *Biophysical Journal 94* (5), 1826-1835.

108. Hsu, P.-C.; Liu, M.-Y.; Hsu, C.-C.; Chen, L.-Y.; Leon Guo, Y., Effects of vitamin E and/or C on reactive oxygen species-related lead toxicity in the rat sperm. *Toxicology* **1998,** *128* (3), 169-179.

109. Niki, E., Interaction of Ascorbate and α-Tocopherol. *Annals of the New York Academy of Sciences* **1987,** *498* (1), 186-199.

110. Mukai, K.; Daifuku, K.; Okabe, K.; Tanigaki, T.; Inoue, K., Structure-activity relationship in the quenching reaction of singlet oxygen by tocopherol (vitamin E) derivatives and related phenols. Finding of linear correlation between the rates of quenching of singlet oxygen and scavenging of peroxyl and phenoxyl radicals in solution. *The Journal of Organic Chemistry* **1991,** *56* (13), 4188-4192.

111. Itoh, S.; Nagaoka, S.-i.; Mukai, K.; Ikesu, S.; Kaneko, Y., Kinetic study of quenching reactions of singlet oxygen and scavenging reactions of free radicals by α-, β-, λ- and σ-tocopheramines in ethanol solution and micellar dispersion. *Lipids* **1994,** *29* (11), 799-802.

112. Fahrenholtz, S. R.; Doleiden, F. H.; Trozzolo, A. M.; Lamola, A. A., ON THE QUENCHING OF SINGLET OXYGEN BY α-TOCOPHEROL. *Photochemistry and Photobiology* **1974,** *20* (6), 505-509.

113. Polizzotti, A.; Schual-Berke, J.; Falsgraf, E.; Johal, M., *Investigating New Materials and Architectures for Grätzel Cells*. 2012.

114. DABBAGH, H. A.; AZAMI, F.; FARROKHPOUR, H.; CHERMAHINI, A. N., UV-VIS, NMR AND FT-IR SPECTRA OF TAUTOMERS OF VITAMIN C. EXPERIMENTAL AND DFT CALCULATIONS. *Journal of the Chilean Chemical Society* **2014,** *59*, 2588-2594.

115. Piacham, T.; Nantasenamat, C.; Suksrichavalit, T.; Puttipanyalears, C.; Pissawong, T.; Maneewas, S.; Isarankura-Na-Ayudhya, C.; Prachayasittikul, V., Synthesis and Theoretical Study of Molecularly Imprinted Nanospheres for Recognition of Tocopherols. *Molecules* **2009,** *14* (8), 2985-3002.